



PCT/AU2004/001118

Patent Office
Canberra

I, JULIE BILLINGSLEY, TEAM LEADER EXAMINATION SUPPORT AND SALES hereby certify that annexed is a true copy of the Provisional specification in connection with Application No. 2004902143 for a patent by QUCOR PTY LTD as filed on 22 April 2004.

| | |
|-------------------|-----|
| REC'D 06 SEP 2004 | |
| WIPO | PCT |



WITNESS my hand this
First day of September 2004

J. Billingsley

JULIE BILLINGSLEY
TEAM LEADER EXAMINATION
SUPPORT AND SALES

**PRIORITY
DOCUMENT**
SUBMITTED OR TRANSMITTED IN
COMPLIANCE WITH RULE 17.1(a) OR (b)

BEST AVAILABLE COPY

AUSTRALIA

Patents Act 1990

Unisearch Limited

PROVISIONAL SPECIFICATION

Invention Title:

Nanoscale Products

The invention is described in the following statement:

Title**Nanoscale Products****Technical Field**

5 This invention concerns nanoscale products, such as electronic devices fabricated to nanometer accuracy. It also concerns atomic scale products and where we use the term nanoscale we intend nanoscale and atomic scale products. Such products could be intermediate products in the fabrication of a quantum computer, but could have many other uses. In further aspects the invention concerns methods of fabricating
 10 such products. It also concerns a quantum computer.

Background Art

The Kane proposal^{1,2} for a silicon-based quantum computer uses the nuclear spin of phosphorus nuclei ($I = \frac{1}{2}$) as the qubits embedded in isotopically pure ²⁸Si ($I = 0$).
 15 At low temperatures the donor electron remains bound to the P nucleus and surface "A" gates control the hyperfine interaction between nuclear and electron spins, enabling polarization of the two. The two P donors need to be ~20 nm apart to allow the adjacent donor electron wavefunctions to overlap. Coupling between adjacent donor electrons is achieved using separate surface "J" gates, enabling an electron mediated interaction
 20 between qubits. Fig. 1(a) shows this proposed structure.

A number of patent applications and papers are relevant to the building of such a device, and these are cited below:

- ¹Kane, B. E. A silicon-based nuclear spin quantum computer. *Nature* 393, 133 (1998).
- 25 ²Kane, B. E. Patent Application PCT/AU98/00778.
- ³Vrijen, R., Yablonovitch, L., Kang Wang, Hong Wen Jiang, Balandin, A., Roychowdhury, V., Mor, T., DiVincenzo, D. Electron-spin-resonance transistors for quantum computing in silicon-germanium heterostructures. *Phys. Rev. A* 62, 012306/1-10 (2000).
- 30 ⁴Swartzentruber, B.S., Mo, Y.W., Webb, M.B. & Lagally, M.G. Scanning tunneling microscopy studies of structural disorder and steps on Si surfaces. *J. Vac. Sci. Tech. A* 7, 2901 (1989).
- ⁵Hata, K., Kimura, T., Ozawa, S. and Miyamoto, N. How to fabricate a defect free surface. *J. Vac. Sci. Technol. A* 18, 1933 (2000).
- 35 ⁶Hata, K., Yasuda, S. and Shigekawa, H. Reinterpretation of the scanning tunneling microscopy images of the Si(100)2x1 dimers. *Phys. Rev. B.* 60, 8164 (1999).

- ⁷Oura, K., Lifshits, V.G., Saranin, A.A., Zotov, A.V. & Katayama, M. Hydrogen interaction with clean and modified silicon surfaces. *Surf. Sci. Rep.* 35, 1 (1999).
- ⁸Feenstra, R. M. *Surf. Sci.* 299-300, 965 (1994).
- ⁹Hamers, R.J., Avouris, Ph. & Bozso, F. Imaging of chemical-bond formation with the scanning tunneling microscope. NH_3 dissociation on Si(001) *Phys. Rev. Lett.* 59, 2071 (1987).
- ¹⁰Thirstrup, C., private communication
- ¹¹Wang, Y., Bronikowski, M.J. & Hamers, R.J. An atomically-resolved STM study of the interaction of phosphine (PH_3) with the silicon (001) surface. *J. Phys. Chem.* 98, 5966 (1994).
- ¹²Hill, E., Freelon, B., Ganz, E. Diffusion of hydrogen on the Si(001) surface investigated by STM atom tracking. *Phys. Rev. B* 60, 15896 (1999).
- ¹³Lin, D.S., Ku, T.S., and Chen, R.P. Interaction of phosphine with Si(100) from core-level photoemission and real-time scanning tunneling microscopy *Phys. Rev. B* 61, 2799 (2000).
- ¹⁴Lin, D.S., Ku, T.S., and Sheu, T.J. Thermal reactions of phosphine with Si(100): a combined photoemission and scanning-tunneling-microscopy study. *Surf. Sci.* 424, 7 (1999).
- ¹⁵Wang, Y., Chen, X. and Hamers, R. J., Atomic-resolution study of overlayer formation and interfacial mixing in the interaction of phosphorus with Si(001) *Phys. Rev. B* 50, 4534 (1994).
- ¹⁶Zhi-Heng Loh, Kang, H.C. Chemisorption of NH_3 on Si(100)2x1: A study by first-principles ab initio and density functional theory. *J. Chem. Phys.* 112, 2444-2451 (2000).
- ¹⁷Northrup, J.E. Theoretical studies of arsine adsorption on Si(100). *Phys. Rev. B* 51, 2218-2222 (1995).
- ¹⁸L. Oberbeck, T. Hallam, N.J. Curson, M.Y. Simmons and R.G. Clark, "STM investigation of epitaxial Si growth for the fabrication of a Si-based quantum computer", *Appl. Surf. Sci.* 212-213, 319 (2003).
- ¹⁹J. W. Lyding, T. Shen, J. S. Hubacek, J. R. Tucker, and G. Abeln, *Appl. Phys. Lett.* 64, 2010 (1994).
- ²⁰J. R. Tucker and T. C. Shen, *Solid-State Electron.* 42, 1061(1998).
- ²¹J. L. O'Brien, S. R. Schofield, M. Y. Simmons, R. G. Clark, A. S. Dzurak, N. J. Curson, B. E. Kane, N. S. McKalpine, M. E. Hawley, and G. Brown, *Phys. Rev. B* 64, 161401 (2001).

- ²²S. R. Schofield, N. J. Curson, M. Y. Simmons, F. J. Rueß, T. Hallam, L. Oberbeck, and R. G. Clark, *Phys. Rev. Lett.* 91, 136104 (2003).
- ²³T. C. Shen, J. Y. Ji, M. A. Zudov, R. R. Du, J. S. Kline, and J. R. Tucker, *Appl. Phys. Lett.* 80, 1580 (2002).
- 5 ²⁴L. Oberbeck, N. J. Curson, M. Y. Simmons, R. Brenner, A. R. Hamilton, S. R. Schofield, and R. G. Clark, *Appl. Phys. Lett.* 81, 3197 (2002).
- ²⁵J. E. Vasek, Z. Zhang, C. Salling, and M. Lagally, *Phys. Rev. B* 51, 17207 (1995).
- ²⁶J. J. Boland, *Phys. Rev. Lett.* 67, 1539 (1991).
- ²⁷E. Hill, B. Freelon, and E. Ganz, *Phys. Rev. B* 60, 15896 (1999).
- 10 ²⁸H. Nakazawa, M. Suemitsu, and N. Miyamoto, *Surf. Sci.* 465, 177 (2000).
- ²⁹M. Dürr, A. Biedermann, Z. Hu, U. H"ofer, and T. F. Heinz, *Science* 296, 1838 (2002).
- ³⁰D. R. Bowler, J. H. G. Owen, C. M. Goringe, K. Miki, and G. A. D. Briggs, *J. Phys. Cond. Matt.* 12, 7655 (2000).
- 15 ³¹B. S. Swartzentruber, Y. W. Mo, M. B. Webb, and M. G. Lagally, *J. Vac. Sci. Technol. A* 7, 2901 (1989).
- ³²R. J. Hamers, R. M. Tromp, and J. E. Demuth, *Phys. Rev. B* 34, 5343 (1986).
- ³³E. J. Buehler and J. J. Boland, *Surf. Sci.* 425, L363 (1999).
- ³⁴Y. Wang, M. J. Bronikowski, , and R. J. Hamers, *J. Vac. Sci. Technol. A* 12, 2051 (1994).
- 20 ³⁴D. P. Adams, S. M. Yalisove, and D. J. Eaglesham, *Appl. Phys. Lett.* 63, 3571 (1997).
- ³⁶M. L. N. Kitamira and M. Webb, *Phys. Rev. Lett.* 71, 2082 (1993).
- ³⁷R. N. A. Natori and H. Yasunaga, *Surf. Sci.* 397, 71 (1998).
- ³⁸E. Kim, C. Chen, T. Pang, and Y. H. Lee, *Phys. Rev. B* 60, 8680 (1999).
- 25 ³⁹Y. Wang, X. Chen, and R. J. Hamers, *Phys. Rev. B* 50, 4534 (1994).
- ⁴⁰F. R. Rueß, L. Oberbeck, M. Y. Simmons, K. E. J. Goh, A. R. Hamilton, T. Hallam, N. J. Curson, and R. G. Clark, *In preparation* (2004).
- ⁴¹D.-S. Lin, T.-S. Ku, and R.-P. Chen, *Phys. Rev. B* 61, 2799 (2000).
- ⁴²G. Bergmann, *Phys. Rep.* 107, 1 (1984).
- 30 ⁴³S. Hikami, A. I. Larkin, Y. Nagaoka, *Prog. Theor. Phys.* 63, 707 (1980).
- ⁴⁴J. R. Tucker, T. -C. Shen, *Int. J. Circ. Theor. Appl.* 28, 553 (2000).
- ⁴⁵G. L. Snider, *J. Appl. Phys.* 85, 4283 (1999).
- ⁴⁶J. C. Kim, J.-Y. Ji, J. S. Kline, J. R. Tucker, T.-C. Shen, *Surf. Sci.* 538, L471 (2003).
- ⁴⁷G.E. Moore, *Electronics* 38, 114 (1965).
- 35 ⁴⁸see e.g. S.M. Sze, *Semiconductor Devices - Physics and Technology* (John Wiley & Sons, New York, 1985).

- ⁴⁹P.M. Fahey, P.B. Griffin and J.D. Plummer, Rev. Mod. Phys. 61, 289 (1989).
⁵⁰J.F. Nützel and G. Abstreiter, Phys. Rev. B 53, 13551 (1996).
⁵¹E. Friess, J Nützel and G. Abstreiter, Appl. Phys. Lett. 60, 2237 (1992).
⁵²K.D. Hobart, F.J. Kub, G.G. Jernigan and P.E. Thompson, J. Vac. Sci. Technol. B 14,
5 2229 (1996).
⁵³R.G. Wilson, F.A. Stevie and C.W. Magee, *Secondary Ion Mass Spectrometry* (John Wiley & Sons, New York, 1989).
⁵⁴J. F. Nützel and G. Abstreiter, Phys. Rev. B 53, 13551 (1996).
⁵⁵S. Hikami, A. I. Larkin, and Y. Nagaoka, Prog. Theor. Phys. 63, 707 (1980).
10 ⁵⁶B. L. Altshuler, A. G. Aronov, A. I. Larkin, and D. E. Khmel'nitskii, Sov. Phys. JETP 54, 411 (1981).

To date there have been no STM studies of the incorporation of single phosphorus atoms from a dopant source such as phosphine into silicon.

This invention demonstrates, for the first time, achievement of a number of the
15 intermediate products and steps necessary to produce a silicon based atomic-scale device such as a quantum computer in line with the Kane proposal.

Summary of the Invention

In a first aspect the invention is a nanoscale product, being an intermediate
20 product of a process for fabricating an atomic scale device such as a quantum computer, the nanoscale product comprising:

a silicon crystal, where donor atoms are substituted for silicon atoms in the surface to form an array of donor atoms spaced apart from each other by 100 nm or less, and where the donor atoms are electrically active;

25 where a hydrogen resist layer has been removed either,
by annealing at $\sim 470 \pm 30^\circ\text{C}$ for less than 10 seconds, and preferably for 5 seconds,

or,

by using the STM tip, preferably with tunnelling conditions in the range of 4 – 7
30 V and 1 – 4 nA.

The following Best Modes of the Invention demonstrate the production of such a structure for the first time.

The silicon surface may be the (100)-oriented surface having a 2x1 unit cell surface structure with rows of σ -bonded silicon dimers. In this case the donor atoms
35 replace silicon atoms in the surface to form donor-silicon hetero-dimers.

The donor may be phosphorus and the phosphorus atoms may be placed with greater precision, such as 50 nm or 20 nm apart.

In a second aspect the invention is a nanoscale product, being an intermediate
 5 product of a process for fabricating an atomic scale device such as a quantum computer, the nanoscale product comprising:

a silicon crystal encapsulating a layer of donor atoms substituted for silicon atoms in the crystal, where substantially all the donor atoms are electrically active;

where a hydrogen resist layer has been removed either,

10 by annealing at $\sim 470 \pm 30^\circ\text{C}$ for less than 10 seconds, and preferably for 5 seconds,

or,

by using the STM tip, preferably with tunnelling conditions in the range of 4 – 7 V and 1 – 4 nA..

15 The encapsulating layers may be epitaxially grown preferably at room temperature over the layer of donor atoms. The encapsulating layers may be between 5 and 50 nm thick.

The silicon surface may be (100)-oriented, where the donor atoms replace silicon atoms to form donor-silicon heterodimers.

20 The donors may be Phosphorus and they may be placed in an array.

According to a third aspect, the invention is a method of fabricating a nanoscale or atomic scale product as defined above, comprising the following steps:

(a) Preparing a clean silicon crystal surface.

25 (b) Passivating the sample surface with atomic hydrogen.

(c) Selectively desorbing single H atoms from the passivated surface using a Scanning Tunnelling Microscope (STM) tip to form a pattern of exposed areas in the hydrogen layer, where the areas are spaced from each other by 100 nm or less.

(d) Exposing the patterned surface to donor molecules to produce an array of
 30 single donor atom bearing molecules in the exposed areas.

(e) Annealing the arrayed surface at between about 300°C and about 650°C to incorporate electrically active donor atoms into the silicon.

(f) Annealing at $\sim 470 \pm 30^\circ\text{C}$ for less than 10 seconds, and preferably for 5 seconds,

35 or,

using the STM tip, preferably with tunnelling conditions in the range of 4 – 7 V and 1 – 4 nA..

The following Best Modes of the Invention demonstrate the performance of this method for the first time.

5 The silicon surface may be (100)-oriented having a 2x1 unit cell surface structure with rows of σ -bonded silicon dimers. In this case the donor atoms replace silicon atoms in the surface to form donor-silicon heterodimers.

The donor may be phosphorus and the phosphorus atoms may be placed with greater precision, such as 50 nm or 20 nm apart.

10 In one embodiment, steps (e) and (f) may be combined.

According to a fourth aspect, the invention is a method of fabricating a nanoscale or atomic scale product as defined above, comprising the following steps:

- (a) Preparing a clean silicon crystal surface.
- 15 (b) Passivating the sample surface with atomic hydrogen.
- (c) Inserting donor atoms into the silicon at lithographically defined areas where the hydrogen was desorbed using an STM tip;
- (d) Annealing at $\sim 470 \pm 30^\circ\text{C}$ for less than 10 seconds, and preferably for 5 seconds,

20 or,

using the STM tip, preferably with tunnelling conditions in the range of 4 – 7 V and 1 – 4 nA..

- (e) Growing silicon over the surface, at between about 0°C and 400°C but preferably at room temperature to prevent diffusion of the donor atoms and to
- 25 encapsulate electrically active donor atoms in the surface.

In the following Best Modes of the Invention we demonstrate this method.

The silicon surface may be (100)-oriented having a 2x1 unit cell surface structure with rows of σ -bonded silicon dimers. In this case the donor atoms replace silicon atoms in the surface to form donor-silicon heterodimers.

30 The donor may be phosphorus and the phosphorus atoms may be place with selected precision, such as 100 nm, 50 nm or 20 nm apart.

According to a fifth aspect, the invention is a method of fabricating a nanoscale or atomic scale product as defined above, comprising the following steps:

- 35 (a) Preparing a clean silicon crystal surface.

(b) Exposing the surface to donor molecules such that the donor molecules adsorb over the silicon surface.

(c) Annealing the arrayed surface at between about 300°C and about 650°C to incorporate electrically active donor atoms into the silicon.

5 (d) Annealing at $\sim 470 \pm 30^\circ\text{C}$ for less than 10 seconds, and preferably for 5 seconds,

or,

using the STM tip, preferably with tunnelling conditions in the range of 4 – 7 V and 1 – 4 nA..

10 (e) Using an STM to view donor atoms on the surface to confirm that the donor atoms are in a substitutional lattice site in the silicon, and are therefore electrically active.

The following Best Modes of the Invention demonstrate the use of this method for the first time.

15 The method may include the further step of: (f) Growing silicon over the surface, at between about 0°C and 400°C, between about 0°C and 250°C or preferably at room temperatures to prevent diffusion of the donor atoms, to encapsulate electrically active donor atoms in the surface.

20 The method may include the further step of: (g) Thermally annealing the surface so that it becomes atomically smooth.

The silicon surface may be (100)-oriented having a 2x1 unit cell surface structure with rows of σ -bonded silicon dimers. In this case the donor atoms replace silicon atoms in the surface to form donor-silicon heterodimers.

25 The donor may be phosphorus and the phosphorus atoms may be placed with selected precision, such as 100 nm, 50 nm or 20 nm apart.

In one embodiment, steps (c) and (d) may be combined.

According to a sixth aspect, the invention is a method of fabricating a nanoscale or atomic scale product as defined above, comprising the following steps:

30 (a) Preparing a clean silicon crystal surface.

(b) Exposing the surface to donor molecules such that the donor molecules adsorb over the silicon surface to form a doped layer.

(c) Annealing the surface at between about 300°C and about 650°C to incorporate electrically active donor atoms into the silicon.

35 (d) Annealing at $\sim 470 \pm 30^\circ\text{C}$ for less than 10 seconds, and preferably for 5 seconds,

or,

using the STM tip, preferably with tunnelling conditions in the range of 4 – 7 V and 1 – 4 nA..

(e) Growing silicon over the surface, at between about 0°C and 400°C but preferably at room temperature to prevent diffusion of the donor atoms, and to encapsulate electrically active donor atoms in the surface.

(f) Measuring the electrical activity of the doped layer.

The following Best Modes of the Invention demonstrate the use of this method for the first time.

10 The silicon growth may take place at between about 0°C and 250°C or preferably at room temperature to prevent diffusion of the donor atoms, to encapsulate electrically active donor atoms in the surface.

The silicon surface may be (100)-oriented having a 2x1 unit cell surface structure with rows of σ -bonded silicon dimers. In this case the donor atoms replace 15 silicon atoms in the surface to form donor-silicon heterodimers.

The donor may be phosphorus and the phosphorus atoms may be placed with selected precision, such as 100 nm, 50 nm or 20 nm apart.

In one embodiment, steps (c) and (d) may be combined.

20 According to a seventh aspect, the invention is a method of fabricating a nanoscale or atomic scale product as defined above, comprising the following steps:

- (a) Fabrication of registration markers;
- (b) Preparing a clean silicon crystal surface;
- (c) Passivating the sample surface with atomic hydrogen;
- 25 (d) Inserting donor atoms into the silicon at lithographically defined areas where the hydrogen was desorbed using an STM tip;
- (e) Annealing at $\sim 470 \pm 30^\circ\text{C}$ for less than 10 seconds, and preferably for 5 seconds,

or,

30 using the STM tip, preferably with tunnelling conditions in the range of 4 - 7V and 1 – 4 nA. to desorb hydrogen from the silicon surface.

Growing silicon over the surface, at between about 0°C and 400°C but preferably at room temperature to prevent diffusion of the donor atoms and to encapsulate electrically active donor atoms in the surface.

35 Fabrication of metallic surface contacts using the registration markers to contact the buried nanoscale or atomic-scale device.

The method may include the additional step of measuring the electrical properties of the device.

In the following Best Modes of the Invention we demonstrate this method.

The silicon surface may be (100)-oriented having a 2x1 unit cell surface structure with rows of σ -bonded silicon dimers. In this case the donor atoms replace silicon atoms in the surface to form donor-silicon heterodimers.

The donor may be phosphorus and the phosphorus atoms may be placed with selected precision, such as 100 nm, 50 nm or 20 nm apart.

The registration markers may be produced by:

(i) Wet-chemical etching of the silicon sample in lithographically structured areas of the sample surface.

(ii) Reactive ion etching (RIE) of the silicon sample in lithographically structured areas of the sample surface.

(iii) Focused ion beam (FIB) milling of the silicon sample surface.

(iv) Deposition of thin metal layers on the silicon sample surface in lithographically structured areas.

The registration markers may have a size between several nm and tens of μm . The registration markers may have a depth or height between several nm and several μm .

The clean silicon surface may be produced in an ultra-high-vacuum environment by:

(i) outgassing for 6 hours at $\sim 600^\circ\text{C}$ by indirect heating.

(ii) flashing the samples to $\sim 1200^\circ\text{C}$ for ~ 1 minute by passing a DC current directly through the sample.

(iii) reducing the sample temperature to $\sim 950^\circ\text{C}$ and then cooling slowly from $\sim 950^\circ\text{C}$ to room temperature.

The surface may be passivated with atomic hydrogen in the same ultra-high-vacuum environment, the dose rate being controlled by monitoring the total pressure of the vacuum system to achieve hydrogen termination of the surface, being a mono layer of hydrogen with one hydrogen atom bonded to each silicon atom (mono-hydride dimer).

The H atoms may be selectively desorbed from the passivated surface using an STM tip in the same ultra-high-vacuum environment, by applying pulses of both high voltage and tunnelling current to the tip for a short time period of the order 1 ms, to form a pattern in the hydrogen layer.

The surface may be exposed to donor molecules in the same ultra-high-vacuum environment, such that the donor molecules bond to the exposed pattern in the surface.

The donor molecules may be phosphine (PH_3) to deliver donor atoms of phosphorus, P.

5 Specifically these processes may form part of a process for producing an atomic array of phosphorus atoms in silicon with the controlled separation for a silicon based quantum computer. Such a solid-state quantum computer may use either the electron spin³ or nuclear spin of phosphorus nuclei ($I = \frac{1}{2}$) as the qubits embedded in isotopically pure ^{28}Si ($I = 0$).

10

In an eighth aspect the invention is a quantum computer fabricated according to any one of the methods defined above.

Brief Description of the Drawings

15 Aspects and examples of the invention will now be described with reference to the following accompanying drawings, in which:

Fig.1(a) is a schematic diagram of the Kane proposal for a silicon based quantum computer.

20 Fig. 2a(a) to (e) and 2b(f) to (k) are a series of eleven steps according to the invention for the fabrication of a nanoscale product.

Fig. 3(a) and (b) are an STM image and a schematic diagram showing a crystalline silicon(100) 2×1 surface.

Fig. 4(a) to (e) are an STM image, schematic diagrams and scanning tunnelling spectroscopy results.

25 Fig. 5(a) to (e) are STM images, schematic diagrams and line profiles showing two dangling bonds arranged along a dimer row on a crystalline silicon surface before phosphine dosing and adsorbed PH_3/PH_2 molecules after phosphine dosing.

Fig. 6(a) to (f) are STM images, schematic diagrams and line profiles showing dangling bonds arranged across a dimer row on a crystalline silicon surface before phosphine dosing and adsorbed PH_3/PH_2 molecules after phosphine dosing.

30 Fig. 7(a) to (e) are STM images of a silicon (100) surface showing a number of defects.

Fig. 8(a) and (b) are STM images of a silicon (100) surface before and after phosphine dosing.

35 Fig. 9(a) to (e) are STM images of a silicon (100) surface after phosphine dosing.

Fig. 10(a) to (i) are a series of STM images and schematic diagrams showing a silicon surface after the phosphine dosing and the effect of heating that surface.

Fig. 11(a) to (f) are a series of diagrams, STM images and line profiles showing phosphine molecules on the surface of a silicon lattice and incorporated into it.

5 Fig. 12(a) to (c) are a series of STM images of the silicon surface after moderate phosphine doses and heating and Auger electron spectroscopy results showing a silicon surface after saturation phosphine dosing and heating.

Fig. 13(a) shows an STM image of a hydrogen terminated silicon surface having a patch where hydrogen has been desorbed; (b) to (d) show a patch after annealing to
10 350°C.

Fig. 14(a) to (h) are a series of STM images and a line profile showing the effect of phosphine dosing and annealing to incorporate phosphorous atoms into a silicon lattice, along a lithographically produced line.

Fig. 14A(a) to (d) are a series of filled state STM images of a hydrogen
15 terminated surface following annealing at different temperatures and for different time periods.

Fig. 14B(a) to (c) are a series of STM images showing deposited phosphine (a), annealing at 350°C for 10 seconds (b), and a detail at (c).

Fig. 14BA is a series of filled state STM images showing a monohydride
20 terminated Si(001) surface (a) and the surface after anneals at 374°C (b), 426°C (c), 470°C (d), 529°C (e), and 581°C (f) for 10 s each. Imaging conditions were (a) -1.6V, 0.15nA. (b) -1.2V, 0.15nA. (c) -1.6V, 0.15nA. (d) -1.2V, 0.14nA. (e) -1V, 0.15nA. (f) -1V, 0.14nA.

Fig. 14BB is a 200 nm × 25 nm region of hydrogen has been desorbed from a
25 monohydride terminated Si(001) surface by biasing the STM tip to +4V at a current of 3nA (a). After phosphine dosing and P incorporation at 350°C (b), a 470°C anneal removes all surface hydrogen, leaving the nanostructured region of phosphorus intact (c).

Fig. 14C is an STM image showing a hydrogen terminated surface after
30 desorption with an STM tip.

Fig. 14D(a) and (b) are STM images showing two dangling bonds exposed in the hydrogen terminated surface using STM lithography (a), and the same surface after phosphine dose, annealing and removal of the hydrogen resist with an STM tip (b).

Fig. 15(a) to (d) are a series of STM images showing the effect of growing
35 silicon at different temperatures, Fig. 15(e) to (h) are a series of STM images showing the silicon surface after growth at room temperature and annealing at different

temperatures; Fig. 15(i), (j) and (k) are a series of schematic diagrams explaining the different temperature dependent growth modes.

Fig. 16(a) to (e) are a series of schematic diagrams and STM images showing the silicon surface before and after growth at 250°C and subsequent annealing at
5 various temperatures.

Figs. 17(a) to (e) are a series of diagrams and STM images showing the silicon surface before and after silicon growth at 250°C on a hydrogen passivated surface and subsequent annealing steps.

Fig. 18(a) is a graph showing the silicon surface roughness after annealing at
10 different temperatures for growth on a clean and on a hydrogen terminated surface; and Fig. 18(b) is a graph showing the defect density after annealing at different temperatures for growth on a clean and on a hydrogen terminated surface.

Fig. 19(a) to (h) are a series of diagrams and STM images showing room temperature encapsulation of a phosphine dosed silicon surface and subsequent
15 annealing.

Fig. 20(a) to (i) are a series of diagrams and STM images showing encapsulation of a phosphine dosed silicon surface at 260°C and subsequent annealing.

Fig. 21 is a series of filled state STM images showing the Si(001) surface after Si overgrowth (a), (e) and annealing at various temperatures (b) - (d) and (f) - (h) from
20 two experiments: 5 ML Si growth at 255°C (left column) and RT (right column). Image size of individual STM images is $50 \times 25 \text{ nm}^2$.

Fig. 21A is a graph showing the relative density of P atoms at the Si(001) surface after 5 ML Si encapsulation at RT and 255°C, respectively, and various annealing steps. The density relative to the initial coverage was determined from STM
25 images. The lines are to guide the eye.

Fig. 22(a) to (d) are a series of diagrams and STM images showing the process of saturating a silicon surface with phosphine, then annealing and encapsulating it by Si growth to fabricate a phosphorus δ -doped layer in silicon.

Fig. 23(a) is a schematic diagram of a phosphorus δ -doped silicon sample; (b)
30 shows the Hall bar structure used for Hall effect measurements; (c) shows the results of the Hall effect measurements; Fig. 23(d) shows the normalized magnetoresistance; and (e) the magneto-conductivities (measurement data and fit curves) as a function of normalized magnetic field of Si:P δ -doped layers for samples encapsulated at RT, 250 and 400 °C.

35 Fig. 24 is a graph showing the mass-31 depth profiles of δ -doped samples grown at RT, 250, 400 and 600°C, respectively, determined by SIMS using a 5.5 keV Cs^+

primary ion energy in an ATOMIKA system. The inset shows the high mass resolution CAMECA SIMS measurement.

Fig. 25 is a schematic illustrating the atomic-scale device fabrication process.

Fig. 26 is an SEM image and enlargement of a set of registration markers etched
5 into the Si(001) surface and the STM tip approached to the Si(001) surface

Fig. 27(a) to (d) illustrate the fabrication process of a $2 \times 2 \mu\text{m}^2$ phosphorus doped 2D device.

Fig. 28(a) shows an STM image of a hydrogen terminated Si(001) surface (dark
10 area) from which hydrogen was removed to form a 100 nm wide and 1 μm long wire with two contact regions on both ends (bright area). Fig. 28(b) is a schematic which shows a wire with two contact regions on both ends contacted by metal fingers.

Fig. 29(a) shows the Hall resistance versus the magnetic field of a $2 \times 2 \mu\text{m}^2$ phosphorus doped 2D device encapsulated with approx. 25 nm of epitaxially grown silicon measured at 4 K sample temperature. Fig. 29(b) shows the sheet resistance
15 versus the magnetic field of this sample.

Fig. 30 (a) shows the magnetoresistance of the $4 \times 4 \mu\text{m}^2$ square device and (b) of the $90 \times 900 \text{ nm}^2$ wire at 4 K and 50 mK. The dashed lines show fits to 2D weak localisation theory. Insets show schematics of the device geometrics.

20 Best Modes of the Invention

FABRICATION APPROACH

Referring first to Fig. 2, it outlines the individual processing steps for the fabrication strategy. A clean Si(100)2x1 surface is formed in an ultra-high-vacuum
25 (UHV) by heating to near the melting point. This surface has a 2x1 unit cell and consists of rows of σ -bonded Si dimers with the remaining dangling bond on each Si atom forming a weak π -bond with the other Si atom of the dimer of which it comprises.

Exposure of this surface to atomic H can break the weak Si π -bonds, allowing H atoms to bond to the Si dangling bonds. Under controlled conditions a monolayer of H
30 can be formed with one H atom bonded to each Si atom, satisfying the reactive dangling bonds, effectively passivating the surface; see Fig. 2(a).

An STM tip is then used to selectively desorb H atoms from the passivated surface by the application of appropriate voltages and tunnelling currents, forming a pattern in the H resist; see Fig. 2(b). In this way regions of bare, reactive Si atoms are
35 exposed, allowing the subsequent adsorption of reactive species directly to the Si surface.

Phosphine (PH_3) gas is introduced into the vacuum system via a controlled leak valve connected to a specially designed phosphine micro-dosing system. The phosphine molecule bonds strongly to the exposed $\text{Si}(100)2\times 1$ surface, through the holes in the hydrogen resist; see Fig. 2(c).

- 5 Subsequent heating of the STM patterned surface for crystal growth causes the dissociation of the phosphine molecules and results in the incorporation of P into the first layer of Si; see Fig. 2(d). It is therefore the exposure of an STM patterned H passivated surface to PH_3 that is used to produce the required P array.

The hydrogen may then be desorbed, as shown in Fig. 2(e), before overgrowing
10 with silicon at room temperature, as shown in Fig. 2(f). An alternative that has been discarded is to grow the silicon directly through the hydrogen layer, as shown in Fig. 2(g).

The next step is to rapidly anneal the surface, shown in Fig. 2(h).

- Silicon is then grown on the surface at elevated temperature, shown in Fig. 2(i).
15 A barrier is then grown as shown in Fig. 2(j). Finally conductive gates are aligned on the surface, as shown in Fig. 2(k).

There are a number of challenges to be met in this fabrication scheme. In all of the processes outlined above, introduction of charge and spin impurities is likely to be
20 fatal to the operation of the quantum computer. Preparation of large areas of defect free $\text{Si}(100)2\times 1$ on which to fabricate the P array is necessary. It is also essential to produce a complete coverage of the Si surface with H with controlled desorption so that PH_3 adsorbs only at the desired sites. A detailed description of how each of these challenges has been met is described below.

25

PREPARATION OF LOW DEFECT DENSITY SURFACE

The (100) surface is well characterised and is the most suitable surface for silicon growth, and as such was chosen as the most suitable candidate on which to attempt placement of an atomically precise phosphorus array for fabrication of the Kane
30 quantum computer.

The system used in this work is a three chamber Omicron UHV variable temperature (VT) STM multiprobe RM system. For the surface passivation stage an atomic hydrogen source is attached to the analysis chamber, consisting of a tungsten filament, water cooled heat shroud and leak valve. Phosphine gas is introduced to the
35 chamber via a UHV leak valve and double containment gas lines.

A separate chamber within the same vacuum environment houses a commercial silicon deposition cell. This instrument allows for surface preparation, placement of phosphorus arrays and subsequent silicon overgrowth all within the one UHV environment.

5 Silicon samples of $2 \times 10 \text{ mm}^2$ dimensions were cleaved from commercially available phosphorus doped *n*-type silicon wafers with resistivities of $1 - 10 \text{ } \Omega\text{cm}$ for use in Omicron direct heating STM sample holders. The sample surfaces were prepared under UHV conditions by following a standard thermal preparation procedure⁴ involving the following steps: (i) The samples were outgassed for 6 hours at $\sim 600^\circ\text{C}$ by
10 indirect heating using a resistive heating element mounted behind the sample holder and outgassed for 3 to 6 hours by direct current heating to a temperature below 600°C . (ii) The samples were flashed to $\sim 1200^\circ\text{C}$ for 30 to 60s by passing a DC current directly through the sample. This step removes the native oxide layer from the surface and allows the surface silicon atoms to become mobile. (iii) The sample temperature was
15 reduced to $\sim 950^\circ\text{C}$ and then cooled slowly from $\sim 950^\circ\text{C}$ to room temperature. It was found that the surface defect density was strongly dependent on the final cool down rate, as has been reported previously⁴. The sample temperature was monitored throughout this procedure using an infrared pyrometer. After the initial outgassing, the pressure in the vacuum chamber remains in the low 10^{10} mbar region or lower
20 (including during flashing to 1200°C).

Fig. 3(a) shows a typical STM image of a low defect density Si(100) 2×1 surface, prepared according to the above procedure. One monatomic step 31 is visible to create two flat (100) terrace regions 32 and 33. The upper terrace 32 is clearly visible, while the lower terrace 33 is hard to see, but it is possible to see that the dimer rows 34 in the
25 two terraces run at right angles to each other. Such steps exist because of a slight misorientation of the surface plane with respect to the (100) crystal direction. It is not possible to produce a completely defect free surface⁵, however, the defect density of the surface shown in Fig. 3(a) is approximately 1% which is consistent with the lowest defect density surfaces reported in the literature (eg., Ref.5). This image was acquired
30 with a negative sample bias and as such is a filled state image with individual dimers appearing as bean shaped protrusions 35 attributed to tunnelling from the π -bond of the dimer⁶.

Fig. 3(b) is a 3-Dimensional diagram of the structure of crystalline silicon.

HYDROGEN RESIST

The next stage of the fabrication procedure is to passivate the Si(100)2x1 surface with hydrogen. In order to do this we use an atomic hydrogen source (AHS). The AHS filament is heated to ~1500°C and a gas flow from a source of 99.999% pure molecular hydrogen is passed through the AHS via a leak valve into the UHV chamber. The AHS converts a significant fraction of the molecular hydrogen to atomic hydrogen, and the atomic hydrogen then reacts with the sample surface, forming the passivation layer. The dose rate is controlled by monitoring the total pressure in the UHV chamber. The purity of the gas being introduced to the chamber is monitored using a mass spectrometer.

Due to the very weak nature of the silicon dimer π bond, the Si(100)2x1 surface is very reactive. Hydrogen atoms impinging onto the Si(100)2x1 surface break the weak dimer π bond⁷, creating two reactive surface sites where hydrogen atoms may adsorb. A dimer with only one H atom adsorbed is called a hemihydride dimer. The silicon atom of the dimer that is not hydrogen terminated is left with a dangling bond where a second hydrogen atom may adsorb. A silicon dimer that has been completely passivated with two hydrogen atoms is called a monohydride dimer.

Several experiments were performed to determine the optimal hydrogen dosing conditions to obtain a uniform monohydride layer. Fig. 4(a) is an STM image of a passivated surface 41 where we have dosed the sample to a chamber pressure of 10⁻⁷ mbar for half an hour with sample temperatures in the range of 300 - 400°C. During dosing the sample surface was positioned directly in front of the AHS UHV inlet at a distance of ~ 10 cm. The result is an almost uniform monohydride 42 layer but having dihydride 43 and the combination 44 of these two phases, known as the H:(3x1) phase. In addition there are dimers missing at the surface at 45.

The monohydride 42 structure is shown in Fig. 4(b), and has both silicon atoms of the dimer terminated with hydrogen.

The dihydride 43 structure is shown in Fig. 4(c), and has each silicon atom bonded to two hydrogen atoms. In Fig. 4(a) this feature has the appearance of a dark spot.

Fig. 4 (d) shows the structure of the combination of these two phases 44, which are identified on the surface.

Fig. 4 demonstrates that we are able to controllably dose the Si(100) surface with hydrogen and identify the resultant surface species. However, to further demonstrate our ability to characterise the clean and hydrided surfaces we have performed a number of scanning tunnelling spectroscopy (STS) experiments⁸. We held

the STM tip at a fixed location and distance from the surface (by disengaging the STM tip feedback mechanism) and ramped the tip bias through -2 V to 2 V, while measuring the tunnel current. Fig. 4(e) shows the results of these STS experiments for both the clean (Fig. 3(a)) and hydrogen terminated (Fig.4(a)) surfaces. The clean surface spectroscopy shows both the π bonding and π^* antibonding peaks. The spectroscopy for the hydrogen terminated surface shows a broad shoulder associated with the silicon bulk density of states and a pronounced Si-H antibonding peak. Both of these results are in agreement with previous studies⁹.

10 HYDROGEN LITHOGRAPHY AND PHOSPHORUS ARRAY

Following the formation of a monolayer of H on the Si surface the next step is to selectively desorb regions in the H resist using the STM tip. This will expose areas of the Si surface for the controlled placement of P atoms.

Achieving atomic resolution desorption places stringent requirements on the STM tip. Controlled desorption can be achieved by applying a large bias to the STM tip, however, it is also possible to desorb hydrogen whilst imaging, thereby exposing regions of the surface unintentionally. We demonstrate that we have overcome this obstacle to controllably and repeatedly desorb H in an array suitable for the fabrication of the Kane quantum computer.

In order to achieve atomic resolution desorption⁶ a very sharp tungsten tip with a large cone angle is required¹⁰. In order to meet these requirements we have used a commercial tip etching device (Omicron W-Tek Semi-Automatic Tip Etching system). A length of W wire (diameter=0.38 mm) is inserted ~ 2 mm into a NaOH solution at the centre of a stainless steel cathode ring. Application of ~5-10 V between electrodes generates an electro-chemical reaction which proceeds preferentially at the surface of the solution. Within ~ 10 min the wire is etched completely through leaving a small radius tip. A 2 min etch in hydrofluoric acid removes any oxide layer. The tip is inspected under an optical microscope to assess the geometry and, if satisfactory, loaded into the UHV system within 30 min to prevent formation of oxide. Other tip materials can be used such as PtIr and will be subject to similar preparation considerations.

An STM tip is used to desorb hydrogen from the surface by application of a controlled voltage pulse between the tip and sample. Careful optimisation of the geometry of the tungsten tip and controlled voltage pulses (sample bias ~6 V and tunnelling current ~1 nA for ~1 ms) makes atomic resolution desorption possible. It is

necessary to desorb an area with the correct phosphine dose so that one phosphine molecule and therefore only one phosphorus atom can bond in this area.

Fig. 5(a) is an STM image showing two desorption sites along a silicon dimer row (before phosphine dosing). The bright circles 51 in the image are two dangling bonds arranged along a dimer row. The desorption sites appear as bright protrusions as a result of the extension of electron density out of the surface due to the silicon dimer surface states of the exposed silicon dangling bonds. The remaining hydrogen on each silicon dimer is known to be transient¹² and we have observed it diffusing from one side of the dimer to the other with time.

10 The next step is to fabricate the P arrays. Following STM lithography to expose small regions of the Si(100)2x1 surface phosphine gas is permitted into the chamber by a controlled leak valve such that individual phosphorus bearing molecules are adsorbed onto the exposed silicon surface.

In order to obtain high purity phosphine gas delivery, the PH₃ micro-dosing 15 system and its connections to the UHV STM employed internally electro-polished gas lines assembled in a clean-room environment. Mass spectra taken in the chamber during the exposure at a pressure of 10⁻⁸ mbar reveal no significant increase in the partial pressure of any other species. The sticking coefficient of phosphine on the clean silicon surface is 1¹³.

20

Fig. 5(b) is an STM image of phosphine molecules being adsorbed at the two dangling bond sites exposed (Fig. 5(a)) with one molecule adsorbed per dangling bond. Fig. 5(c) is a line profile across the dimer rows of Fig. 5(a) through one of the dangling bonds and shows the typical 0.12 nm height. Fig. 5(d) shows a line profile through one 25 of the adsorbed phosphine molecules with a typical height of 0.17 nm.

Fig. 6(a) to (d) show equivalent images to Fig. 5 (a) to (d) but for three dangling bond sites perpendicular to the dimer row direction.

The STM images in Figs. 5(a) and 6(a), with such a close spacing between sites, highlight the atomic resolution desorption achieved. The distance between sites can 30 easily be increased to the required qubit spacing of 20 nm, and we have performed controlled lithography of single desorption sites in a line >100 nm in length. The images demonstrate that these desorption sites are sufficient to allow only one phosphine molecule to bond to the surface at each site.

All images were acquired at a sample bias of -1.8 V and tunnelling current of 35 0.4 nA.

Figs. 5(d) and 6(d) show the same area as Figs. 5(a) and 6(a) after exposure to phosphine gas at room temperature.

The effectiveness of the hydrogen resist as a barrier to phosphine adsorption is demonstrated by the uniform hydrogen coverage after phosphine dosing except at the previously desorbed hydrogen sites. In order to observe any changes after phosphine exposure we have specifically chosen single hydrogen desorption sites, rather than larger desorption sites and present high resolution images where the spacing between sites is very small.

Analysis of the line profiles in Figs. 5(f) and 6(f) show a characteristic increase of ~ 0.05 nm in the height of the protrusion after phosphine dosing. Such a difference can frequently occur due to minor changes in imaging conditions between scans, which results in the STM tip extending further into the gap between dimer rows. However the height difference due to PH_3 adsorption is measured from the top of the dimer rows to the top of the protrusion and is not therefore affected by this.

The ~ 0.05 nm height increases in the line profiles, observed at all adsorption sites over several images, was calibrated against an atomic step edge on the same surface (not shown) both before and after phosphine dosing. This reproducible increase confirms the adsorption of a PH_3 molecule and corresponds to the difference between the exposed silicon dangling bond and the adsorbed phosphine. The transient nature of the hydrogen atom on the silicon dimer can account for the asymmetry of the final image where one phosphine molecule has bonded to the left silicon atom in the dimer (upper) and another phosphine molecule has bonded to the right silicon in the dimer (lower).

Studies of the interaction of phosphine with clean $\text{Si}(100)2\times 1$ surface^{11, 14, 15} suggest that PH_3 molecularly adsorbs to one end of a silicon dimer and can then dissociate to PH_2 provided silicon dangling bonds are available nearby for the re-adsorption of the dissociated H. The absence of available dangling bond sites on the hydrogen-terminated surface can inhibit this dissociation step. A similar dissociative process and Si-XH_2 configuration is understood to occur in the adsorption of NH_3 ¹⁶ and AsH_3 ¹⁷ on the $\text{Si}(100)2\times 1$ surface, where both nitrogen and arsenic are isoelectronic with phosphorus.

The above results are important since for the first time we have demonstrated the effectiveness of the hydrogen resist as a barrier to phosphine adsorption and used this technique for the controlled placement of single phosphorus bearing molecules on a silicon surface – a central step in the construction of a silicon based quantum computer. This process, shown for closely-spaced controlled doping, demonstrates the

achievability of more widely-spaced (~ 20 nm), precisely positioned phosphorus qubit arrays over large areas. This fabrication process is also applicable to the production of other micro- or nanoelectronic devices that could utilise ordered atom or dopant arrays.

5 DETECTION OF PH_x ON THE $\text{Si}(100)$ SURFACE

In order to understand the incorporation of phosphorus atoms from phosphine gas into the silicon $(100)2\times 1$ it is first necessary to be able to identify phosphorus related species on a silicon surface and distinguish these from other features on the surface, including $\text{Si}(100)$ surface defects. Fig. 7(a) is an STM image of a silicon (100) surface showing a number of defects. The defects, which occur in several forms, are seen as dark features on the dimer rows and four such defects are characterised with filled and empty state imaging in Fig. 7(b) to (e). The fact that the defects (and any other feature on the surface) have a characteristic appearance in both filled and empty state images means that we can obtain a characteristic 'fingerprint' for each feature and thus distinguish one feature from another.

The images in Fig. 7b to 7e are filled and empty state images of the following defects: (b) missing dimer defect, (c) multiple missing dimer defect, (d) C-defect, and (e) split-off dimer defect.

All images were obtained using a tunnelling current of 0.1 nA. The bias voltages used were (b) -1.8 V, (c) $+1.6$ V, (d) -1.8 V, (e) $+1.2$ V, (f) -1.8 V, (g) $+1.2$ V, (h) -1.3 V, (i) $+1.2$ V.

Fig. 8 shows a $25 \times 25 \text{ nm}^2$ area of a $\text{Si}(100)$ surface (a) before and (b) after the surface is exposed to a low dose of phosphine. Before dosing (Fig. 8(a)) there are a few defects on the surface. One such multiple missing dimer vacancy which is circled and labelled 81 is present after dosing. However, generally after dosing (Fig. 8(b)) it can be seen that most of the defects have changed in appearance and that the number of features on the surface has increased significantly. For instance a bright protrusion 82 has appeared. Such changes to the appearance of the surface result from the adsorption of PH_3 molecules and from species formed from the partial dissociation of PH_3 .

The imaging conditions were (a) -1.6 V, 0.2 nA and (b) -1.6 V, 0.2 nA.

Fig 9(a) shows a filled state STM image of a $50 \times 50 \text{ nm}^2$ area of a $\text{Si}(100)$ surface dosed with a low dose of PH_3 . There are several features seen in the image that are not seen in images of the clean $\text{Si}(100)$ surface. In order to characterise the adsorption species formed after PH_3 dosing we have performed high-resolution filled

and empty state imaging of a PH_3 dosed surface. Studying the characteristic appearance of each of the features in filled and empty state images, and the apparent height of the features in the filled state images (see Figs. 9(b) to (e)) we find that there are four new species. (b) and (c) are phosphorus containing molecules (PH_x where $x=2,3$); (d) is a hemihydride i.e. a silicon dimer with one dangling bond saturated with a hydrogen atom and the other dangling bond unreacted. Figures 9 (biv), (ciii), (diii) and (eiii) show the features in empty state images. Figures 9 (bii), (cii), (dii) and (eii) show height profiles of the features in filled state images discussed above.

All images were obtained using a tunnelling current of 0.1 nA. The filled (empty) state images were obtained with using a bias of -1.8 V ($+1.2$ V).

INCORPORATION OF P INTO THE SURFACE – FIG. 2(d)

Fig. 10(a) shows a $\text{Si}(100)2\times 1$ surface dosed with a low dose of phosphine, it is similar to Fig 9(a). Fig. 10(b) shows the surface after subsequent annealing to 350°C , Fig. 10(c) after annealing to 475°C and Fig. 10(d) after annealing to 700°C .

After phosphine dosing, the features imaged on the surface in Fig. 10(a) are those described in Fig. 9(a).

After the 350°C anneal the bright spots known to be phosphine molecules are gone. Large bright lines 101 perpendicular to the dimer rows were investigated by taking the filled state and empty state images shown in Fig. 10(e) and (f) which revealed them to be 1-dimensional silicon dimer chains. The chains are made up from Si atoms that are ejected from the surface when P atoms are incorporated into the silicon to form Si-P heterodimers. The images in (e) and (f) were obtained using sample biases of -1.6 V and $+1.6$ V respectively.

Dark bars 102, more easily seen in the enlargement of Fig. 10(g), are monohydrides, and their structure is illustrated in Fig. 10(h).

Zigzag patterns 103, again more easily seen in the enlargement of Fig. 10(g), are the Si-P heterodimers, and their structure is illustrated in Fig. 10(i).

After annealing to 475°C the silicon chains 101 have disappeared and after annealing to 700°C the monohydrides 102 and Si-P heterodimers 103 are no longer present on the surface.

The images in Fig. 10 provide detailed analysis of what reactions are occurring at the silicon surface as a function of temperature. At room temperature phosphine adsorbs onto the surface as PH_3 , most of which quickly dissociates to form PH_2 and H. Heating this surface to 350°C sees dissociation of the PH_x ($x = 2-3$) to form a P-Si heterodimers, involving the incorporation of P atoms into the surface layer and the

ejection of Si from the surface layer onto the surface to form 1-dimensional Si chains. The dissociation of PH_x also results in the adsorption of H onto the surface in the monohydride phase. When the surface is heated to 475°C the Si atoms in the 1-dimensional chains are supplied with enough energy to diffuse to step edges so the chains disappear from the surface. Once the surface temperature has been raised to 700°C the monohydrides and the P atoms have desorbed from the surface, as H_2 and P_2 , respectively.

A clear demonstration of the fact that it is possible to incorporate P into the top layer of a clean Si(100) surface is provided in Fig. 11. The diagram of Fig. 11(a) explains what is shown in the filled state STM image of Fig. 11(b), namely, a pair of P containing molecules after adsorption onto the bare Si(100) surface. This is confirmed by the line profile of Fig. 11(c).

By contrast, the diagram of Fig. 11(d) explains what is shown in Fig. 11(e), namely that a pair of P atoms have been incorporated into the surface as a result of annealing a phosphine dosed surface to 400°C . The line profile of Fig. 11(f), when compared to Fig. 11(c) show that there is a characteristic height difference of ~ 0.06 nm between the non-incorporated and incorporated P, with the former extending higher above the surface plane. The reason for this height difference is apparent from the schematic models in Figs 11(a) and (b), which show the P coordination geometry for the two cases.

Fig. 12(a) is an STM image of a surface that has been given a low dose of phosphine and heated to 350°C , and shows the same features as Fig. 10(b). Fig. 12(b) is a similar image but the dosing was for six times as long. As a result the silicon chains are much longer and more numerous, confirming that the ejected chains are related to the presence of P incorporated on the surface.

In order to confirm that P remains in the region of the surface after annealing we use a chemically specific technique, Auger electron spectroscopy (AES), to analyse the P dosed surface. The characteristic phosphorus AES peak at 120 eV was monitored for a succession of doses until the peak intensity became saturated, as shown at 122 in Fig. 12(c). The surface was then annealed to 590°C , which is approximately the upper limit of the temperature range used for P incorporation, and another AES spectra was taken, 123 as shown in Fig. 12(c). Although, the intensity of the P 120 eV peak has decreased by $\sim 40\%$, possibly due to some desorption of physisorbed PH_3 , its intensity is high enough to conclude that there is a significant amount of P in the region of the surface.

INCORPORATION OF P INTO A LITHOGRAPHICALLY DEFINED REGION

Fig. 13 shows STM-based lithography using an H-passivation layer on Si(100) as a resist for spatially controlled adsorption of phosphine. Desorbing H with the tip of an STM results in the formation of a $\sim 200 \times 50 \text{ nm}^2$ "patch 131 and two $\sim 100 \text{ nm}$ long lines 132 and 133 of bare Si on the H-passivated surface, as shown in Fig. 13(a).

After dosing the surface with phosphine and annealing to $\sim 375^\circ\text{C}$, the incorporation of P atoms into the surface, within the desorption patch, can be inferred from the appearance of silicon dimer chains 134, see Fig. 13(b). However the H-termination of the surrounding surface has not been effected by the phosphine exposure.

High resolution images of the dosed and annealed patch, shown in Fig. 13(c) and (d) are filled and empty state images, respectively, of the area indicated by the box in (b). In the empty state image, the ejected Si-Si dimer chains show splitting characteristic of Si-Si dimers.

Fig. 14 demonstrates the incorporation of P dopant atoms along a lithographic line. Fig. 14(a) shows a $\sim 1 \text{ nm}$ wide line 141 of bare Si fabricated in a H-terminated Si(100) surface. Exposure to 0.3 Langmuirs of phosphine gas produces adsorption of PH_x species and H, see Fig. 14 (b). After annealing to $\sim 375^\circ\text{C}$ there is full dissociation of the PH_x species. This produces further H adsorption and incorporation of P and ejection of Si. Some of the H repassivates the silicon surface to cause it to look darker in Fig. 14(c). Fig. 14 (d) and (e) show filled and empty state images, respectively, of the phosphine dosed and annealed line, and they confirm the appearance of a silicon dimer chain 142 in the region of the line. The characteristic splitting of the substrate H-terminated dimer rows is observed in the empty state image. Several single dangling bonds 144 appear as single bright protrusions in both filled and empty state images, as do several dangling bond pairs 145 which are due to bare Si-Si dimers on the surface.

The single ejected dimer chain 142 is visible near the centre of the images. This chain is identified by the fact that it is oriented perpendicular to the substrate dimer rows and also that it splits into pairs of protrusions in the empty state. Unlike the bare silicon dimer chains seen in Fig. 13, this dimer chain is hydrogen terminated, as is evidenced by the fact that the intensity of the chain is comparable to the surrounding dangling bonds – a bare Si-Si dimer chain would be much brighter than the dangling bonds on the surface. The H to produce this termination comes from the dissociation of PH_3 molecules. Fig. 14(f) shows a high-resolution filled state image of the dosed and

annealed line that has been contrast enhanced to highlight features of the surface that are otherwise overshadowed by the very bright dangling bonds of the surface. The arrows point to P-Si-H heterodimers, several of which have been formed along the length of the lithographic line.

5 In Fig. 14(h) a line profile, obtained from between X and X' in Fig. 14(g), is displayed, along with a diagram of the part of the surface through which the line profile was obtained. The highest peak in the line profile results from the presence of a P-Si-H heterodimer. The above results show that we are able to incorporate P dopant atoms into the Si(100) surface with sub-nanometre accuracy at spatial locations defined using
10 an STM.

THERMAL HYDROGEN DESORPTION - FIG 2a(e)

Figures 14A, 14B, 14BA, 14BB, 14C and 14D are all concerned with removing the hydrogen resist layer from the silicon surface before encapsulation with epitaxial
15 silicon. Studies undertaken by us have confirmed that whilst it is possible to grow epitaxial silicon through the hydrogen resist, the quality of the silicon crystal grown is significantly degraded as compared with removing the resist completely before growth¹⁸. To this end a series of experiments have been conducted to remove the resist layer.

20

In the first experiment a silicon (100) surface is terminated with atomic hydrogen to form a monohydride-terminated surface. This surface was then subjected to several different thermal anneals to determine the appropriate temperature required to remove the hydrogen resist layer effectively. Each surface shown in Figure 14A (a-d)
25 was initially hydrogen terminated to a complete coverage of 1ML.

Figure 14A(a) shows an filled state STM image of hydrogen terminated surface following annealing to 500°C for 10 seconds. The resulting surface is very rough as a result of the incomplete removal of the hydrogen resist. The many bright protrusions on this surface are silicon dangling bonds where hydrogen has been removed from these
30 silicon dimers. The greater proportion of the surface is still terminated with hydrogen and appears darker. The significant amount of hydrogen remaining on the surface after this treatment makes this surface unfavourable for epitaxial silicon growth.

Figure 14A(b) shows a section of the hydrogen terminated surface following heating to a slightly higher temperature of 530°C for 10 seconds. The nine bright
35 'zigzag' features are hemi-hydride or singly hydrogen occupied silicon dimers which still remain on the surface. The remaining dark features are dimer vacancies. The

density of hydrogen on this surface is $<0.1\%$ and is low enough that epitaxial growth will not be affected on this surface.

Figure 14A(c) shows a section of the hydrogen terminated surface following an even higher anneal of 560°C for 10 seconds. This surface exhibits 5 bright hemi-hydride features indicating that there is still some hydrogen on the surface. However there is a considerable increase in the dark features (dimer vacancies). These vacancies align together indicating significant rearrangement of the surface. This rearrangement is detrimental to the stability of lithographically placed dopant arrays such as those fabricated for the quantum computer. As a result we can conclude that this anneal temperature is too high.

The optimal anneal temperature seems to be $\sim 530^{\circ}\text{C}$ when using a single anneal to desorb the hydrogen. In order to minimise the amount of thermal energy needed to remove the hydrogen we repeated this experiment in Figure 14A(d) but not only annealing for 5 seconds rather than 10. This surface shows the same characteristics as the surface in Figure 14A(b) (i.e. a small number of hemi-hydride features and no aligned defects) indicating that the shorter heating time removes the hydrogen as effectively with a smaller thermal budget.

In order to determine the stability of lithographically placed dopant arrays to these heating conditions a monohydride surface was lithographically patterned with an STM tip as outlined in HYDROGEN LITHOGRAPHY AND THE PHOSPHORUS ARRAY.

The lithographically defined regions onto which the phosphine is deposited can be seen in Figure 14B(a). The structure is a castellation pattern in the upper part of the image and four $\sim 5\text{nm}$ points in the lower left of the image. The bright protrusions over the rest of the surface are silicon dangling bonds which have been inadvertently exposed by the STM lithography. This surface is then dosed with phosphine for three minutes at a pressure of 1×10^{-9} mbar and heated to 350°C for 10 seconds to incorporate the phosphorus into the surface silicon monolayer. The resulting surface is heated to 530°C for 5 seconds to remove the hydrogen as in figure 14A(b).

Figure 14B(b) shows the remnants of the dopant pattern after the 5 second 530°C step. Some parts of the upper castellation pattern are seen but more importantly two of the point structures in the lower part of Figure 14B(a) have survived.

Figure 14B(c) shows a high resolution image of one of the points in Figure 14B(b) exhibiting most importantly a bright protrusion perpendicular to the dimer rows. This is characteristic of silicon ejected by the phosphorus incorporation process.

The identification of ejected silicon localised in regions defined by STM lithography, demonstrates that the phosphorus which has been incorporated at controlled locations remains in the same location after hydrogen is removed using thermal processing of 530°C for 5 seconds.

- 5 The results of a detailed high resolution STM study of the thermal desorption of hydrogen from the Si(001)2×1 surface using successive anneals are shown in Fig. 14BA.

All experiments were performed in an ultra-high vacuum system. Sample preparation, hydrogen termination and phosphine dosing have been described above.
10 Hydrogen was desorbed by passing a current directly through the sample and cooling to room temperature at a rate of $\sim 2^{\circ}\text{C.s}^{-1}$. The substrate temperature was determined with an infrared pyrometer giving an accuracy of $\pm 30^{\circ}\text{C}$.

Fig. 14BA (a)-(f) shows high resolution STM images of a hydrogen terminated Si(001) 2×1 surface (a) before and (b-f) after a succession of 10 s anneals at 374, 426, 15 470, 529 and 581°C. Fig. 1 (a) shows an STM image of a nearly perfect Si(001):H terminated surface where each silicon atom of a dimer bonds to one hydrogen atom, resulting in 1 ML hydrogen coverage. The bright protrusions in the top left of the image, are single and double dangling bonds (labelled S and D respectively) that result from an incomplete termination of the surface on the upper terrace. Also visible on the 20 surface are a C-type defect (labelled C) and two double-dihydride dimers (labelled DH) in which two hydrogen atoms bond to each Si dimer atom. A monohydride terminated surface with such a low density of dangling bonds provides an ideal resist layer for STM lithography experiments.

Fig. 14BA (b) shows the H terminated surface after a 10 s anneal to 374°C 25 during which the density of both single and double dangling bonds has increased. Whilst some single dangling bonds have rearranged to form dangling bond pairs during this anneal, the limited hydrogen mobility at this temperature, combined with the short anneal time has meant that not all single dangling bonds have paired up. Hence, both single and double dangling bonds still appear on the surface.

30 Fig. 14BA (c) shows the same surface after a further 10 s anneal at 426°C. Here the surface is dominated by bare silicon, rather than monohydride, and as a result, the monohydride terminated Si dimers appear dark against the brighter non-terminated Si(001). This change in the surface appearance adds a complication to the interpretation of the STM images since dimer vacancies (DVs) also appear as darkened dimer-sized 35 patches in filled state STM images, similar to the monohydride terminated dimers. We estimate the defect density from interpolating the DV density observed in filled state

imaging before (Fig. 14BA (b)) and after (Fig 14BA (d)), the 426°C anneal. From this comparison we can determine that there was no significant increase in DV density during the annealing process and that the hydrogen coverage in Fig. 14BA (c) is approximately 25%.

5 Fig. 14BA (d) shows the same surface after a further 10 s anneal at 470°C. A few final H atoms of the resist layer still remain on the surface but now in the form of hemihydrides (where a single isolated H atom bonds to one atom of a Si dimer). At this coverage the probability for one hemihydride (labelled HH) to desorb as H₂ by finding
10 another hemihydride as it diffuses across the surface becomes diminishingly small. We can conclude that at this anneal temperature the resist layer has been effectively removed since the presence of such small coverages of H are not expected to significantly degrade subsequent epitaxial Si overgrowth. We also note the presence of a few C-type defects and DV defects. Whilst the number of C-type defects has remained unchanged the density of DV defects is slightly higher than for the initial
15 clean surface. There may be two reasons for this increase. Firstly, Si etching can occur during annealing if there are dihydrides on the surface. However, the density of dihydrides seen in Fig. 14BA (a) is very low and the amount of etching that would be expected to occur would therefore be small. Secondly, dimer vacancies are known to be generated during annealing of a Si surface. This means that any further annealing will
20 also serve to further increase the DV defect density as seen in Fig. 14BA (e) and (f).

Fig. 14BA (e) shows the surface after a further anneal to 529°C for 10 s. Here the number of hemi-hydrides has been further reduced whilst the number of C-defects remains approximately the same as in Fig. 14BA (d). However, as expected the density of dimer vacancies has increased significantly as a result of the continued annealing. At
25 these temperatures many of the DV defects have rearranged from a random distribution to align perpendicular to the dimer rows. This DV alignment occurs only after the hydrogen has been desorbed implying that hydrogen inhibits the migration of dimer vacancies on the surface in the same way that it inhibits silicon dimer migration. The formation of aligned DV defects called dimer vacancy rows (DVR) is energetically
30 favorable at temperatures above ~500°C, at which DVs become mobile. The density of DVRs increases after another anneal at 581°C for 10 s shown in Fig. 14BA (f). Subsequent annealing at even higher temperatures (not shown) leads to more pronounced DVRs but no significant morphological changes.

Having studied the desorption of a H resist layer from a Si(001) surface in detail
35 using successive anneals we find that there is a temperature range of $470 \pm 30^\circ\text{C}$ within which the H resist can be removed effectively from the surface with minimal defect

generation. The optimal anneal temperature is slightly lower compared to the previous study shown in Fig. 14A where single shot anneals were used to desorb the hydrogen. This is due to the fact that during successive anneals hydrogen is partially desorbed even below the hydrogen desorption temperature thus decreasing the temperature
 5 necessary to completely remove the hydrogen. We now address the important question whether a phosphorus doped nanostructure patterned into the H resist layer survives intact during a thermal anneal to remove the resist.

Figure 14BB (a) shows a hydrogen terminated surface where a $200 \times 25 \text{ nm}^2$ patch of hydrogen has been removed using the STM tip. The H resist appears darker
 10 because of the higher density of surface states associated with unterminated surface. A low density of single and double dangling bonds is observed around the lithographic region arising from an incomplete hydrogen termination. The surface is then exposed to 0.135 L of PH_3 gas which is adsorbed only in the patch region. Subsequent annealing to 350°C for $\sim 1 \text{ s}$ causes the phosphine to dissociate and the phosphorus to incorporate
 15 into the nanostructured region of the surface.

The region of incorporated phosphorus atoms can be seen in Fig. 14BB (b). This STM image shows a slight increase in dangling bond density on the hydrogen terminated surface after the 350°C anneal due to a small amount of hydrogen desorption.

20 An anneal to 470°C for 10 s is now applied to remove the hydrogen resist from the doped nanostructure. Fig. 14BB (c) shows that almost all of the hydrogen has been removed from the surface with some DV defect generation. Importantly, the boundary between the phosphorus doped region and the surrounding silicon surface is sharp as indicated by the presence of bright elongated features in the phosphorus doped region.
 25 These features are chains of silicon atoms ejected during the P incorporation process. The sharp boundary arises since the ejected silicon is mobile during the anneal and diffuses to the edge of the lithographic region. Further diffusion of the silicon atoms appears to be inhibited by the hydrogen resist as it desorbs. It can be seen that silicon accumulates at the boundary of the phosphorus doped region nucleating small silicon
 30 islands. A closer inspection of individual features in the STM images of the nanostructure reveals that, within our detection accuracy, no phosphorus has diffused out of the nanostructured region. The fact that a 470°C anneal does not result in diffusion has also been independently confirmed by electrical measurements from an STM patterned nanostructure device in which a 10 s, 470°C hydrogen desorption
 35 anneal was used for a P doped nanostructure of width 90 nm (see Fig. 30). The surface in Fig. 14BB (c) also shows an increased defect density with significant DV ordering

close to the P doped region. Such ordered defects are not seen away from the nanostructured region. We attribute the formation of DVRs to the relief of surface strain caused by the localized high phosphorus density in the nanostructure. The surface in Fig. 14BB (c) shows almost complete removal of the H resist while the phosphorus dopant structure remains in place. This surface provides an ideal starting point for epitaxial Si growth to encapsulate the phosphorus doped nanostructure.

STM TIP INDUCED HYDROGEN DESORPTION

Using the STM tip for hydrogen removal for the lithography process can also be applied to completely removing the resist after phosphine dosing and incorporation.

Figure 14C shows a 1ML monohydride terminated surface was subjected to repeated passes in a raster pattern of the STM tip under conditions of +4V sample bias, 3nA constant current to almost completely desorb hydrogen from the surface. The top of Figure 14C shows a portion of the surface which is still hydrogen terminated. This region has many random dangling bonds due to the high bias and current used to desorb the patch. The exposed silicon surface shows a small amount of remnant hydrogen in the form of monohydride and hemi-hydride dimers but is otherwise undamaged by the desorption process. This means that hydrogen can be removed in large areas using the STM tip leaving behind a suitable surface for subsequent epitaxial silicon growth.

To demonstrate the effectiveness of this technique for removing the hydrogen whilst maintaining the integrity of the lithographically incorporated phosphorus atoms we highlight the experiment performed in Figure 14D. Figure 14D(a) shows two bright features on a hydrogen terminated silicon surface corresponding to two dangling bonds that have been exposed by STM lithography. The surface is then phosphine dosed and annealed to incorporate P atoms into the top layer of the silicon surface before an STM tip is then used to remove the hydrogen resist completely.

Figure 14D(b) shows the same surface after the hydrogen has been almost completely removed from this region of the surface using the STM tip with +4V, 3nA tunnelling conditions. The two bright protrusions are clearly observed at the surface corresponding to the two incorporated phosphorus atoms, which are seen to be in the same locations as the dangling bonds prior to phosphorus dosing in Figure 14D(a). Other dark features in the image are thought to be hemi-hydride features resulting from incomplete desorption of hydrogen. This result clearly demonstrates that the hydrogen resist can be almost completely removed from the surface using the STM tip whilst maintaining the integrity of the carefully created STM patterned array of P atoms in silicon.

ENCAPSULATION OF INCORPORATED P BY HIGH PURITY SILICON

Figures 15 to 24 are all concerned with the silicon encapsulation process, and in particular the best way to achieve an atomically smooth layer so that we can image the buried Si-P heterodimers and ensure that they do not move out of their arrays.

GROWING SILICON – FIG. 2(f) and (g)

Fig. 15 illustrates two approaches to the growth of silicon with no P present. Fig. 15(a) to (d) are concerned with encapsulation at room temperature and elevated temperatures. Figs. 15(e) to (h) are concerned with encapsulation at room temperature and subsequent annealing. Fig. 15(i) to (k) show schematics which illustrate the temperature dependent epitaxial growth modes of silicon.

Fig. 15(a) shows silicon epitaxial layers with a thickness of about 12 monolayers on a Si(100)2x1 substrate deposited at room temperature. The mobility of silicon adatoms on the surface is strongly restricted by the low substrate temperature. Thus, the silicon adatoms stick on the surface close to the place where they were deposited from the gas phase and 3D Si islands form. This process is explained in the diagram of Fig. 15(k), where the random growth can be seen to result in a high surface roughness.

With increasing substrate temperature, the mobility of the Si adatoms on the surface increases and elongated Si islands grow. Depending on the substrate temperature several layers grow simultaneously:

At 220°C, shown in Fig. 15(b), three layers grow at one time, and the mechanism is explained in Fig. 15(j).

At 420°C, shown in Fig. 15(c), only two layers grow at one time.

At higher substrate temperatures, such as 590°C shown in Fig. 15(d), Si grows in the step-flow growth mode, and the mechanism is explained in Fig. 15(i). Here the mobility of Si adatoms is high enough to diffuse on the terraces and to reach the step edges where they incorporate into the crystal. The result is a smooth crystalline surface in much the same way as a reconstructed Si(100)2x1 surface after sample flashing.

Figs. 15(e) to (h) show an alternative encapsulation procedure. Fig. 15(e) is the same as Fig. 15(a). However, Fig. 15(f) and (g) show the effect of annealing at 335 °C for 1 minute and additional 9 min, and Fig. 15(h) shows the effect of subsequent annealing at 660 °C for 1 minute.

Overall, surface roughness and defect density can be seen to decrease with increasing annealing temperature and time. Thus, the structural quality of the epitaxial Si layer increases with increasing growth or annealing temperature. The STM images in

Fig. 15 show that similar surface morphologies are achieved with the two different approaches.

Figure 16 shows the results of a more detailed study where five monolayers of silicon are grown at 250°C and then annealed at different temperatures and times.

Fig. 16(a) is a schematic and Fig. 16(e) shows the corresponding filled state STM image of the Si(100) surface before any silicon growth.

Fig. 16(b) is a schematic and Fig. 16(f) is the corresponding filled state STM image of the Si(100) surface after Si growth of 5 monolayers (ML) at 250°C. At a substrate temperature of 250 °C, silicon grows in the layer-by-layer growth mode.

The remaining images in Fig. 16 show the results after various annealing steps. The rough surface structure is still clearly visible after annealing at 328 °C. Annealing at 363 °C and 407 °C leads to the formation of a terrace structure similar to the structure of the clean Si surface. However, the terraces contain small Si islands, vacancy areas, and antiphase domain boundaries. The surface also displays a high density of missing dimer defects. After additional annealing at 456 °C and 490 °C mobile single missing dimers formed multiple missing dimer defects. Further annealing at 548 °C and 605 °C recovers the initial terrace structure of the Si(100) surface without Si islands or holes, however, the density of missing dimer defects is significantly higher than on the initial clean Si surface after flashing. The image size of the STM images is $50 \times 50 \text{ nm}^2$.

Fig. 17 shows the results of a similar study, but where the silicon surface has been passivated by hydrogen prior to silicon growth.

Fig. 17(a) is a schematic and Fig. 17(e) the corresponding filled state STM image of a clean Si(100) surface.

Fig. 17(f) is a filled state STM image of a hydrogen terminated Si(100) surface. The monohydride terminated surface shows a low density of Si dangling bonds which appear as bright protrusions in the STM image.

Fig. 17(b) is a schematic and Fig. 17(g) the corresponding filled state STM image of the sample surface after Si growth of 5 ML at 250 °C on the hydrogen terminated surface. As diffusion of Si atoms on the hydrogen terminated surface is largely suppressed by the presence of hydrogen, silicon grows in island growth mode as opposed to layer-by-layer growth on a clean Si(100) surface at 250 °C.

Figs. 17(c) and (d) are schematic and the remainder of Fig. 17 are filled state STM images of the surface after various annealing steps. The 'island' structure remains even after annealing at 315, 345, 350, and 400 °C.

Further annealing at 401 °C for 55 s, however, changes the surface morphology.

5 The islands flatten and have an elongated dimer row structure. The dimer rows exhibit dark areas similar to single missing dimer defects. These dark features appear to be monohydrides which are still adsorbed on the Si surface. After the next annealing step at 456 °C for 5 s, the surface displays a lower density of the dark features indicating that hydrogen desorption occurs during annealing. The reduced density of hydrogen at

10 the surface allows for a higher Si diffusivity and, thus, for a change of the surface morphology. After annealing for 5 s at 508 °C Si atoms have rearranged to form terraces. However, small Si islands and holes as well as antiphase domain boundaries and a high density of missing dimer defects are present on the terraces. After further annealing at 507, 561, and 560 °C the Si terraces show a high density of missing dimer

15 defects which are aligned to energetically favorable defect rows perpendicular to the dimer rows. The defect density is significantly higher than on the initial clean surface prior to growth and also higher than after growth on a clean Si surface and annealing. In order to rearrange Si atoms to form a terrace structure after growth, an annealing step of

20 561 °C for 5 s is necessary. This is about 100 °C higher than for growth on a clean Si surface, where the terrace structure is already formed at a temperature of 456 °C (see Fig. 16). The size of the STM images is $50 \times 50 \text{ nm}^2$.

Fig. 18(a) shows the RMS (root mean square) Si surface roughness of STM images displayed in Fig. 16 (without H) and Fig. 17 (with H). For annealing

25 temperatures below about 500 °C, growth on the H terminated surface leads to a higher surface roughness compared to growth on a clean, non-H terminated surface. Annealing of the samples at temperatures below about 400 °C does not significantly change the surface roughness. The samples show a surface roughness comparable to the roughness of a clean Si surface (after flashing) for annealing temperatures of about 550 °C and

30 higher. The lines are guide to the eye.

Fig. 18(b) shows the density of missing dimer defects determined from STM images from growth on a clean and hydrogen terminated Si(100) surface, respectively. For equal thermal budget, i.e. growth at 250 °C and subsequent annealing steps, the Si surface shows a significantly higher defect density after growth at 250 °C on a

35 hydrogen terminated surface than after growth on a clean Si(100) surface. The main reason for the higher defect density appears to be the island growth mode as opposed to

the layer-by-layer growth on the clean Si(100) surface at 250 °C. The coarsening process of an initially high density of islands leads to the formation of antiphase domain boundaries and vacancy areas in the terraces. Both samples, however, display higher defect densities even after annealing at more than 600 °C for one minute than a clean Si surface after flashing. The lines are guide to the eye.

These results demonstrate that to obtain smooth layers it is best to remove the hydrogen first. This gives better atomic flatness and a reduced number of defects.

10 GROWING SILICON OVER DOPED SURFACES

Fig. 2 (f) and (h) (RT growth and rapid annealing)

Figs. 19 to 21 show the effects of different growth temperatures during silicon encapsulation and subsequent annealing steps, on the segregation and diffusion of P atoms to the surface.

15

Fig. 19 shows room temperature encapsulation of a phosphorus doped surface and subsequent annealing.

Fig. 19(ai) is a schematic and Fig. 19(aii) is a filled state STM image of a clean Si(100) 2×1 reconstructed surface.

20

Fig. 19(bi) is a schematic and Fig. 19(bii) is a filled state STM image of the surface after phosphine saturation dosing for 15 min at a chamber pressure of 1×10^9 mbar and annealing to 600 °C to incorporate phosphorus atoms and desorb hydrogen.

Fig. 19(ci) is a schematic and Fig. 19(cii) is a filled state STM image of the surface after epitaxial growth of 5 monolayers (ML) of silicon at room temperature

25 (RT).

Fig. 19(di) is a schematic and Fig. 19(dii), (diii), (div) and (dv) are filled state STM images of the surface after annealing of the sample for 1 min at 325 °C, 450 °C, 600 °C and 750 °C, respectively. The surface after epitaxial growth is covered with 3D silicon islands and flattens during subsequent annealing steps. The annealing steps at 325 °C to 600 °C show an increasing density of bright zigzag features on the surface. These features are related to Si-P heterodimers at the Si(100) surface and demonstrate an increase of the density of phosphorus atoms at the surface due to diffusion of these atoms from the highly phosphorus doped layer beneath the epitaxially grown silicon layer.

35

Fig. 19(ei) is a schematic and Fig. 19(eii) is a filled state STM image of the surface after annealing of the sample for 1 min at 900 °C. After this final annealing

step, the initial clean silicon surface has recovered after desorption of surface phosphorus atoms.

Fig. 20 shows encapsulation of a phosphorus doped surface at 260 °C and subsequent annealing.

Fig. 20(ai) is a schematic and Fig. 20(aii) is a filled state STM image of a clean Si(100) 2×1 reconstructed surface.

Fig. 20(bi) is a schematic and Fig. 20(bii) is a filled state STM image of the surface after dosing with phosphine at room temperature annealing at 600°C for 60 s to incorporate the phosphorus atoms into the Si surface as Si-P heterodimers. The Si-P heterodimer appears as a bright zigzag feature along the dimer row.

Fig. 20(ci) is a schematic and Fig. 20(cii) is a filled state STM image of the surface after five ML of Si are grown at 260 °C. This occurs in the layer-by-layer growth mode.

Fig. 20(di) is a schematic and Fig. 20(dii), (diii), (div), (dv), (dvi) and (dvii) are filled state STM images of the surface after it has been annealed for 5 s at temperatures of 350, 399, 454, 500, 552, and 609 °C, respectively. The Si surface after growth shows single dimer rows and elongated dimer row islands as well as a low density of bright zigzag features in the dimer rows. These zigzag features are identified as Si-P heterodimers. The density of the bright zigzag features increases with increasing annealing temperature. Annealing also changes the surface morphology similar to growth on a clean Si(100) surface and annealing (Fig. 16). After annealing for 5 s at 454 °C the terrace structure reappears, however, even after annealing at 500 °C small islands are still present on the surface.

Figs. 19 and 20 show, for the first time the use of STM imaging to measure dopant segregation and diffusion directly.

Figures 21 (a) - (h) show filled state STM images taken at RT of two separate growth experiments. For each experiment STM images of the Si(001) surface are shown after Si overgrowth at different temperatures (a), (e) and successive annealing steps for 5 s at ~350°C, ~500°C, and ~600°C (b) - (d) and (f) - (h). Note that for space reasons only selected STM images of the annealing sequence are shown here. The two experiments only differ in the Si overgrowth step (Figs. 21 (a) and (e)): 5 ML of Si were grown at 255°C or at RT.

Figure 21 (a) shows small 2D islands and short Si dimer chains at the surface after 5 ML growth at 255°C. Subsequent annealing of the surface at temperatures of 345 (b), 498 (c), and 600°C (d) causes the Si surface to flatten due to island coarsening

and diffusion of Si atoms to step edges. The bright asymmetric features that occur result from segregated P atoms, forming Si-P heterodimers and the density of these can be seen to increase during successive anneals.

After 5 ML growth at RT 3D Si islands are formed due to the small mobility of Si atoms on the surface, see Fig. 21 (e). Figures 21 (f) - (h) show that successive annealing steps flatten the surface as with the 5 ML growth at 255°C. Interestingly, the Si surface morphology in the different experiments looks very similar for the same annealing temperature, even for the first annealing step at ~350°C for 5 s (b), (f). However, Figs. 21 (b) - (h) clearly show that the density of Si-P heterodimers at the Si surface is much lower for a given anneal temperature if the Si encapsulation occurs at RT compared with 255°C Si growth.

Figure 21 (e) highlights an important limitation in the use of STM to investigate P segregation/diffusion: the high surface roughness that results from low temperature growth makes identification of Si-P heterodimers at the surface difficult. To identify a Si-P heterodimer a sufficient brightness contrast between the heterodimer and the surrounding Si surface is necessary, which can only be obtained for atomically flat surfaces. Therefore, Si-P heterodimers only become clearly visible in our experiments after a short anneal at ~350°C for 5 s. As a consequence the P density at the Si surface after the first anneal is a result of not only P segregation that occurs during growth but also arises from diffusion of P atoms that occurs during the subsequent anneal. Nonetheless it is reasonable to assume that P diffusion, with an energy barrier of 3.66 eV, is negligible for short anneals at such low temperatures. The P density observed at the surface after the first anneal therefore is most likely a result of P segregation that occurs during Si growth.

25

To quantify the density of P atoms at the Si(001) surface observed in the STM images of Fig. 21 we have counted the number of Si-P heterodimers after each anneal. Figure 21A shows the increase in the density of P atoms at the surface following subsequent annealing steps for the two different experiments. The relative density is obtained by comparison of the P density after Si growth and sample annealing, with the initial density of incorporated P atoms after PH₃ dosing and 600°C annealing of the clean Si surface.

If we consider the first 5 s annealing step at 350°C for the P atoms encapsulated in Si grown at 255°C already ~25% of the P atoms have segregated to occupy surface lattice sites. After subsequent annealing at 400, 450, 500, 550, to 600°C nearly 60% of the P atoms are present at the surface. These results demonstrate that even with a short,

35

low temperature anneal encapsulation of P atoms in epitaxial Si, grown at $\sim 250^\circ\text{C}$, results in significant P segregation.

In contrast, if P atoms are overgrown with 5 ML of Si deposited at RT and annealed at 350°C for 5 s, only $\sim 5\%$ of the initial number of P atoms are present at the surface. During subsequent annealing at 400, 450, 500, 550, and 600°C the P density only increases slightly to $\sim 10\%$ due to diffusion of P atoms from subsurface layers to the surface. The reduced density of P atoms at the Si surface compared to the 255°C Si growth experiment is a direct consequence of the strongly suppressed segregation of P atoms during Si overgrowth at RT.

To calculate the segregation length Δ of P in Si at 250°C and RT from the STM data we use the relation⁵⁴

$$p_{inc} = a_0/4\Delta$$

where p_{inc} is the incorporation probability and $a_0/4 = 0.1358$ nm, the distance between two subsequent Si(001) monolayers. We know that in Fig. 21A we find about 25% of P atoms at the surface after 5 ML Si growth at 255°C and the first anneal at $\sim 350^\circ\text{C}$. This means that 75% of the P atoms were incorporated. From this value (assuming that only segregation during growth occurred and that the diffusion of P atoms during the first annealing step at $\sim 350^\circ\text{C}$ is negligible) we get an incorporation probability $p_{inc} = 0.24$. According to the relation above this value corresponds to a segregation length of $\Delta = 0.58$ nm. For 5 ML Si growth at RT, the same analysis gives a segregation length of $\Delta = 0.29$ nm.

PHOSPHORUS DELTA DOPING

In order to determine the electrical activation of the phosphorus atoms epitaxially overgrown by silicon, a phosphorus delta doped layer was grown and made into a Hall bar device structure; see Fig. 23 (a). The fabrication steps for such a device are outlined in Fig 22.

Fig. 22(ai) is a schematic and Fig. 22(aii) is an STM image which shows a clean (100)2x1 silicon surface.

Fig. 22(bi) is a schematic and Fig. 22(bii) is an STM image and enlargement which shows the surface after phosphine saturation dosing at room temperature.

Fig. 22(cii) is a schematic and Fig. 22(cii) is an STM image which shows the surface after annealing at 550°C to incorporate the phosphorus atoms into the surface as P-Si dimers.

Fig. 22(di) is a schematic and Fig. 22(dii) is an STM image which shows the surface after growing 24 nm of epitaxial silicon at 250°C (the silicon surface after growth at room temperature is not shown here).

Fig. 23(a) is a schematic and Fig. 23 (b) is an optical microscope photo of the resulting Hall bar device after formation of ohmic contacts. Fig. 23(c) shows the normalised sheet resistivity, $\rho_{xx}/\rho_{xx}(0)$ as a function of magnetic field, B at a sample temperature of 4 K for samples grown at either 250°C or room temperature. The resulting data shows peaks at $B=0$, characteristic of weak localisation of electrons. Removing the weak localisation correction, and calculating the Hall slope (from Fig. 23(c)) allows us to estimate the mobility of the 2D layer as $70 \text{ cm}^2\text{V}^{-1}\text{s}^{-1}$ for the sample grown at 250°C and $30 \text{ cm}^2\text{V}^{-1}\text{s}^{-1}$ for the sample grown at room temperature. Fig. 23(c) also shows the Hall resistivity for these phosphorus delta doped samples giving a carrier density of $1.7 \times 10^{14} \text{ cm}^{-2}$ for both samples. This density is in excellent agreement with the 2D dopant density demonstrating that all of the phosphorus dopants that are incorporated into the silicon crystal are electrically active within the measurement error for both samples. This is a significant result for the fabrication of electronic device structures since it demonstrates that the phosphorus atoms incorporated using this process will be electrically active at these high doping densities.

Fig. 23(d) shows the magnetoresistance (MR) of P-in-Si δ -doped samples grown at RT, 250 and 400 °C. The negative MR behaviour is a clear signature of weak localization (WL) which arises from coherent backscattering of electrons in time-reversed trajectories. From the shape of the MR curve, we can extract the phase relaxation time τ_ϕ and phase coherence length l_ϕ which are measures of the characteristic scales for which quantum interference effects become observable. In order to do this, we fitted the WL correction to the conductivity σ using the Hikami model⁵⁵ for a disordered 2D-system of non-interacting electrons:

$$\Delta\sigma_{wl} = -\frac{\alpha e^2}{\pi h} \left[\Psi\left(\frac{1}{2} + \frac{B_0}{B}\right) - \Psi\left(\frac{1}{2} + \frac{B_\phi}{B}\right) \right] \quad (1)$$

where α is a scaling factor, Ψ is the digamma function and B_0 and B_ϕ are the characteristic magnetic fields associated with elastic transport and phase relaxation rates respectively. The fitting range was limited to $B < 0.1 B_0$. In Fig. 23(e), we plot the magnetoconductivity $\Delta\sigma = \sigma_{xx}(B) - \sigma_{xx}(0)$ of the δ -doped layer as a function of normalized magnetic field B/B_0 and compare it to the theoretical predictions from the

Hikami model. The values of the fitting parameters α , B_o , B_ϕ and the corresponding τ_ϕ and l_ϕ extracted from data fitting are listed in Table I.

TABLE I: Results from SIMS, 4.2 K magnetoresistance measurements and data fitting for samples encapsulated at various temperatures T.

| T(°C) | RT | 250 | 400 | 600 |
|--|-------|-------|------------------|-------------------|
| l_{seg} (nm) | 1.5 | 2.3 | 100 ^a | 1000 ^a |
| n_{31} (10^{14} cm ⁻²) | 1.3 | 1.4 | 1.7 ^b | 0.4 ^b |
| n_s (10^{14} cm ⁻²) | 1.67 | 1.64 | 0.22 | - |
| $\rho_{xx}(0)$ (k Ω \square) | 1.66 | 0.63 | 3.32 | - |
| μ (cm ² V ⁻¹ s ⁻¹) | ~23 | ~61 | ~86 | - |
| τ (fs) | ~4 | ~10 | ~15 | - |
| l (nm) | ~3 | ~9 | ~5 | - |
| α | 1.1 | 1.2 | 1.5 | - |
| B_o (T) | 22.1 | 3.7 | 10.2 | - |
| B_ϕ (T) | 0.062 | 0.031 | 0.36 | - |
| τ_ϕ (ps) | 1.6 | 1.3 | 0.5 | - |
| l_ϕ (nm) | 52 | 72 | 21 | - |

^aExtrapolation of literature data.

^bIncludes contributions from both ³¹P and ³⁰SiH.

An important parameter for quantum devices is l_ϕ . It increases from 52 nm for the RT sample to 72 nm for the 250 °C sample and then decreases to 21 nm for the 400 °C sample. As $l_\phi \propto \sqrt{\tau n_s \tau_\phi}$, the increase in l_ϕ from the RT to the 250 °C sample is mainly due to the corresponding increase in τ since these two samples have similar n_s and τ_ϕ . The smaller value of l_ϕ for the 400 °C sample is due to the smaller values of τ_ϕ and n_s , which offset the higher value of τ . In addition, the significant spread of dopants within the ~25 nm Si epilayer of the 400 °C sample implies that the thickness of the P-doped layer is of the same order as l_ϕ and the sample is thus on the border of the 2D limit.⁵⁶ The above analysis gives a measure of l_ϕ and τ_ϕ , and shows that the 250 °C encapsulation is most suitable for making devices that show quantum coherent effects.

In order to determine the extent of the confinement of the P atoms within the δ -doped layer we have performed secondary ion mass spectrometry (SIMS) measurements on our δ -doped samples. Fig. 24 shows the mass 31 depth profiles for phosphorus δ -doped samples encapsulated at RT, 250, 400 and 600 °C determined by SIMS. Both the RT and 250 °C samples show two separate mass 31 peaks: a broad peak near the surface and a sharper peak at the interface between the substrate and epitaxial layer. The higher mass resolution SIMS measurement (inset of Fig. 24),

however, shows only one ^{31}P peak at the interface between substrate and epitaxial layer demonstrating that the peak near the surface is due to ^{30}SiH . The full width at half maximum of the ^{31}P peak is 4 nm for the RT sample and 6 nm for the 250 °C sample. From SIMS measurements, we determined the P segregation length to be 1.5 nm for RT and 2.3 nm for 250 °C overgrowth thus showing the smaller degree of segregation during RT encapsulation. For the 400 and 600 °C samples, we see only one broad mass 31 peak near the surface. We attribute this to the strong segregation of P atoms to the surface at these high growth temperatures. The corresponding segregation lengths extracted from extrapolating literature data⁵⁴ are 100 nm for 400 °C growth and 1000 nm for 600 °C growth. From the SIMS measurements, we determine the ^{31}P concentration n_{31} by integrating the area under the ^{31}P peak of the samples encapsulated at RT and 250 °C, respectively. Within the SIMS measurement error of ~20%, the ^{31}P concentrations for the RT and 250 °C samples are in agreement with the expected value of $1.7 \times 10^{14} \text{ cm}^{-2}$ (see Table I). However, this analysis is not possible for the higher temperature encapsulation because the single mass 31 peak is so broad that it now includes contributions from both ^{30}SiH and ^{31}P . For the 400 °C, this gives a higher value of n_{31} than for RT and 250 °C. For the 600 °C sample, n_{31} is significantly lower indicating the strong segregation of ^{31}P to the surface where it is not detected by SIMS and possibly the onset of P desorption from the surface.

REGISTRATION OF ATOMIC-SCALE DEVICES AND ATOMIC-SCALE DEVICE FABRICATION

Figs. 25 to 30 are all concerned with the fabrication and electrical measurement of atomic-scale devices using registration markers on the silicon surface to register the atomic-scale device to metallic surface gates needed for electrical measurements. The fabrication of registration markers which are visible in optical or scanning electron microscopes is a basic requirement for connecting atomic-scale devices to the outside world. The registration markers have to survive all processing steps such as sample heating and silicon growth.

Fig. 25 is a schematic illustrating the atomic-scale device fabrication process. The device process starts with the fabrication of registration markers which are needed to identify the exact location of the atomic-scale device for the formation of ohmic metal contacts at the final stage of the device process. These registration markers can have various sizes between a few nm and several μm to be identified in scanning electron microscope (SEM) images or optical microscope images. Registration markers

can be fabricated using e.g. focused ion beam (FIB) milling or etching of the silicon surface. The silicon surface can be etched using either wet-chemical etching or reactive ion etching (RIE) of lithographically structured areas which are defined by optical or e-beam lithography (EBL). A set of differently sized registration markers can be used
 5 (see Fig. 26) to more accurately define the position of atomic-scale devices and to make sure that registration markers survive all subsequent processing steps such as sample heating and Si epitaxial growth.

After fabrication of the registration markers the sample is heated to remove oxide and other contaminants from the sample surface and the sample surface is then
 10 terminated with a monolayer of hydrogen atoms as described previously.

Using the SEM the STM tip is then approached to the sample surface with respect to the registration markers (see Fig. 26). The following processes of atomic-scale lithography to define the desired device structure, phosphine dosing, phosphorus incorporation, removal of the hydrogen resist layer and encapsulation of the
 15 incorporated P atoms with epitaxially grown silicon have been described previously. Finally, using the registration markers and optical lithography or EBL a metal layer is deposited on parts of the silicon surface to form ohmic metallic contacts which are needed for electrical measurements to the buried atomic-scale device.

Fig. 27(a) to (d) illustrate the fabrication process of a buried $4 \times 4 \mu\text{m}^2$ phosphorus doped 2D device. Fig. 27 (a) is an STM image showing a bright area from which hydrogen was desorbed using the STM tip and two dark areas at the top and bottom of the image where hydrogen still remains on the surface. Fig. 27(b) is a schematic which shows the P doped device area (bright square) and metal finger contacts. Fig. 27(c) shows an optical microscope image of the device region after
 25 complete fabrication of the device. Metal finger contacts and registration markers are clearly visible. Fig. 27(d) shows a larger scale optical microscope image of the device region including large metal contact areas used for bonding of thin metal wires to the device which are needed for electrical measurements.

Fig. 28(a) shows an STM image of a hydrogen terminated Si(001) surface (dark
 30 area) from which hydrogen was removed to form an approx. 100 nm wide and 1 μm long wire with two contact regions on both ends (bright area). Fig. 28(b) is a schematic which shows a wire with two contact regions on both ends contacted by metal fingers.

Fig. 29(a) shows the Hall resistance versus the magnetic field of a $4 \times 4 \mu\text{m}^2$ phosphorus doped 2D device encapsulated with 25 nm of epitaxially grown silicon
 35 measured at 4 K sample temperature. The Hall slope corresponds to an electron density of $1.79 \times 10^{14} \text{ cm}^{-2}$ in excellent agreement with the expected value of $1.7 \times 10^{14} \text{ cm}^{-2}$

from the phosphine dosing/phosphorus incorporation process (see also Figs. 23c and 24). This demonstrates full electrical activation of the encapsulated phosphorus dopant atoms. Fig. 29(b) shows the sheet resistance versus the magnetic field of this sample. The peak of the sheet resistance at zero magnetic field is due to weak localisation of the
 5 electrons which demonstrates the 2D structure of the device.

Four terminal magnetoresistance measurements of two STM-patterned devices ($4 \times 4 \mu\text{m}^2$ patch and $90 \times 900 \text{ nm}^2$ wire) were performed at $0.05 - 4 \text{ K}$ to confirm the suitability of the fabrication strategy for the creation of nano-scale devices. In particular
 10 we aimed to determine the influence of the STM-patterned device geometry on electron transport in the presence of a magnetic field.

Figure 30(a) shows the magnetoresistance of the $4 \times 4 \mu\text{m}^2$ phosphorus δ -doped square device both at 4 K and 50 mK . The magnetoresistance of the square device in Figure 30(a) shows a peak centered around $B=0$ that becomes more pronounced as the
 15 sample is cooled to 50 mK . Note that the peak resistivity is similar at both temperatures, as expected for a highly doped metallic system.

The strong increase in the magnitude of the negative magnetoresistance with decreasing temperature is a characteristic signature of weak localization. Weak localization arises from coherent backscattering of forward and time reversed electron
 20 waves around a loop as electrons diffuse through the sample, leading to an increase of the resistance over the classical Drude value. This quantum correction to the resistance becomes larger as the temperature is lowered, because the phase coherence length increases as $T \rightarrow 0$ and more loops (with larger circumferences) can contribute to the total backscattering. The application of a magnetic field breaks the time reversal
 25 symmetry in these loops and suppresses coherent backscattering, resulting in a negative magnetoresistance that is more pronounced at lower temperatures.

We can extract the phase coherence length of the electrons by performing a three-parameter fit of the magnetoresistance (see dotted lines) to the Hikami expression for weak localization in the diffusive regime. At 4 K we obtain a phase coherence
 30 length of $l_\phi = 38 \text{ nm}$, which increases to $l_\phi = 131 \text{ nm}$ as the temperature is reduced to 50 mK . This suggests that if we make a STM-defined structure with a width below $w \sim 130 \text{ nm}$, we would expect to see evidence of the lateral confinement in the weak localization i.e. in the magnetoresistance.

In Figure 30(b) we present the magnetoresistance of the 90 nm -wide quantum
 35 wire device. We can see that the overall resistance of the wire is much higher than the square device, as expected from the sample geometry. At 4 K the resistance of the wire

device shows a similar peak in the magnetoresistance around $B = 0$. From fitting the data to the Hikami formula for weak localization we can again extract the phase coherence length l_ϕ , which is smaller than the width of the wire. Electron transport in the wire is essentially two-dimensional, as electrons are unable to distinguish if they are
 5 traveling through a 4 μm -wide square or a 90 nm-wide wire. As the temperature is reduced to 50 mK however, l_ϕ becomes larger than the wire width, and the lateral confinement of the wire limits the maximum size of electron loops that can contribute to the backscattering mechanism that causes weak localization. Thus although the negative magnetoresistance becomes stronger in the wire as T is reduced, it is
 10 significantly less pronounced than for the square device. This is highlighted if we consider the 2D Hikami fit applied to the wire. Here we can clearly see a suppression of the 2D weak localization around $B=0$ due to a cross-over from two-dimensional to one-dimensional electron transport as the phase coherence length increases.

We can use the suppression of the 2D weak localization to independently
 15 measure the width of the quantum wire. As the magnetic field is increased, the maximum size of electron loops for which there is constructive interference of backscattered electrons decreases – the constructive interference is destroyed when a magnetic flux quantum threads a loop of radius r , i.e. when $r^2 = \hbar/(eB) = l_B^2$. When the magnetic length l_B is much larger than the wire width w , the magnetic field has
 20 relatively little effect, which results in the plateau around $B = 0$. As the magnetic field increases the size of the constructively interfering loops becomes smaller, so that it is B , and not the wire width, that determines the magnitude of the weak localization effect. Thus the wire approaches the two-dimensional behavior of the square when $2l_B \sim w$. From Figure 30(b) we see that the measured data merges with the dashed line of the 2D
 25 theory at $|B| \sim 0.3$ T, which implies a wire width of ~ 90 nm, in excellent agreement with the STM-defined geometry.

Our results open the way for the realization of sophisticated atomic-scale devices in silicon such as single electron transistors (SETs), quantum cellular automata and a Si based solid-state quantum computer.

30

Finally, it is important to note that the fabrication strategy demonstrated here is also directly applicable to other silicon based quantum computer architectures³.

It will be appreciated by persons skilled in the art that numerous variations and/or modifications may be made to the invention as shown in the specific
 35 embodiments without departing from the spirit or scope of the invention as broadly

described. The present embodiments are, therefore, to be considered in all respects as illustrative and not restrictive.

DATED this twenty second day of April 2004

Unisearch Limited
Patent Attorneys for the Applicant:

F.B. RICE & CO

11/53

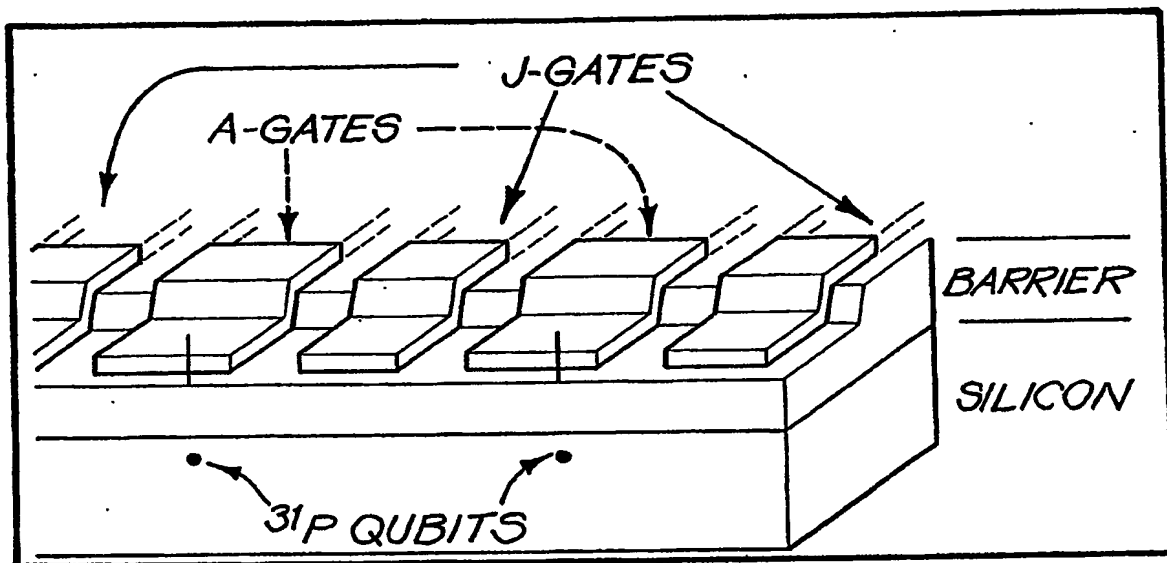


FIG. 1

2/53

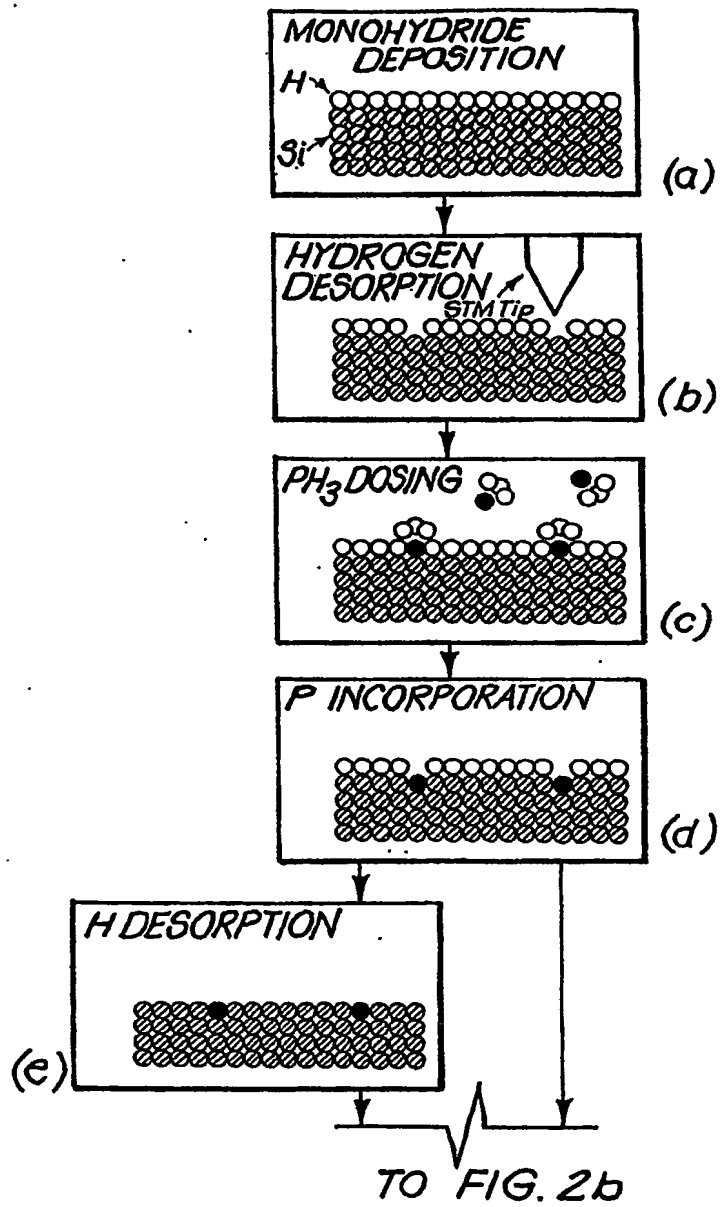


FIG. 2a

3/53

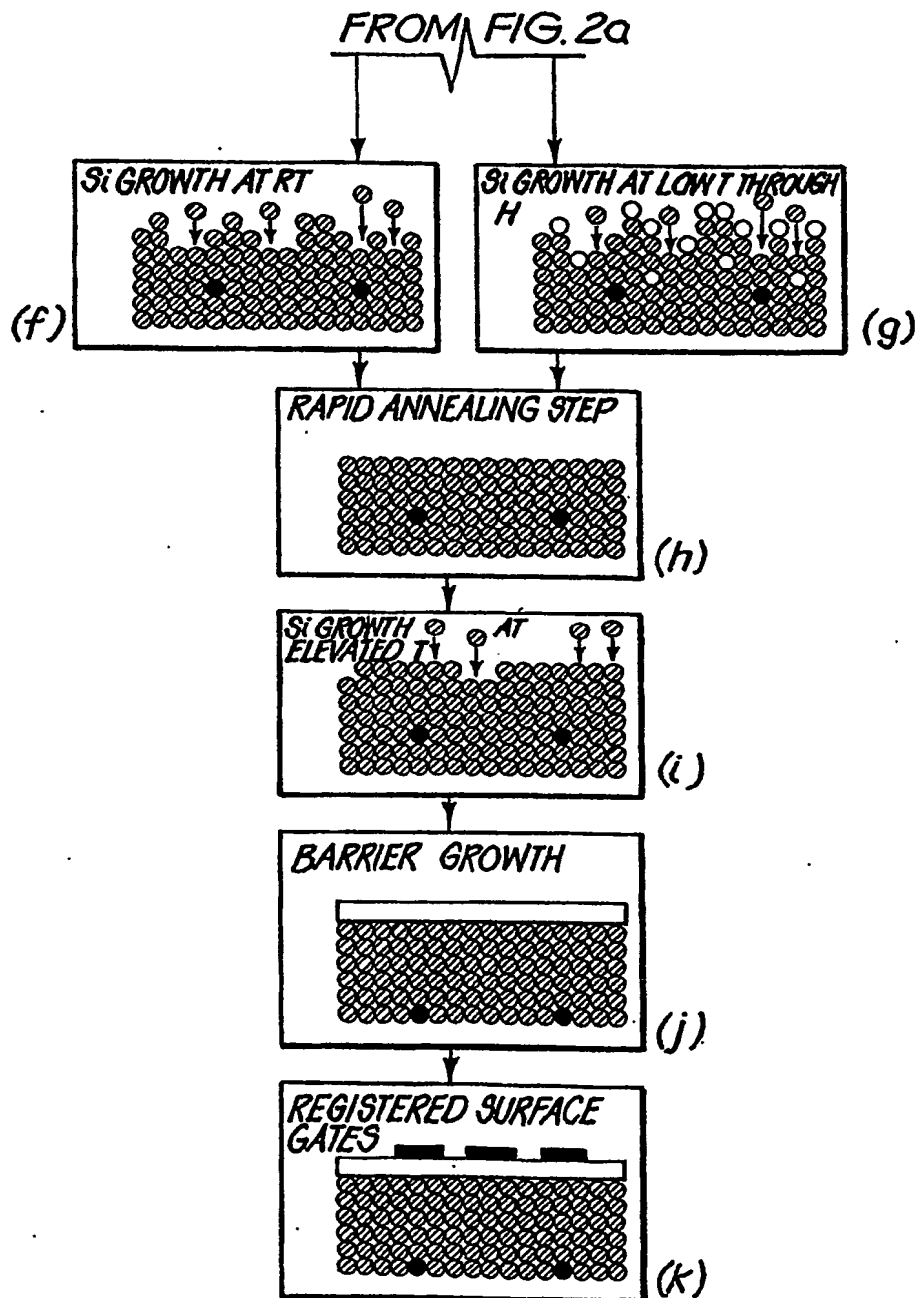


FIG. 2b

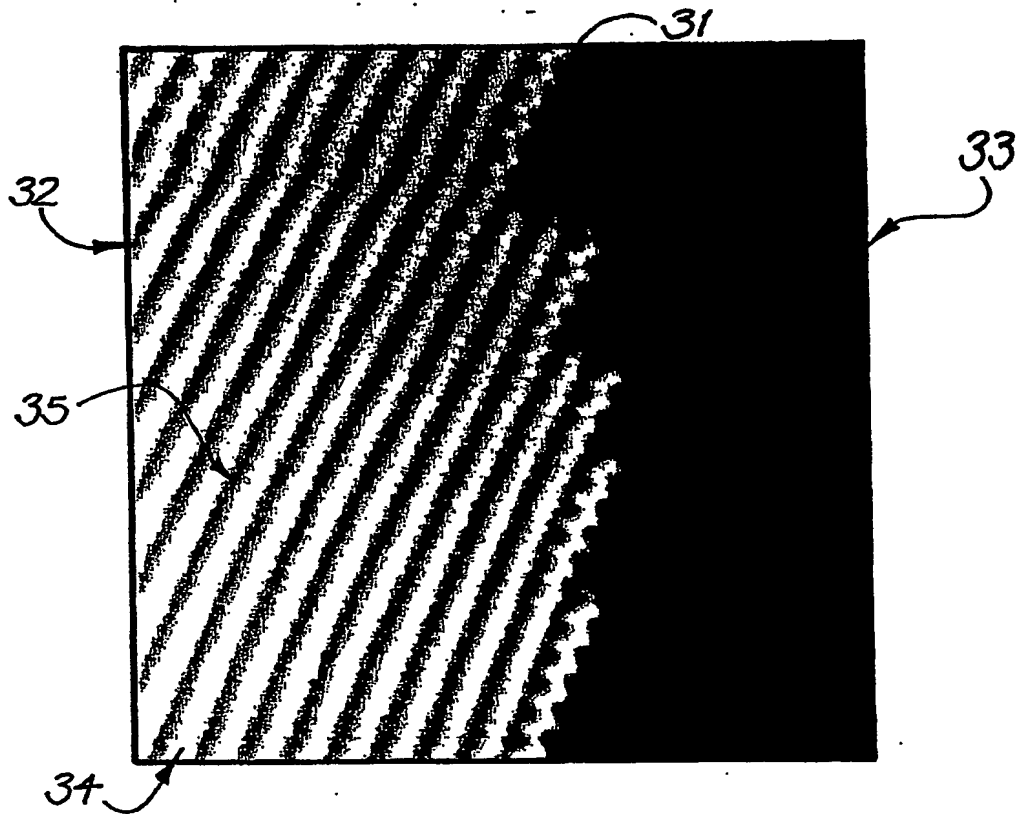


FIG. 3a

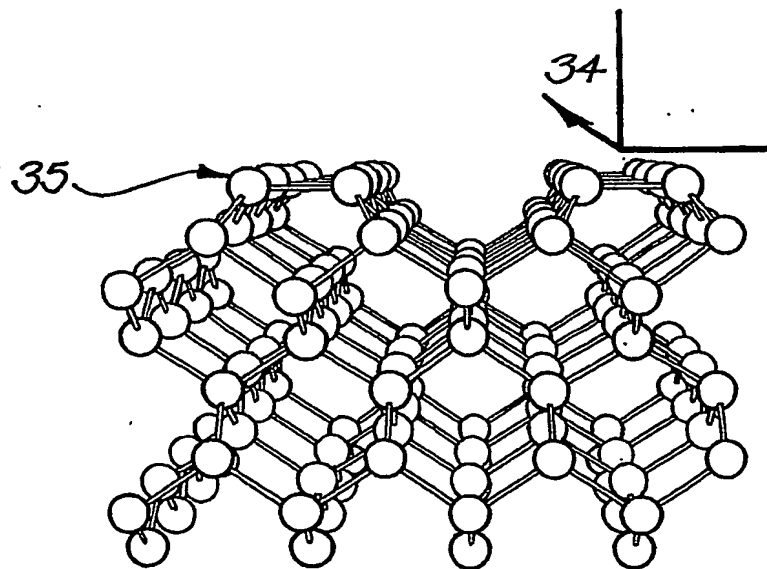


FIG. 3b

5/53

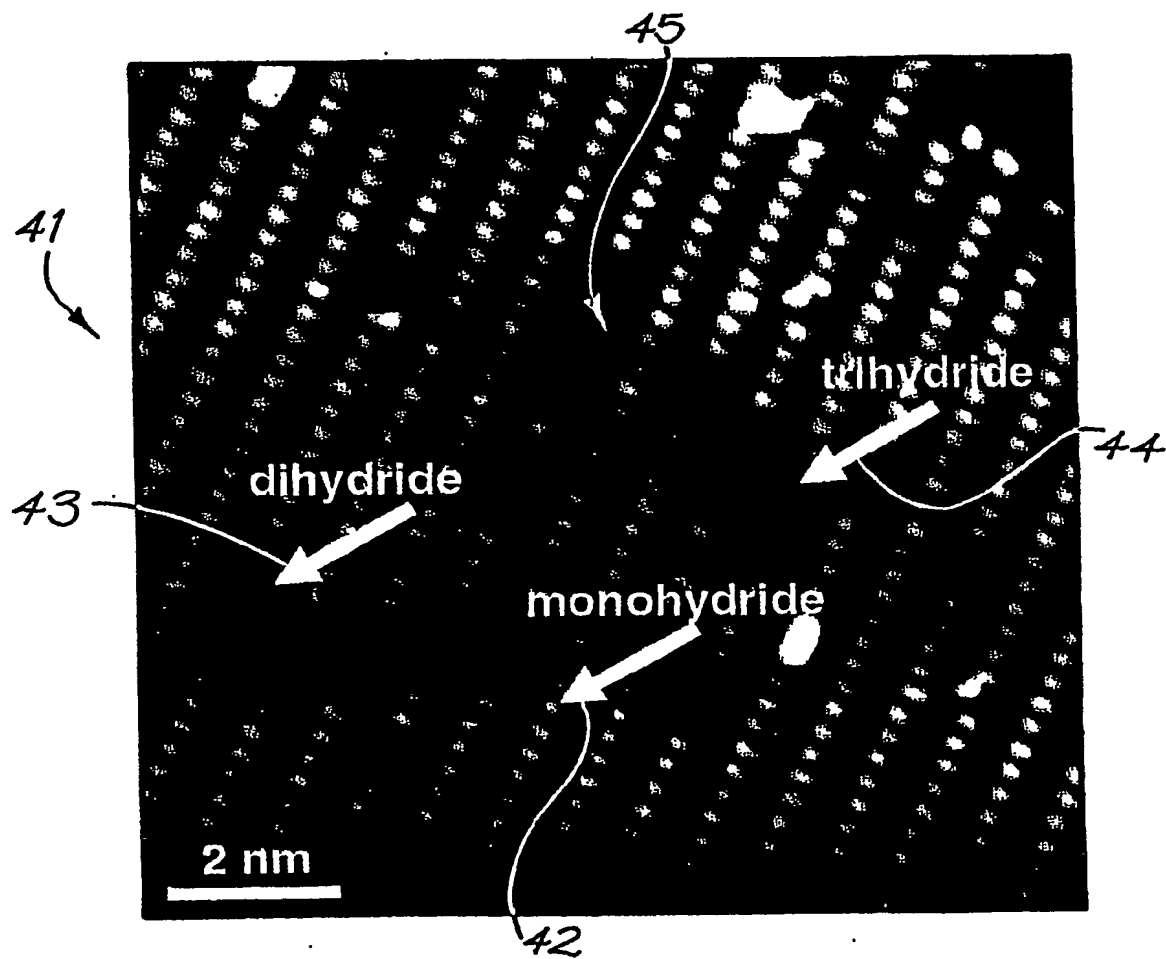


FIG. 4a

6/53

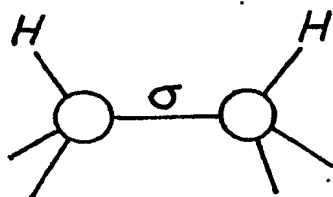


FIG. 4b

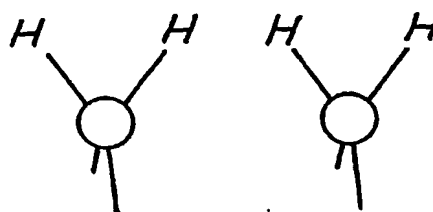


FIG. 4c

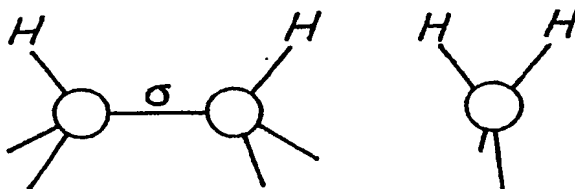


FIG. 4d

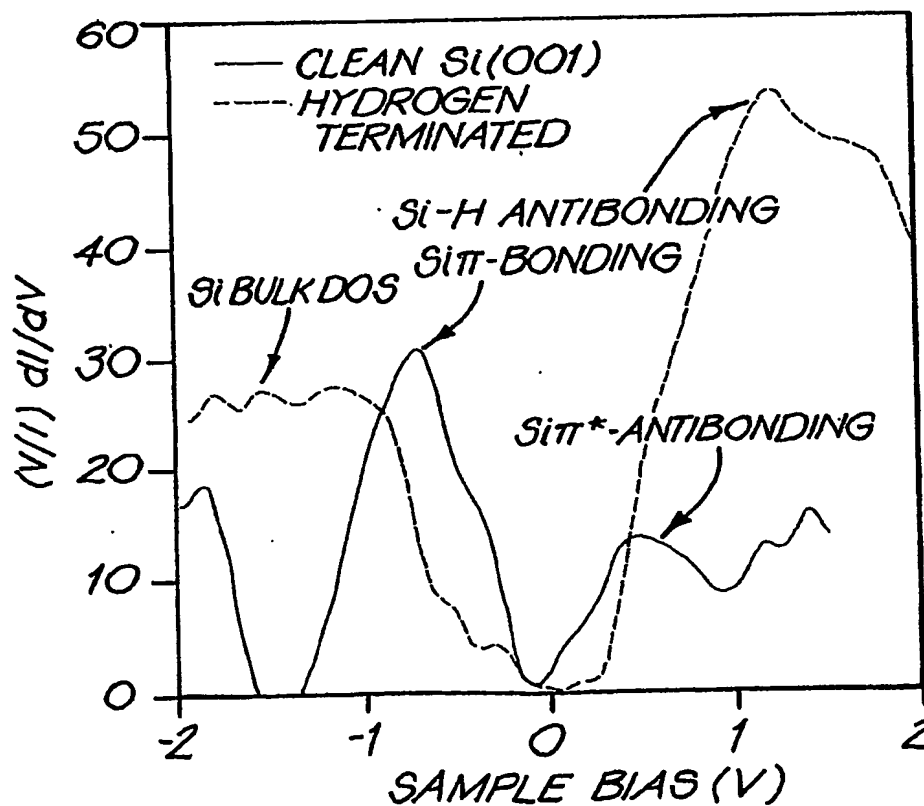


FIG. 4e

7/53

DANGLING BOND

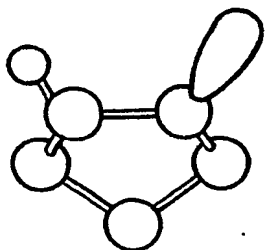


FIG. 5b

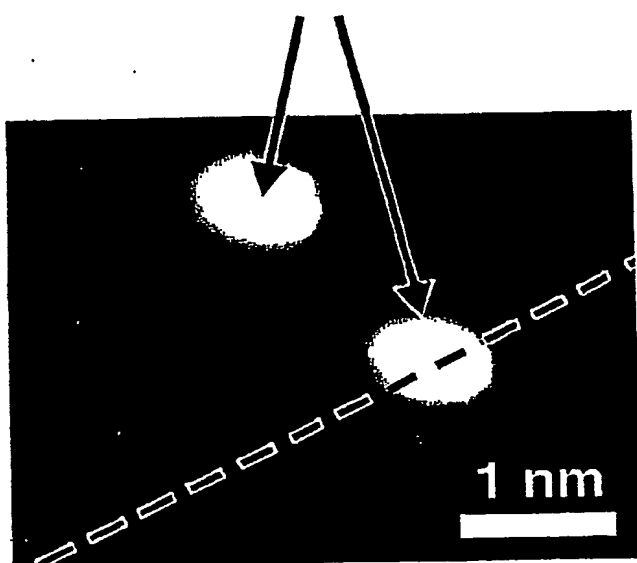


FIG. 5a

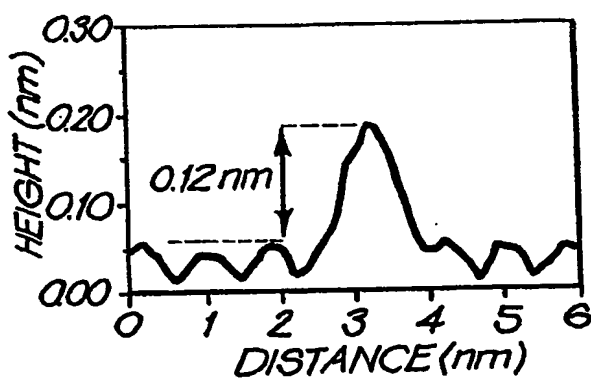


FIG. 5c

8/53

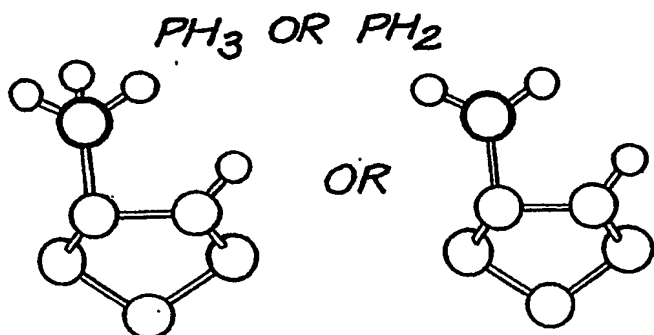


FIG.5e

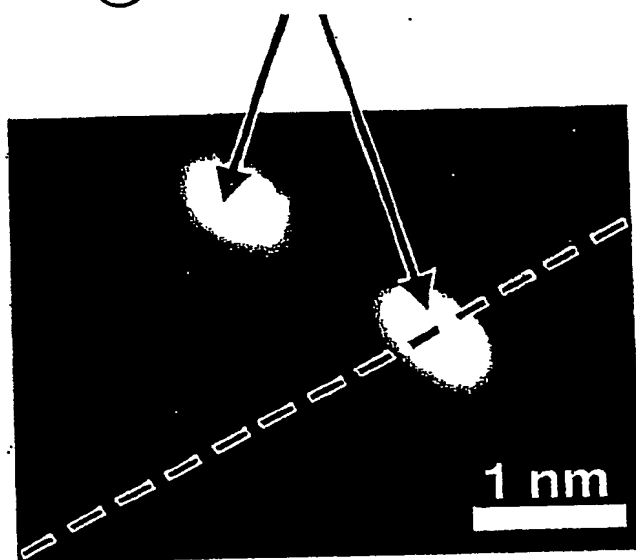


FIG.5d

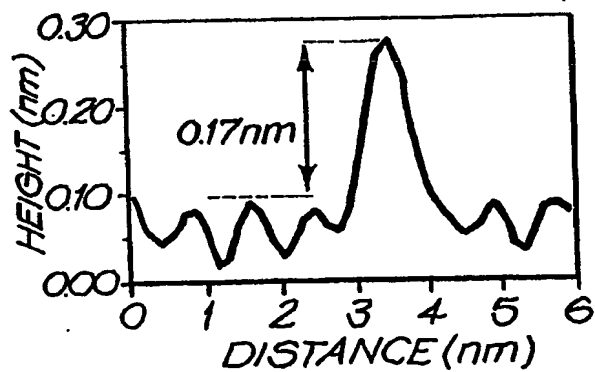


FIG.5f

9/53

DANGLING BOND

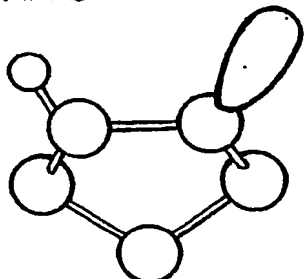


FIG. 6b

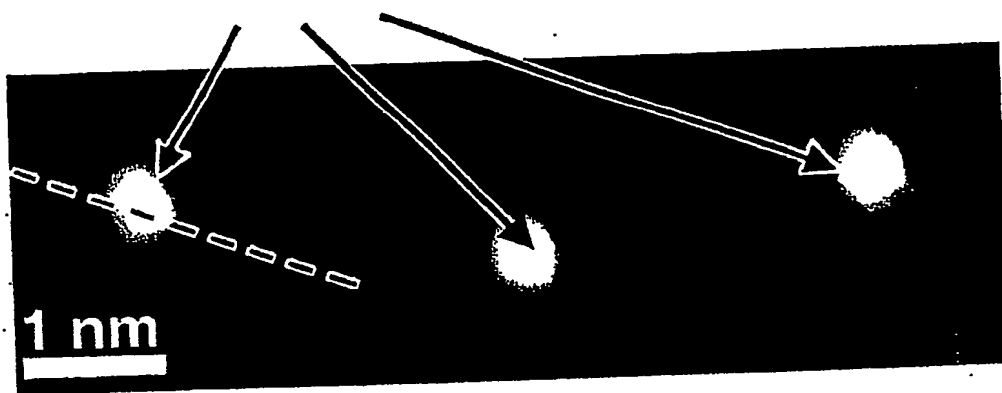


FIG. 6a

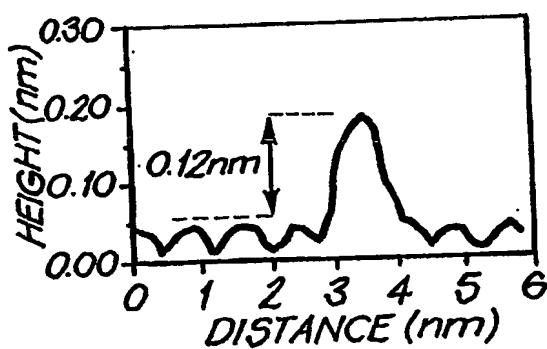


FIG. 6c

10/53

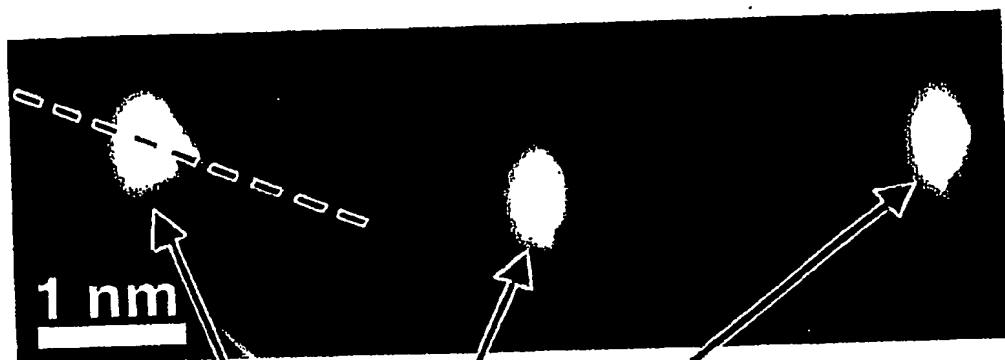
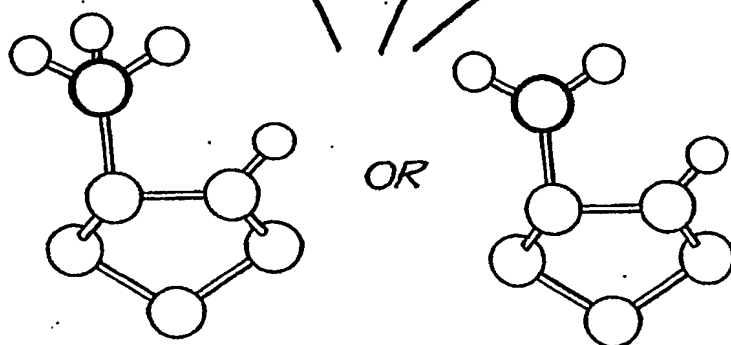


FIG. 6d



PH₃ OR PH₂

FIG. 6e

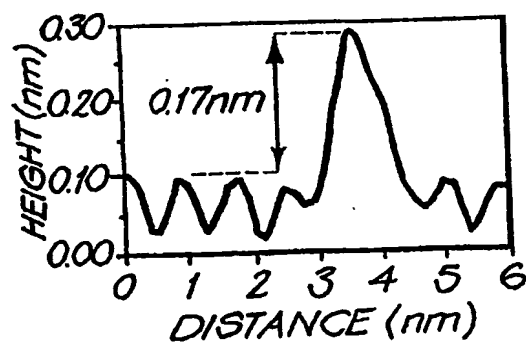
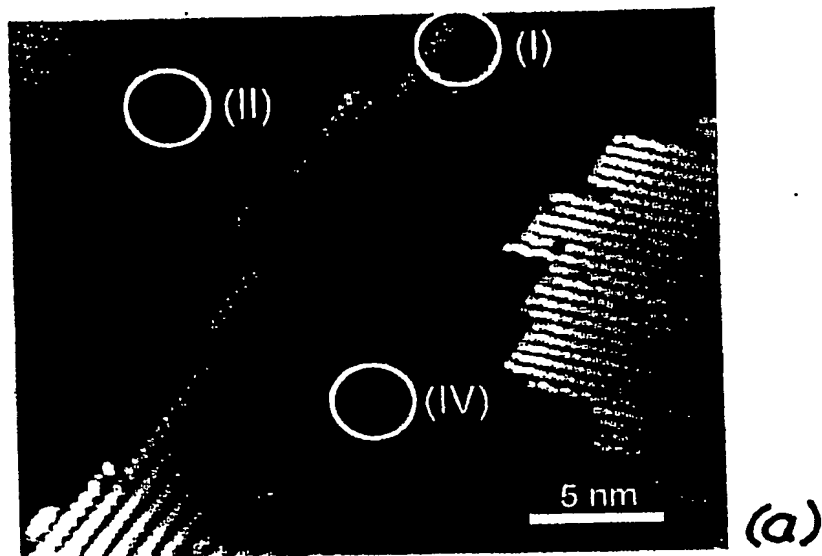


FIG. 6f

11/53



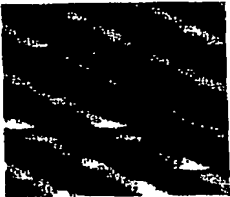







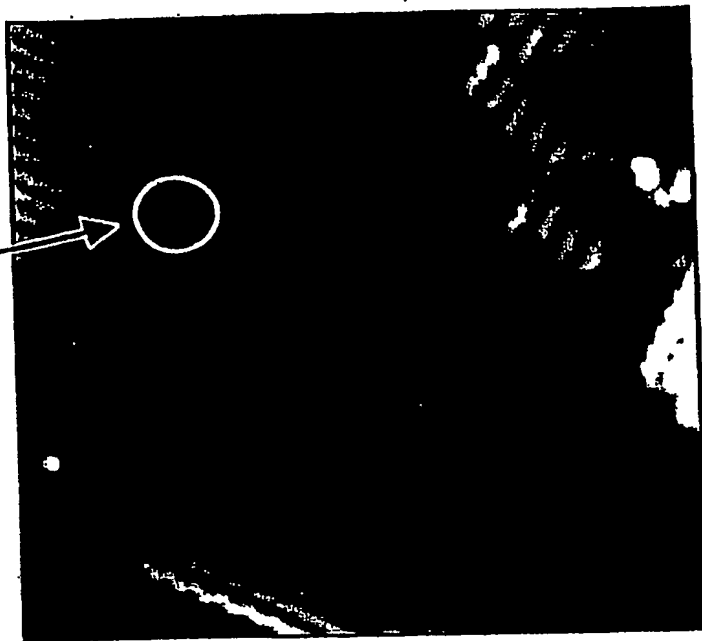
| | DEFECT | FILLED STATE | EMPTY STATE |
|-----|-------------------------------|--|---|
| (b) | MISSING DIMER DEFECT |  (bi) |  (bii) |
| (c) | MULTIPLE MISSING DIMER DEFECT |  (ci) |  (cii) |
| (d) | C DEFECT |  (di) |  (dii) |
| (e) | SPLIT-OFF DIMER DEFECT |  (ei) |  (eii) |

FIG. 7

12/53

CIRCLED
FEATURE
SAME
BEFORE &
AFTER
DOSING
81



BEFORE PHOSPHINE DOSING

SURFACE CHANGES DUE TO PHOSPHINE DOSING

AFTER PHOSPHINE DOSING

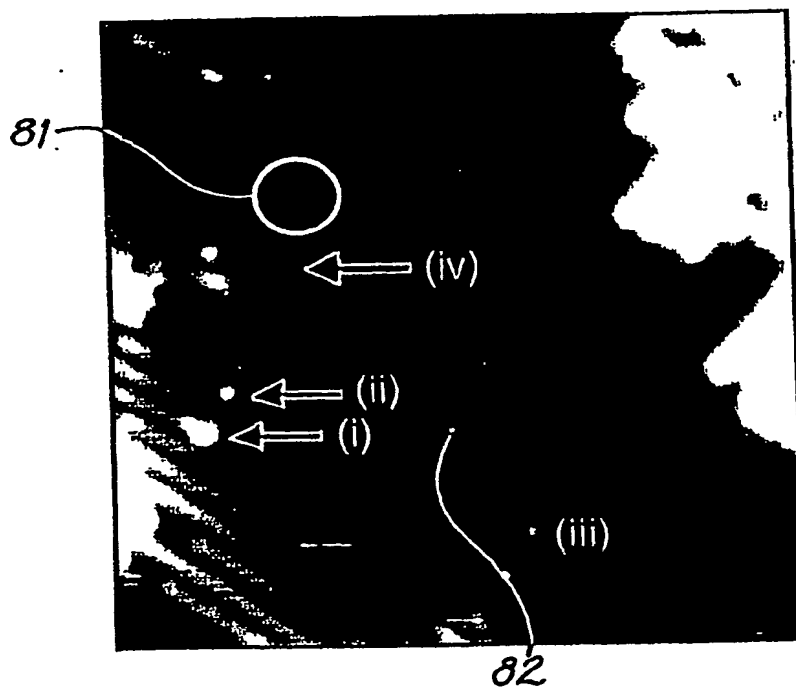


FIG. 8

13/53

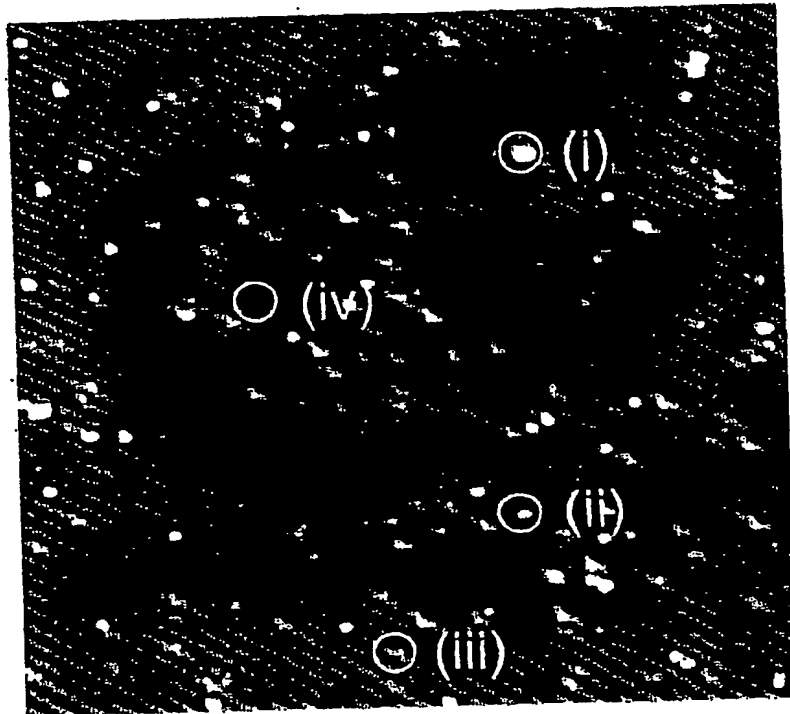


FIG. 9a

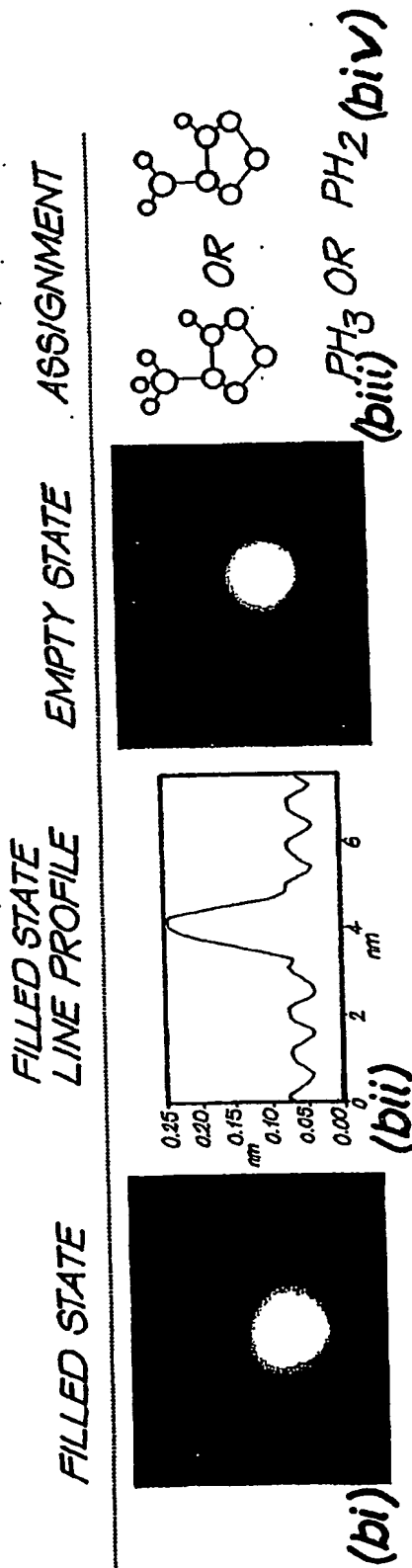


FIG. 9b

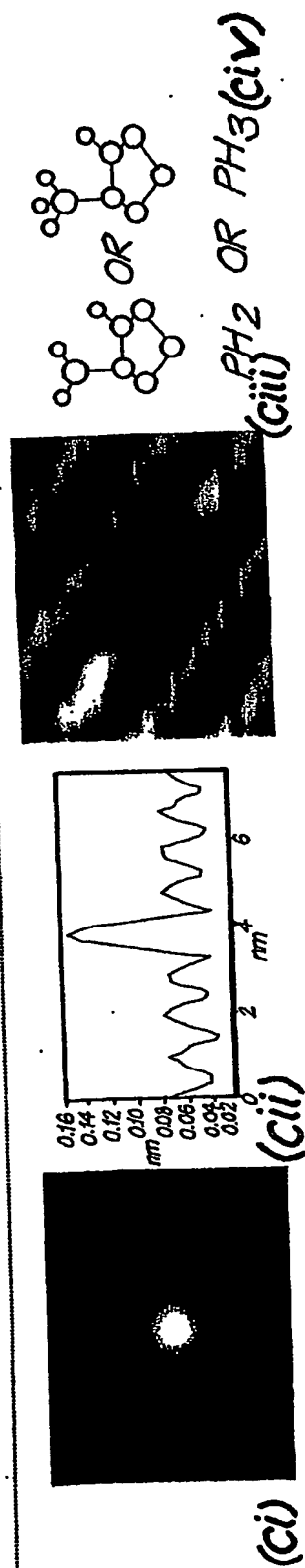


FIG. 9c

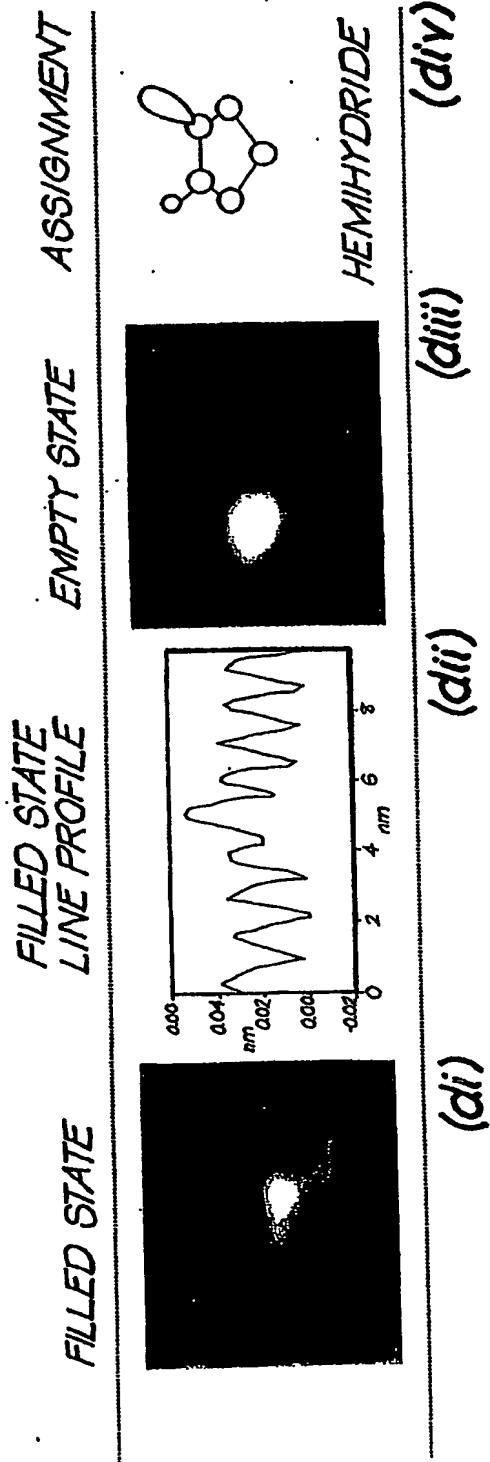


FIG. 9d

15/53

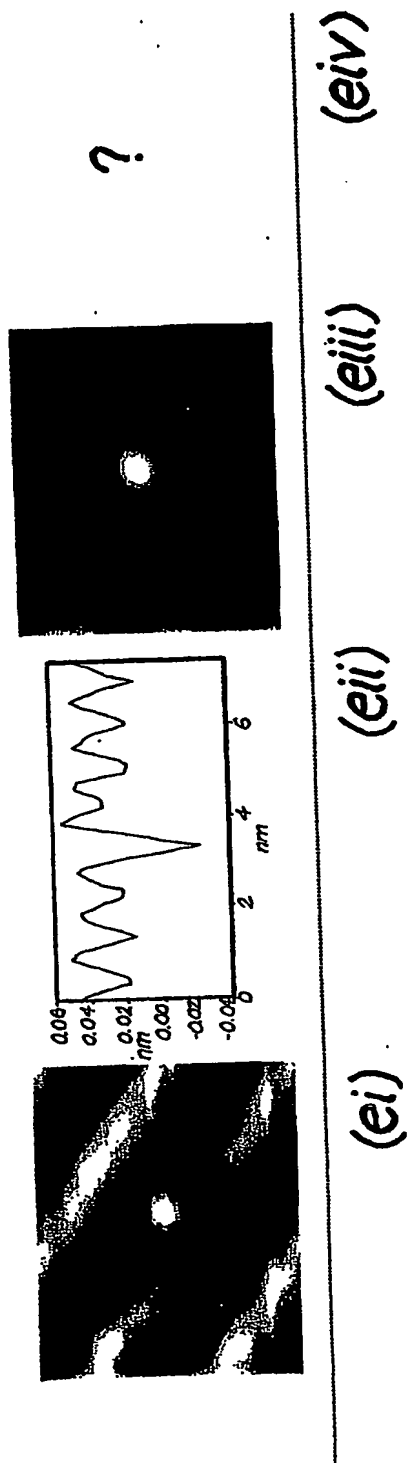


FIG. 9e

16/53

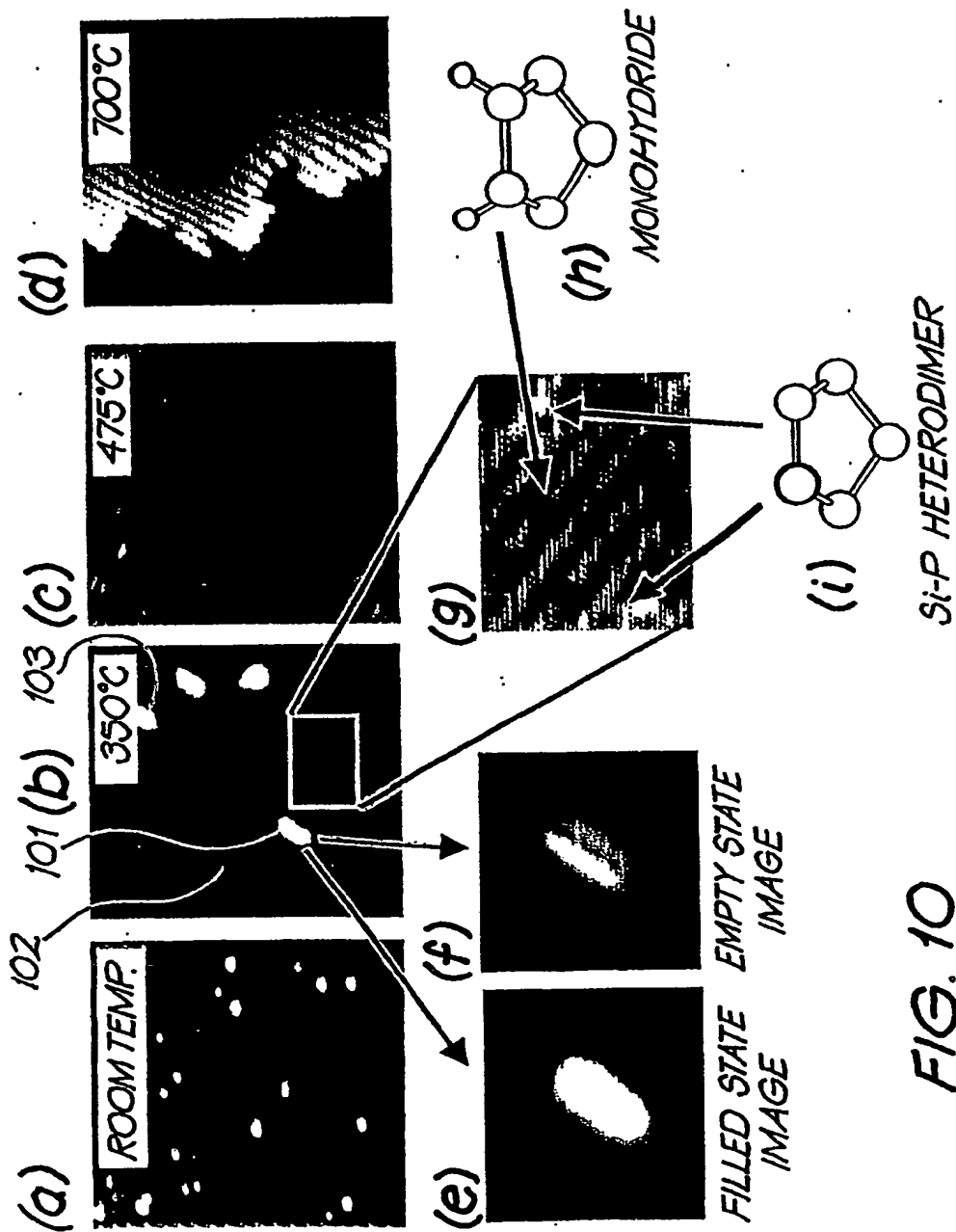


FIG. 10

17/53.

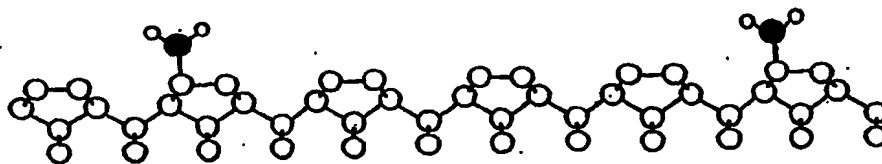
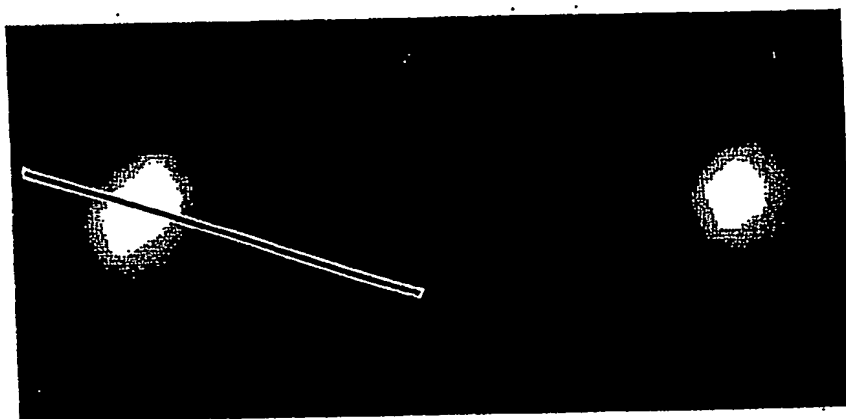


FIG. 11a



BIAS = -3.0V
 $I_t = 0.1 \text{ nA}$

FIG. 11b

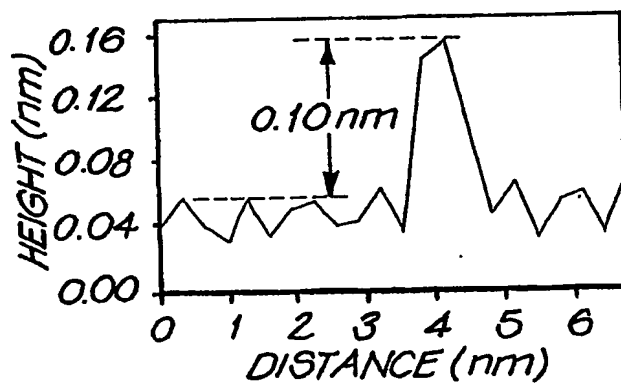


FIG. 11c

18/53

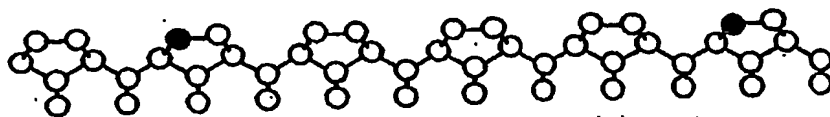
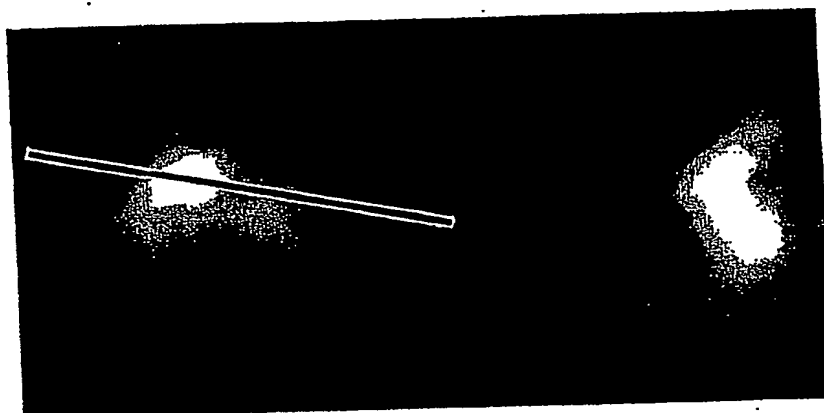


FIG. 11d



BIAS = -1.6 V
 $I_t = 0.2 \text{ nA}$

FIG. 11e

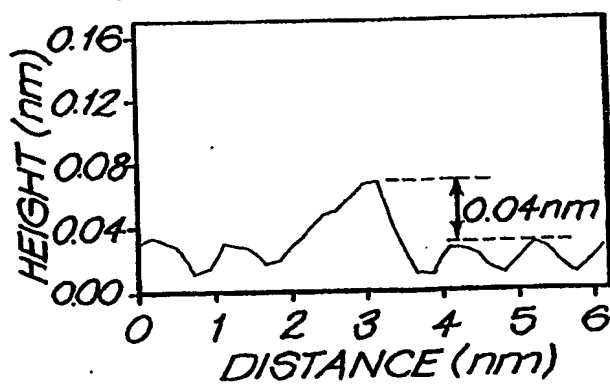


FIG. 11f

19/53

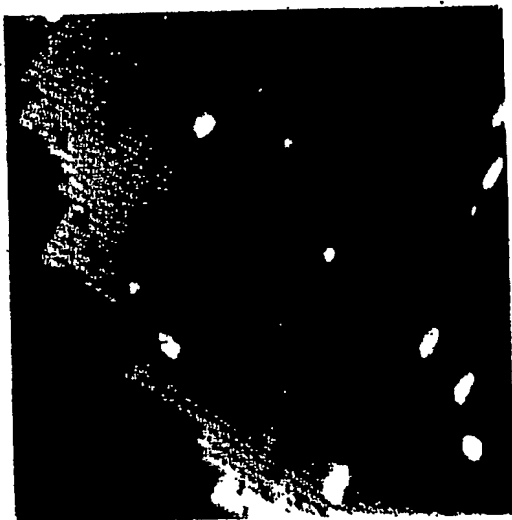


FIG. 12a



FIG. 12b

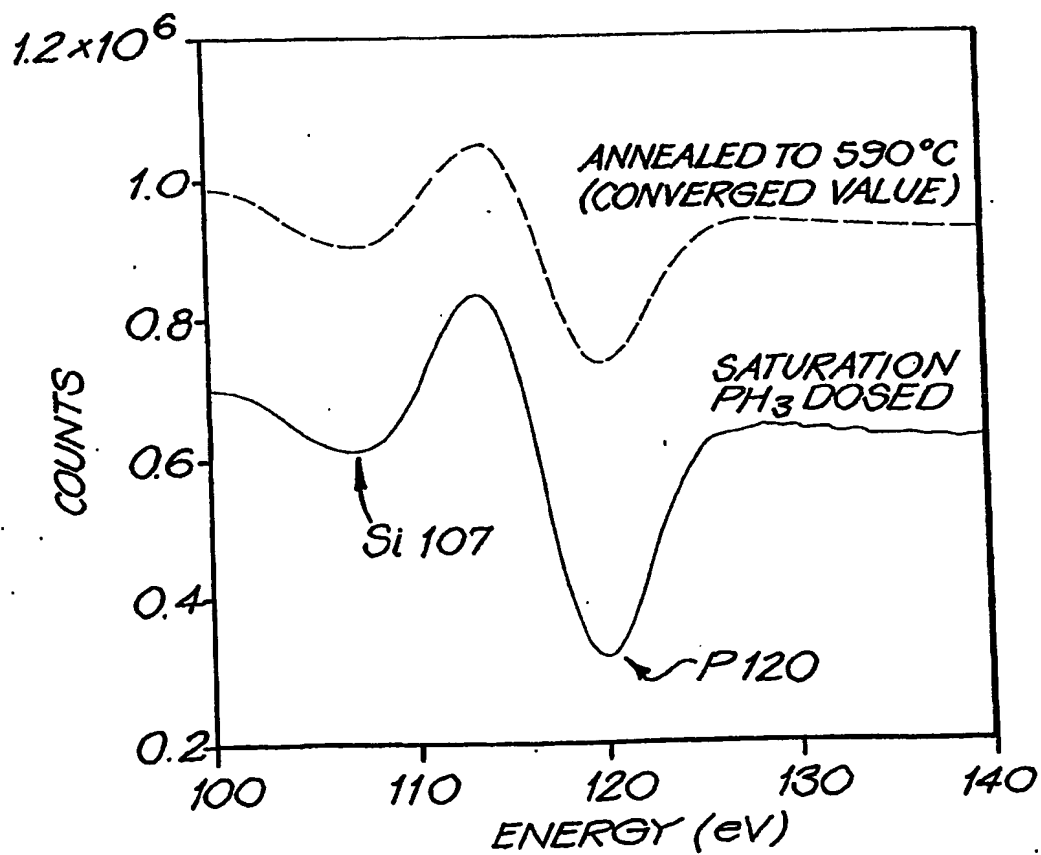


FIG. 12c

20/53

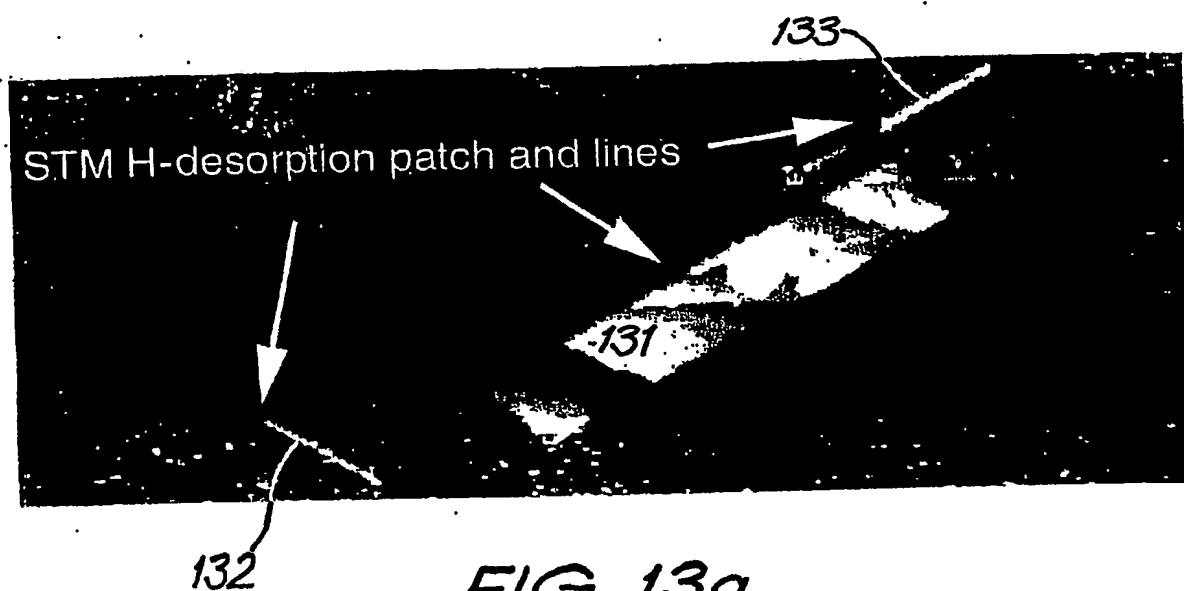


FIG. 13a

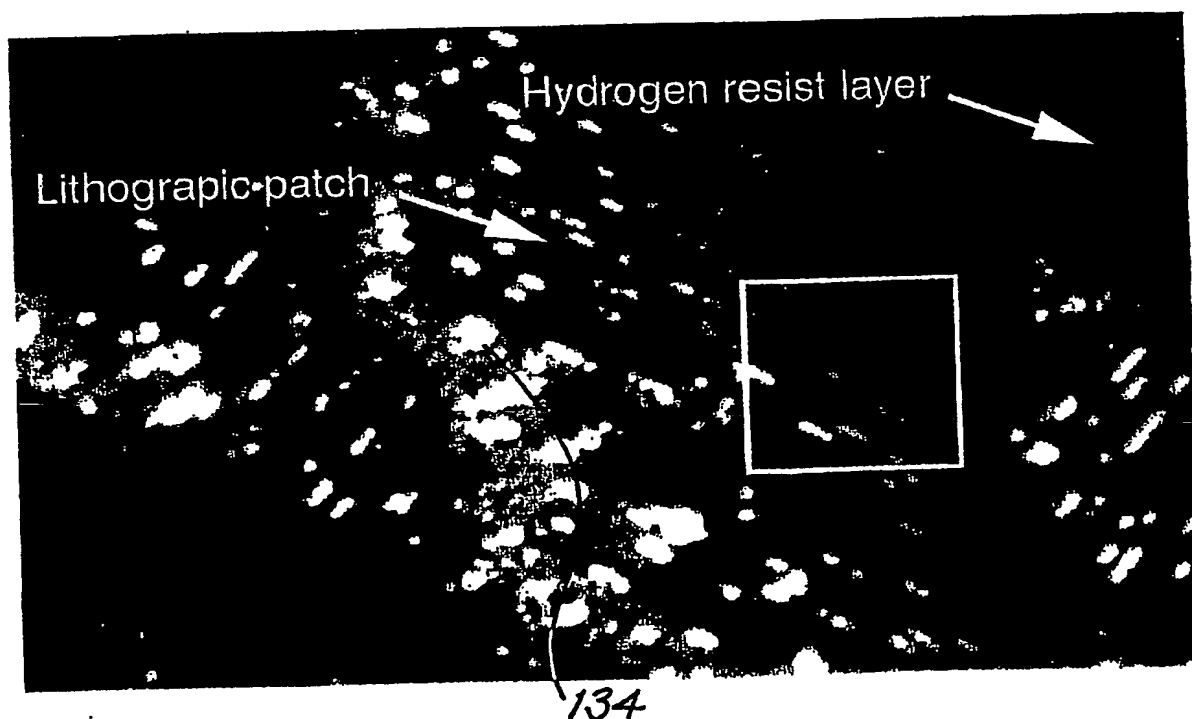


FIG. 13b

21/53



FIG. 13c

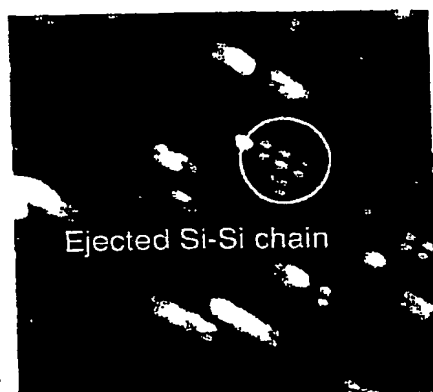


FIG. 13d

22/53

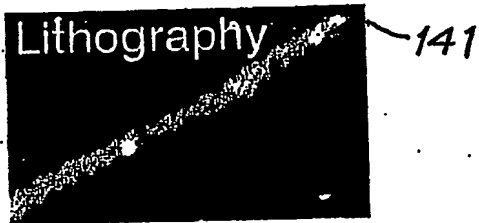


FIG. 14a



FIG. 14b



FIG. 14c

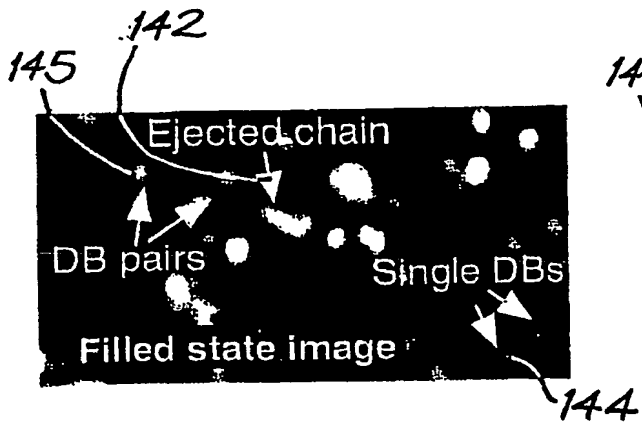


FIG. 14d

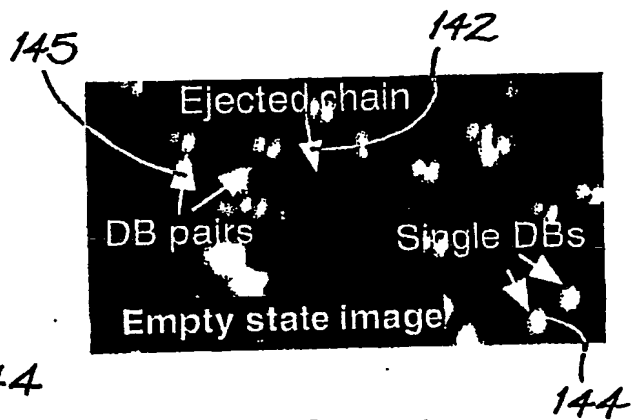


FIG. 14e

23/53



FIG. 14f

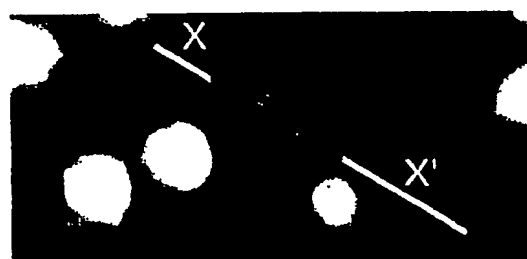


FIG. 14g

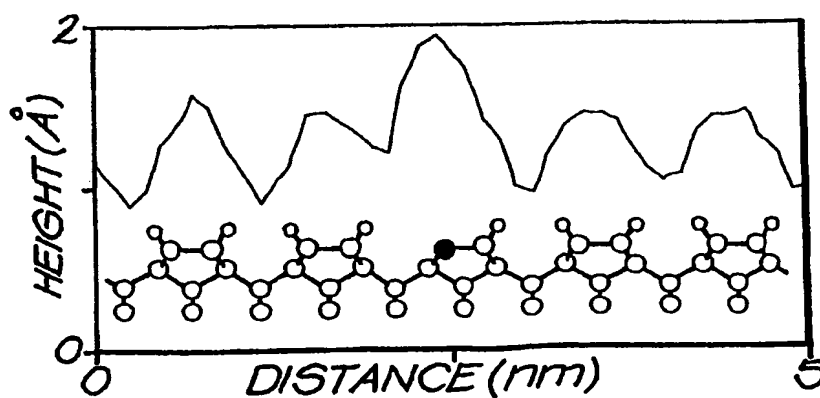


FIG. 14h

24/53.

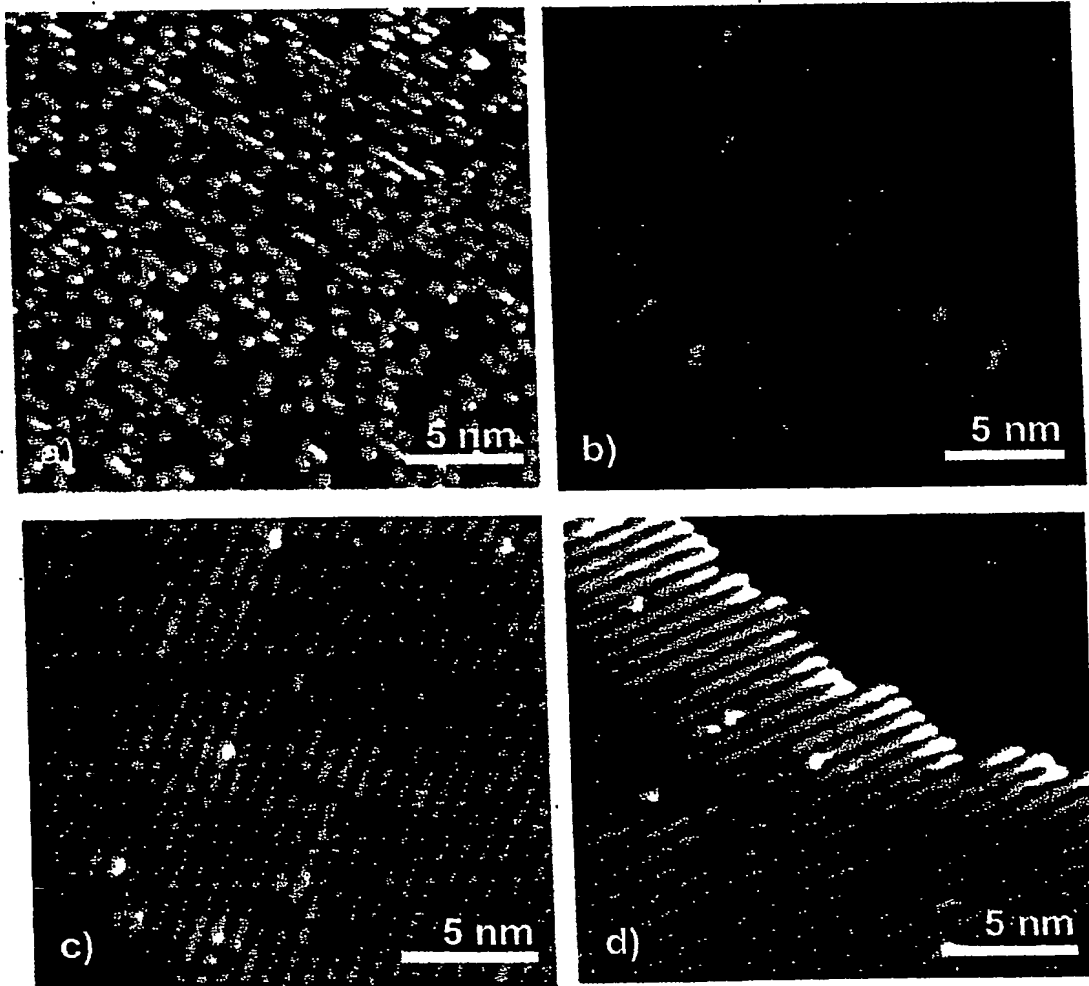


Figure 14 A.

25/53

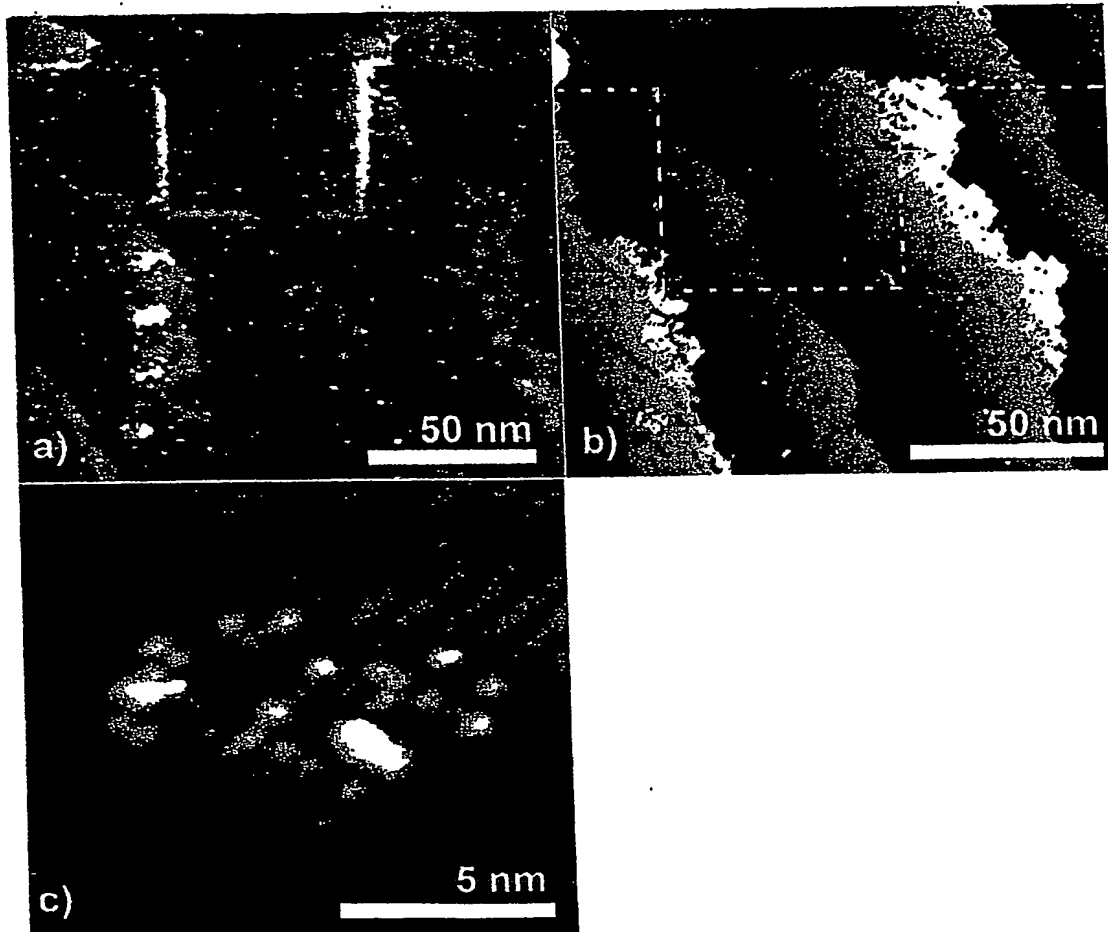


Figure 14-6

26/53

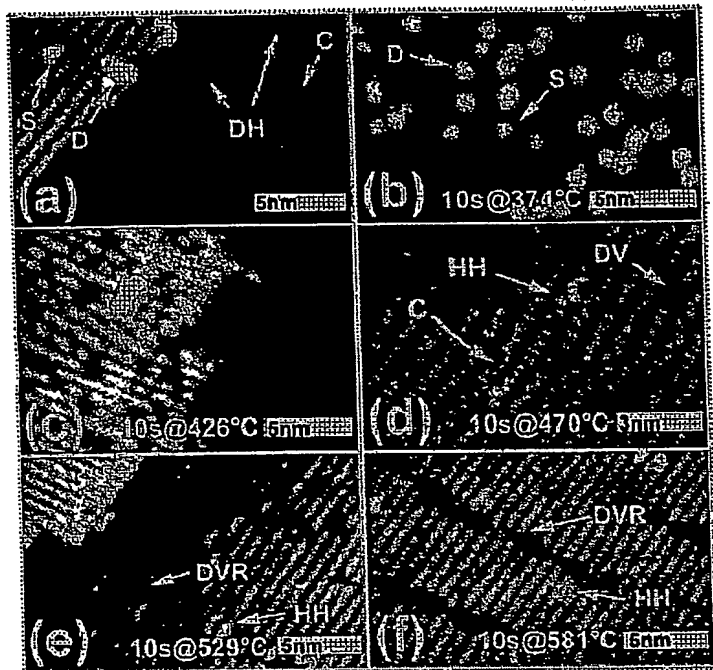


Fig. 14BA

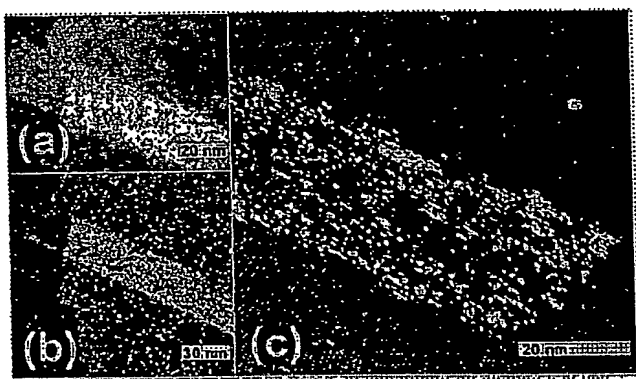


Fig. 14BB

27/53

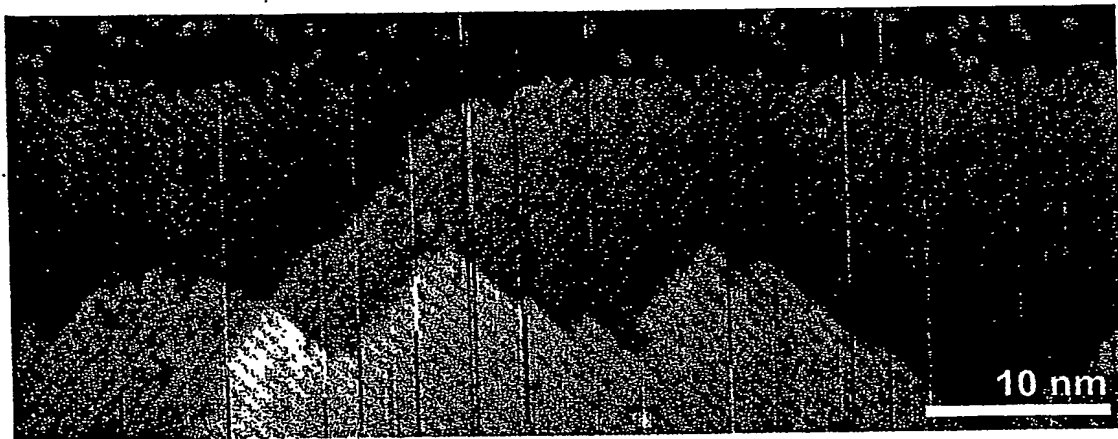


Figure 14C

28/53

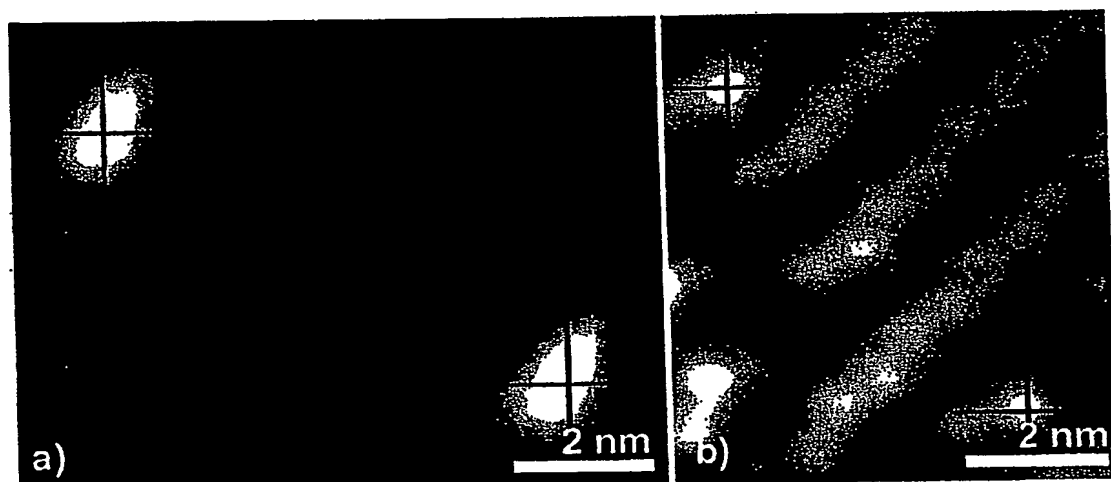


Figure 14 D

29/53



12 ML growth @ RT

FIG. 15a



12 ML growth @ 220°C

FIG. 15b



12 ML growth @ 420°C

FIG. 15c



12 ML growth @ 590°C

FIG. 15d

30/53



12 ML growth @ RT

FIG. 15e



annealed 60s @ 335°C

FIG. 15f



annealed 600s @ 335°C

FIG. 15g



annealed 60s @ 660°C

FIG. 15h

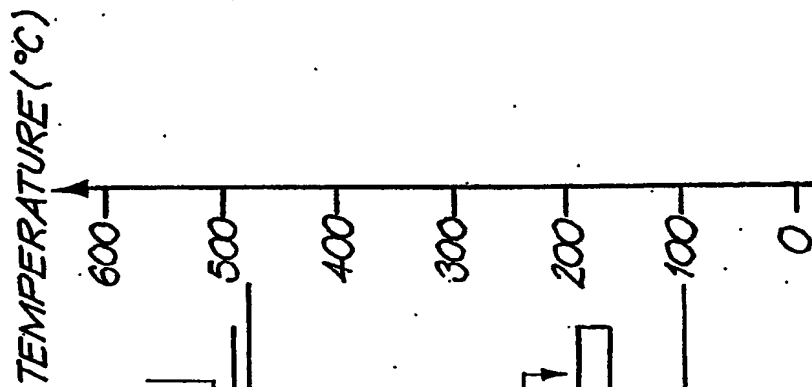


FIG. 15i

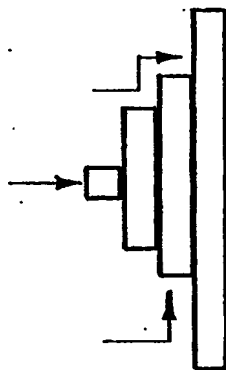


FIG. 15j

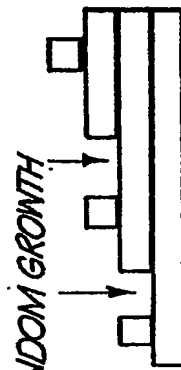


FIG. 15k

32/53



FIG. 16a

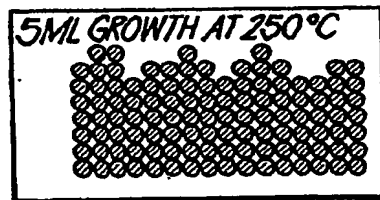


FIG. 16b



FIG. 16c

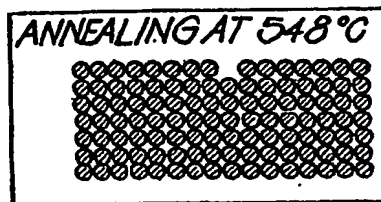


FIG. 16d

33/53

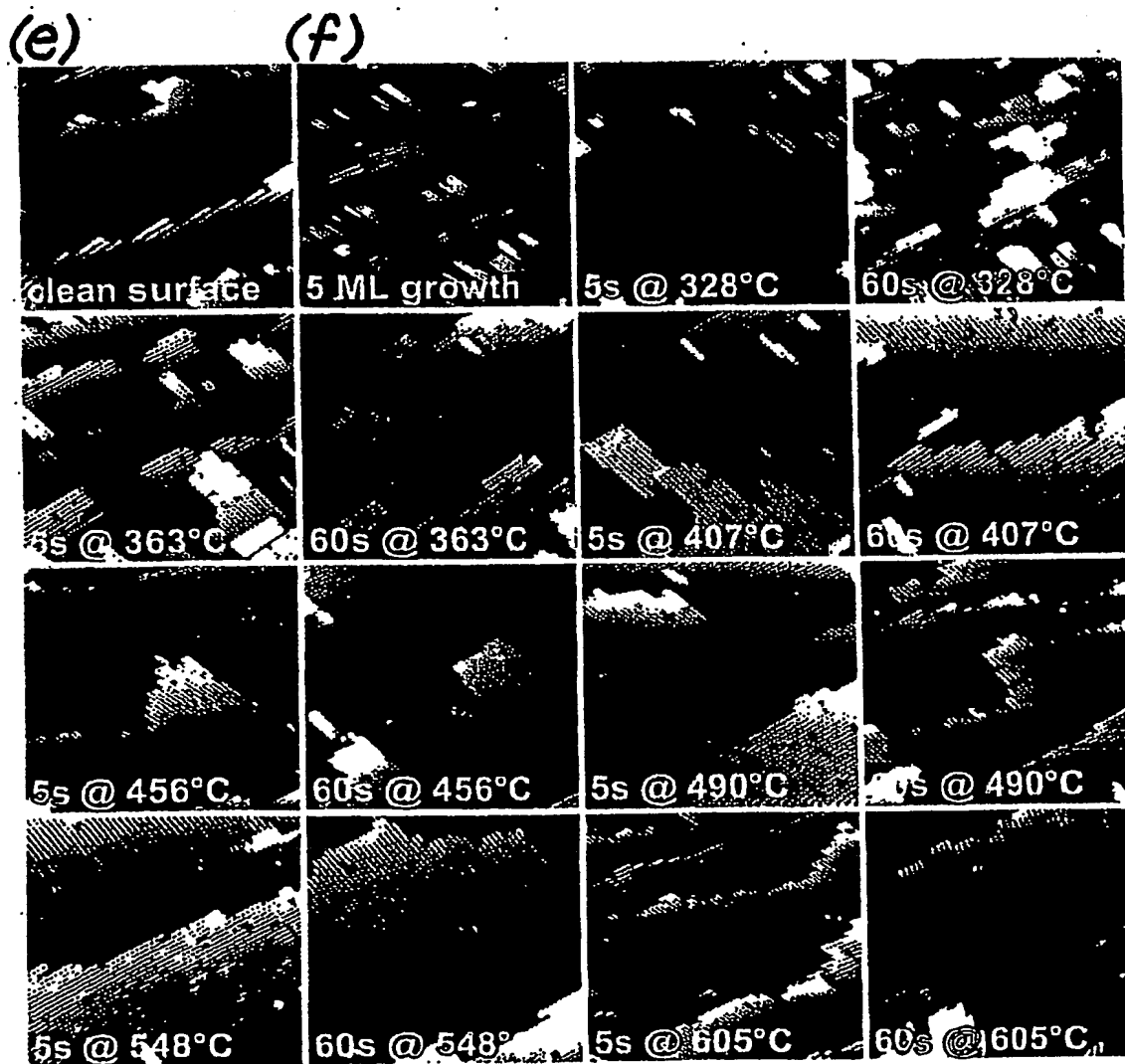


FIG. 16

34153



FIG. 17a

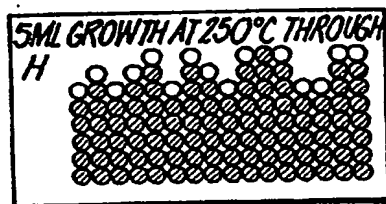


FIG. 17b

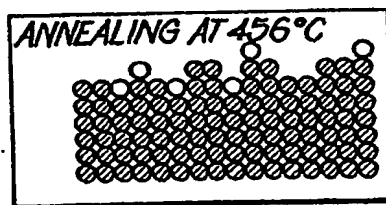


FIG. 17c



FIG. 17d

35 | 53

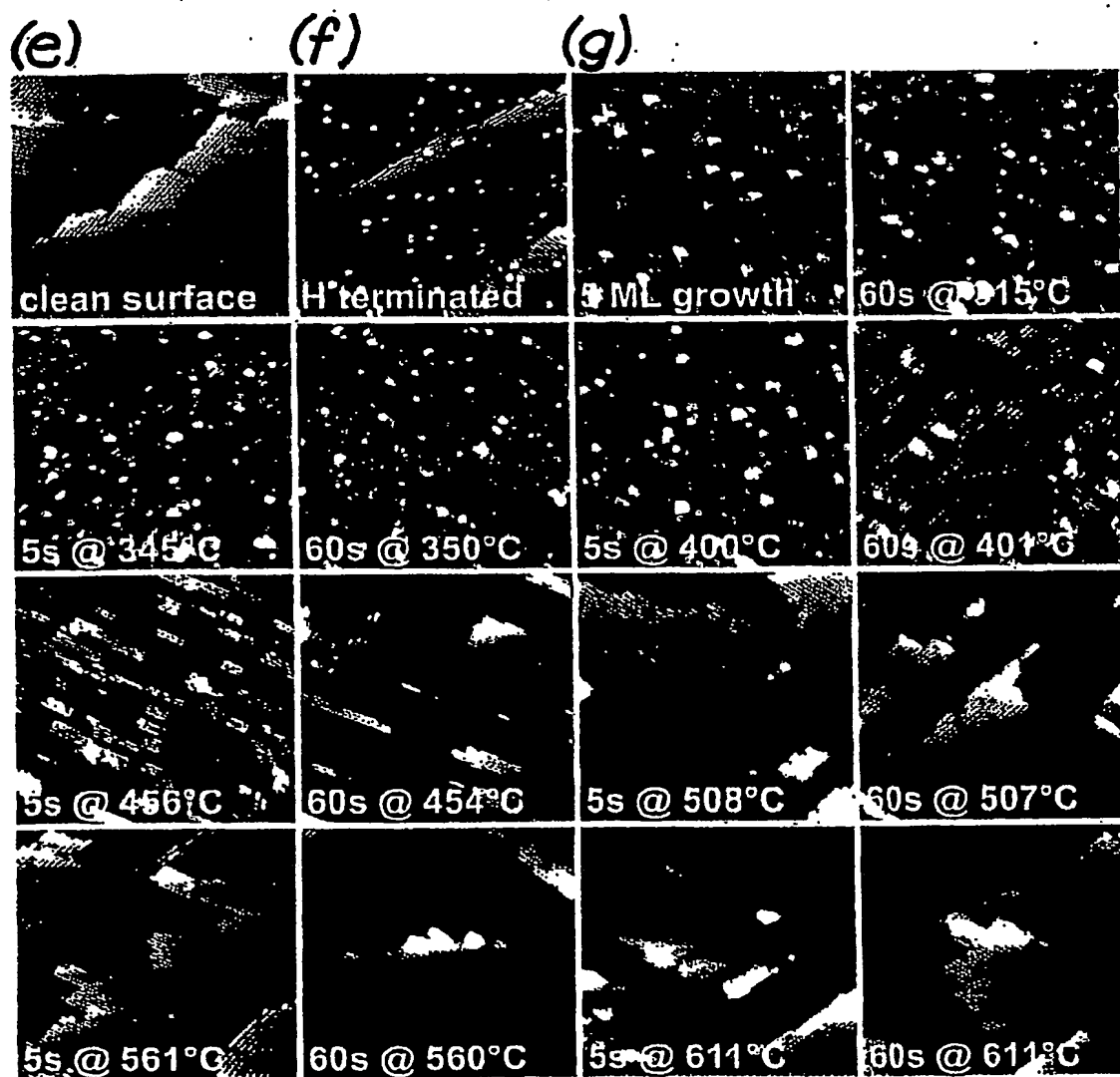


FIG. 17

36/53

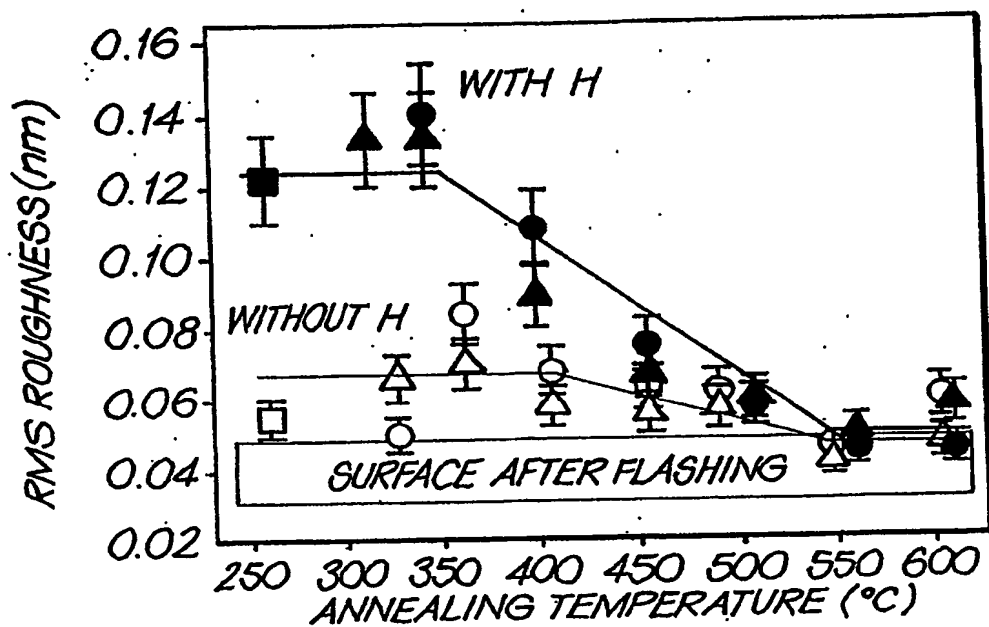


FIG. 18a

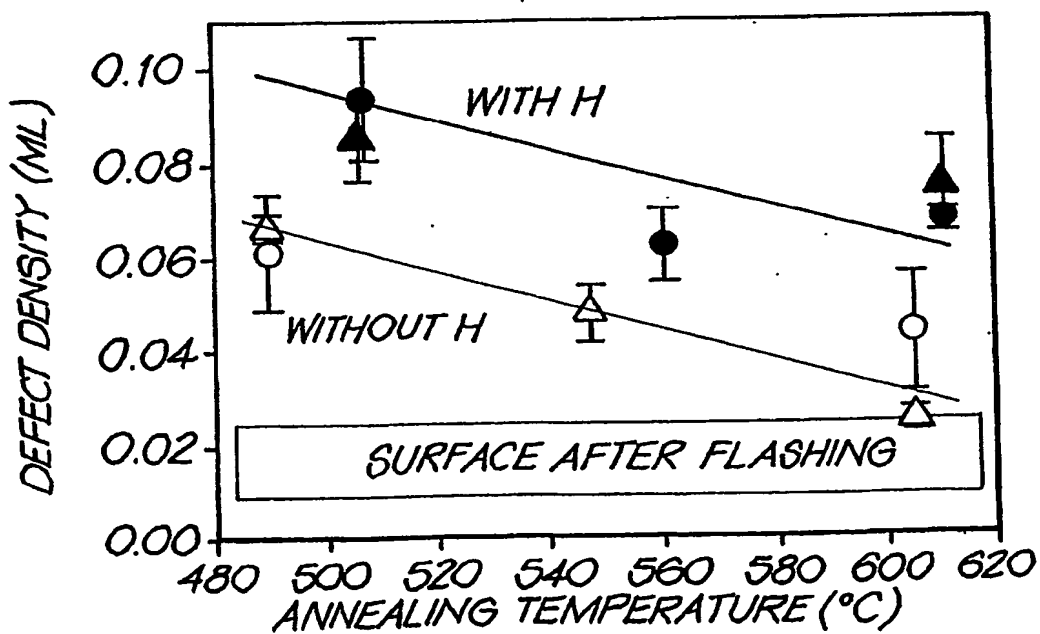
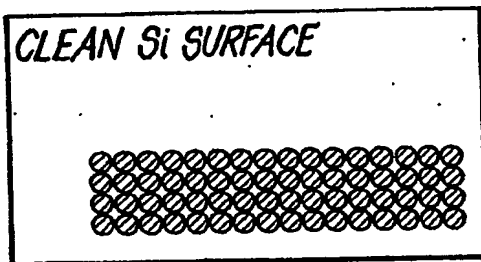
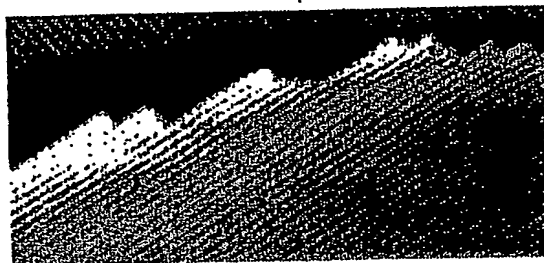


FIG. 18b

37/53

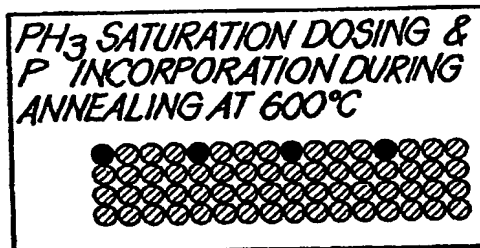


(i)

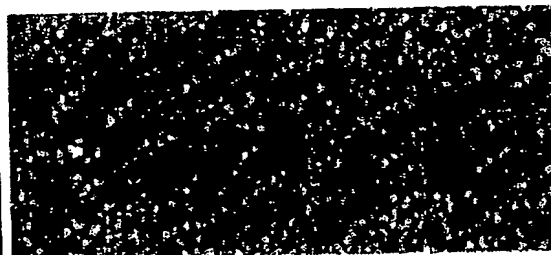


(ii)

FIG. 19a

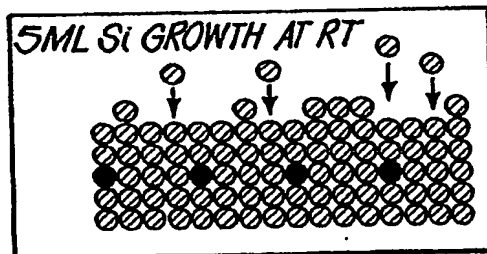


(i)

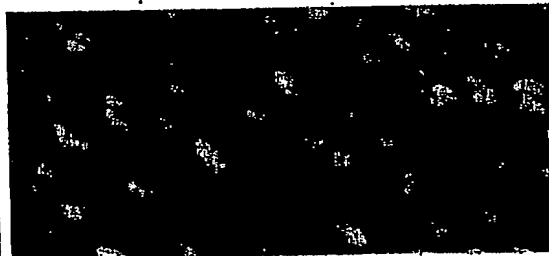


(ii)

FIG. 19b



(i)



(ii)

FIG. 19c

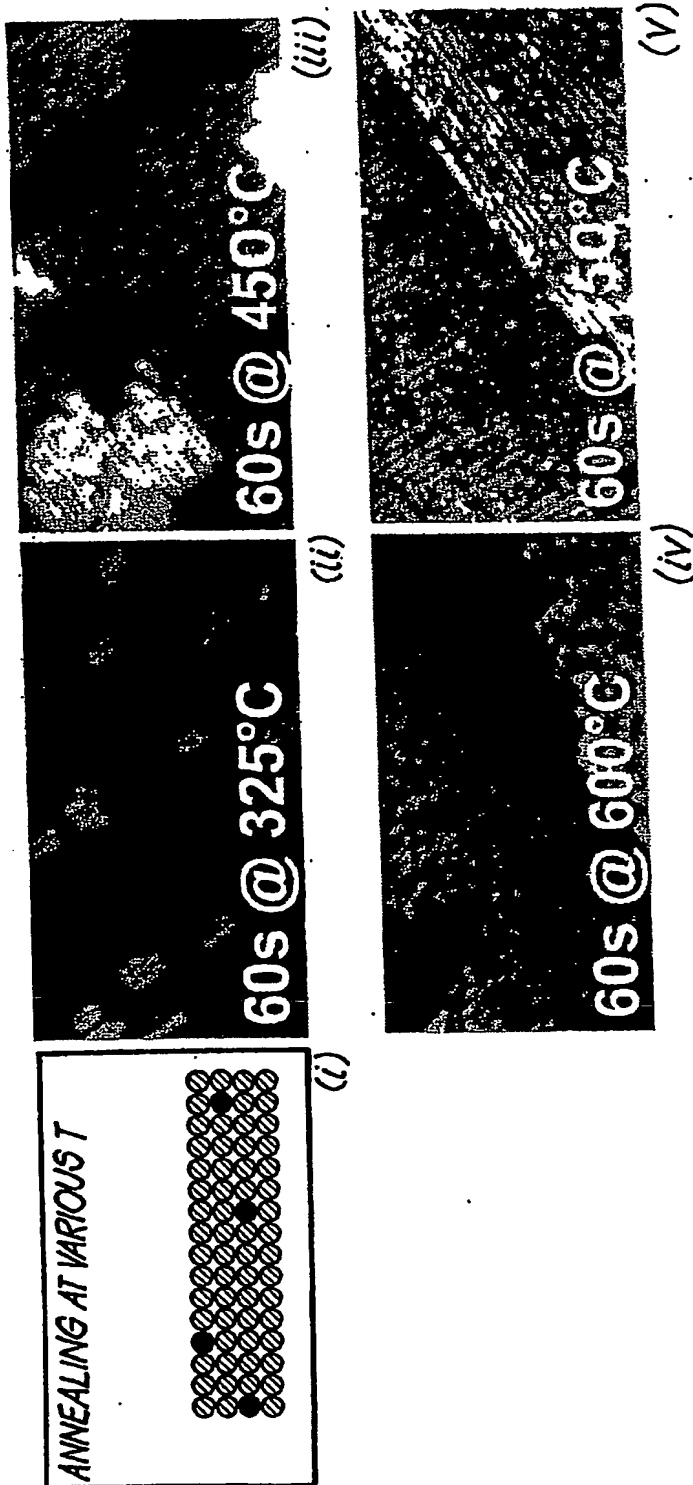


FIG. 19d

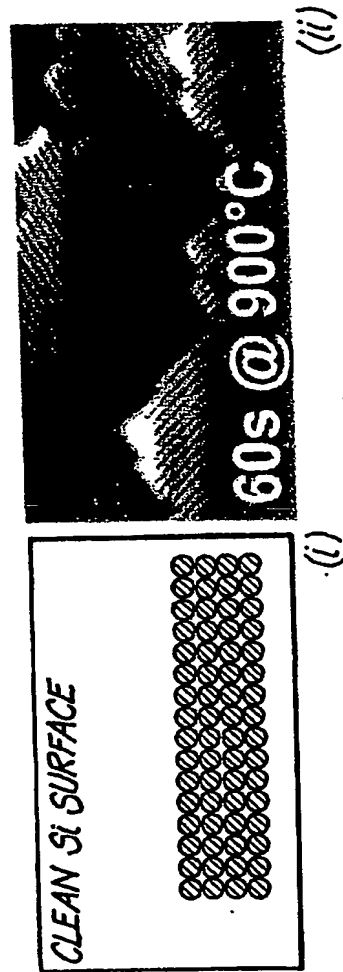
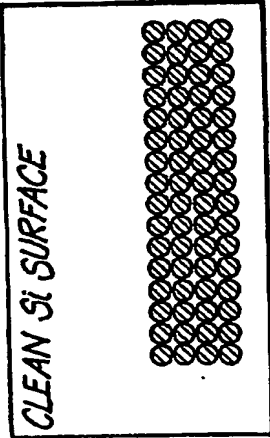
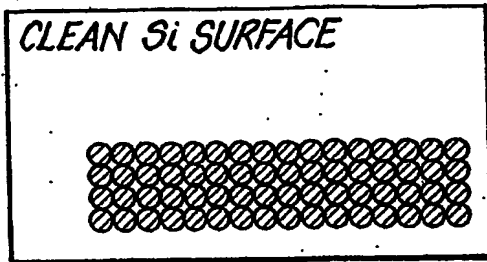


FIG. 19e



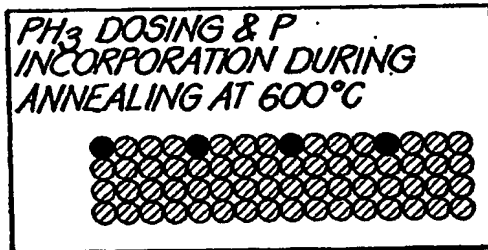
39(53



(i)

(ii)

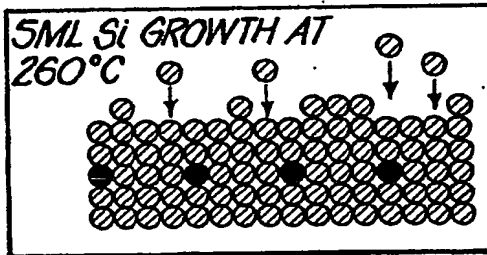
FIG. 20a



(i)

(ii)

FIG. 20b



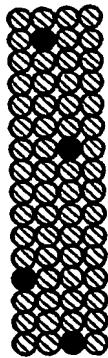
(i)

(ii)

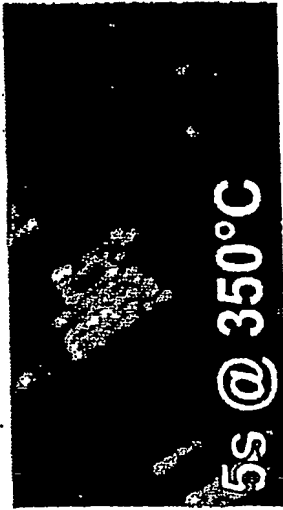
FIG. 20c

40(53

ANNEALING AT VARIOUS T



(i)



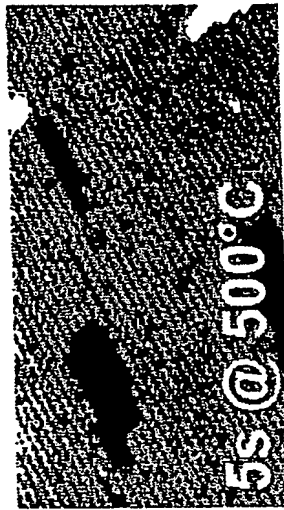
(ii)



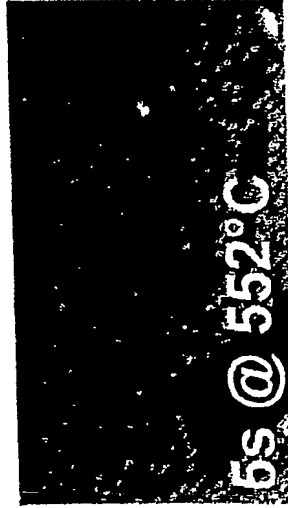
(iii)



(iv)



(v)



(vi)



(vii)

FIG. 20

41/53

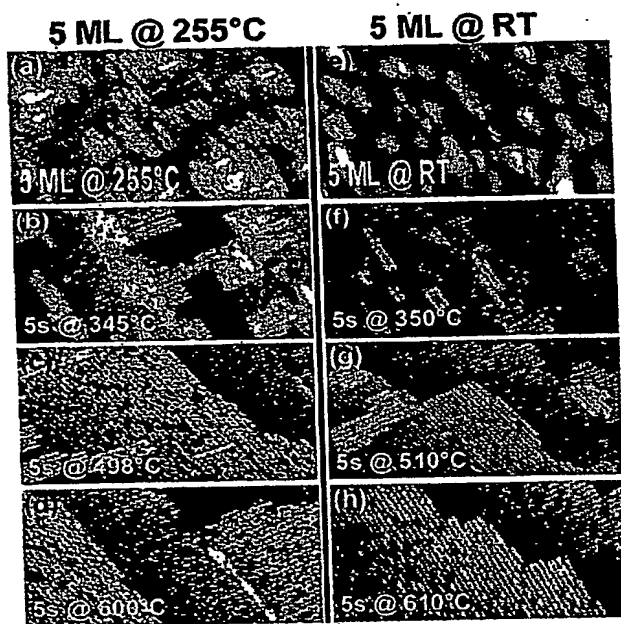


Fig. 21

42/53

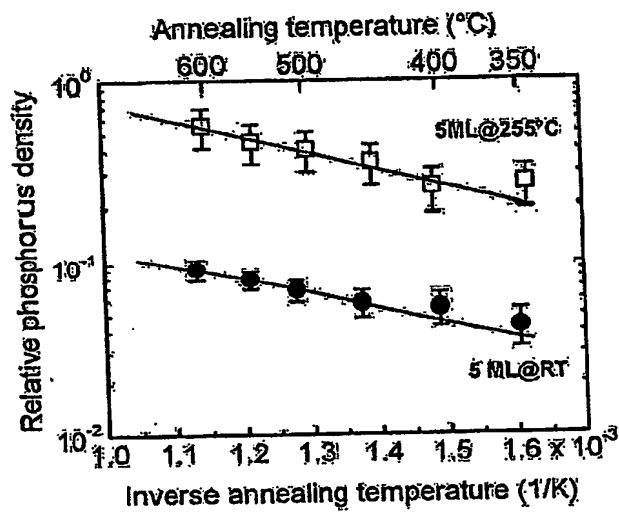
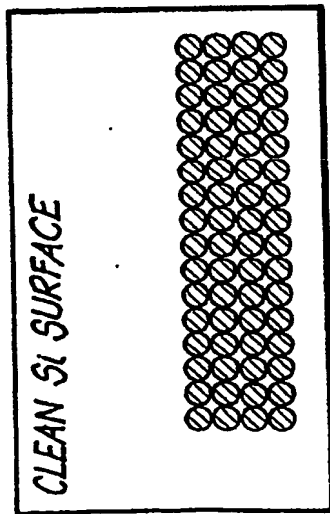
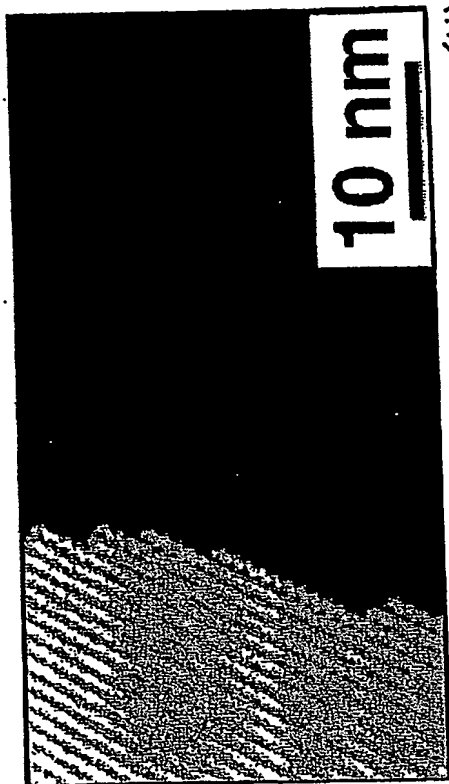


Fig. 21A

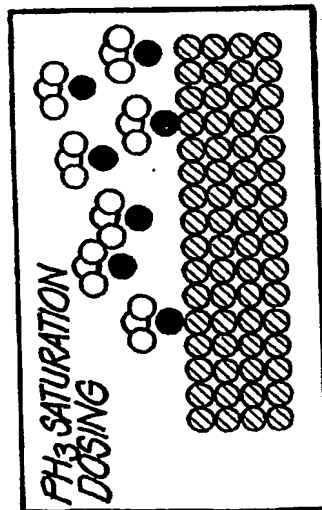


(i)

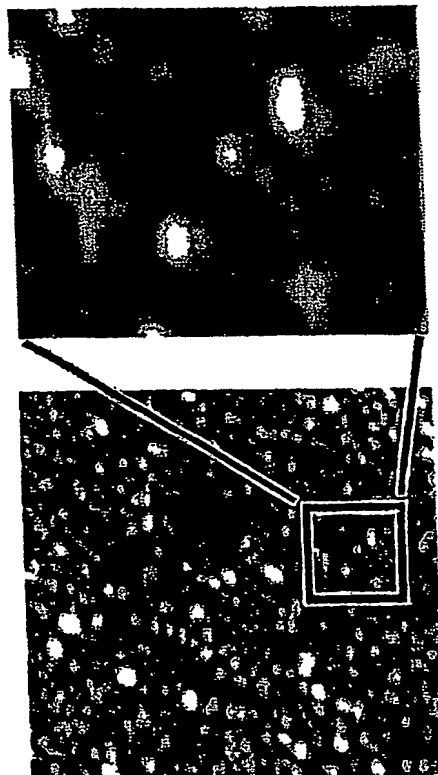


(ii)

FIG. 22a

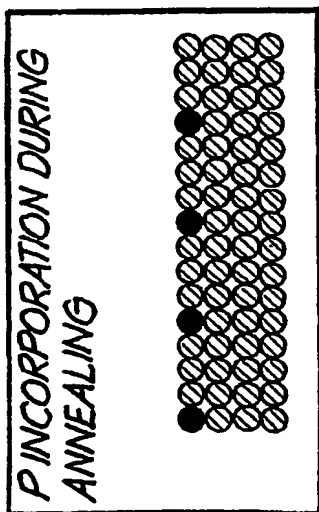


(i)



(ii)

FIG. 22b



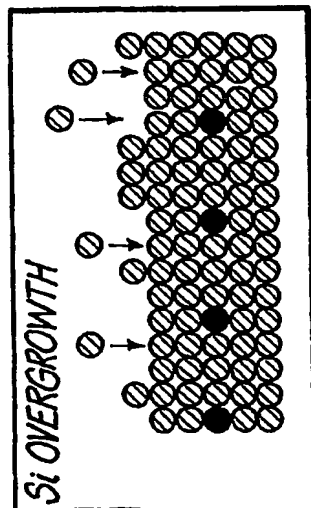
(i)



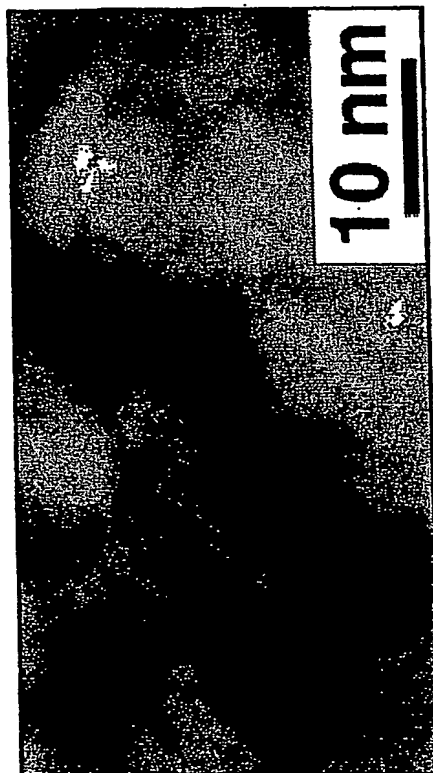
10 nm

(ii)

FIG. 22c



(i)



10 nm

(ii)

FIG. 22d

45/53

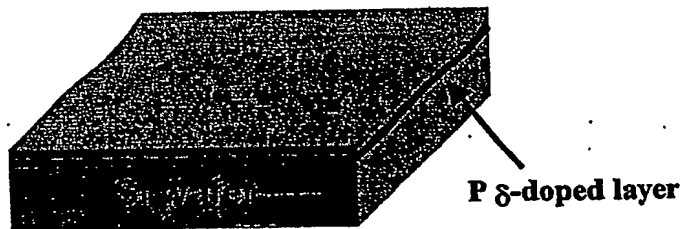


FIG. 23a

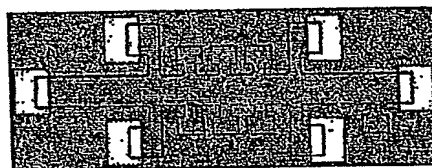


FIG. 23b

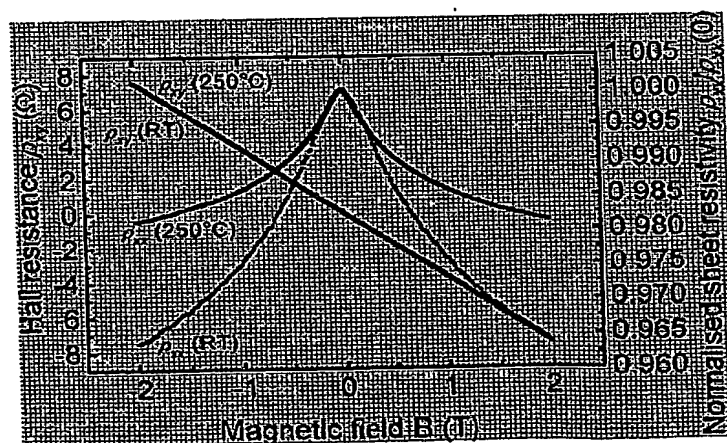


FIG. 23c

46/53

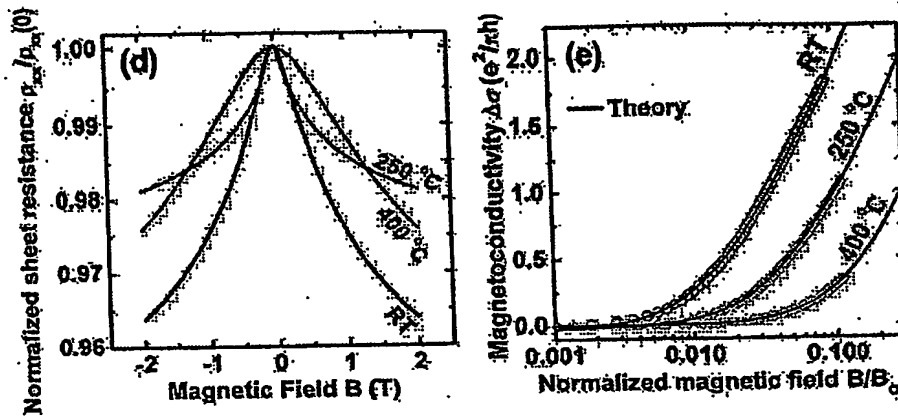


Fig. 23(d)

Fig. 23(e)

47/53

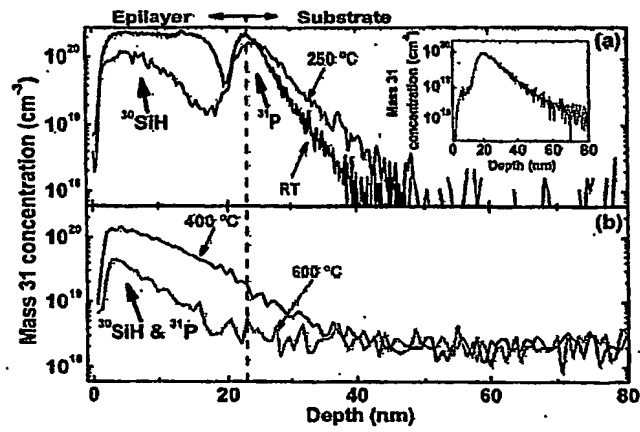


Fig. 24

48/53

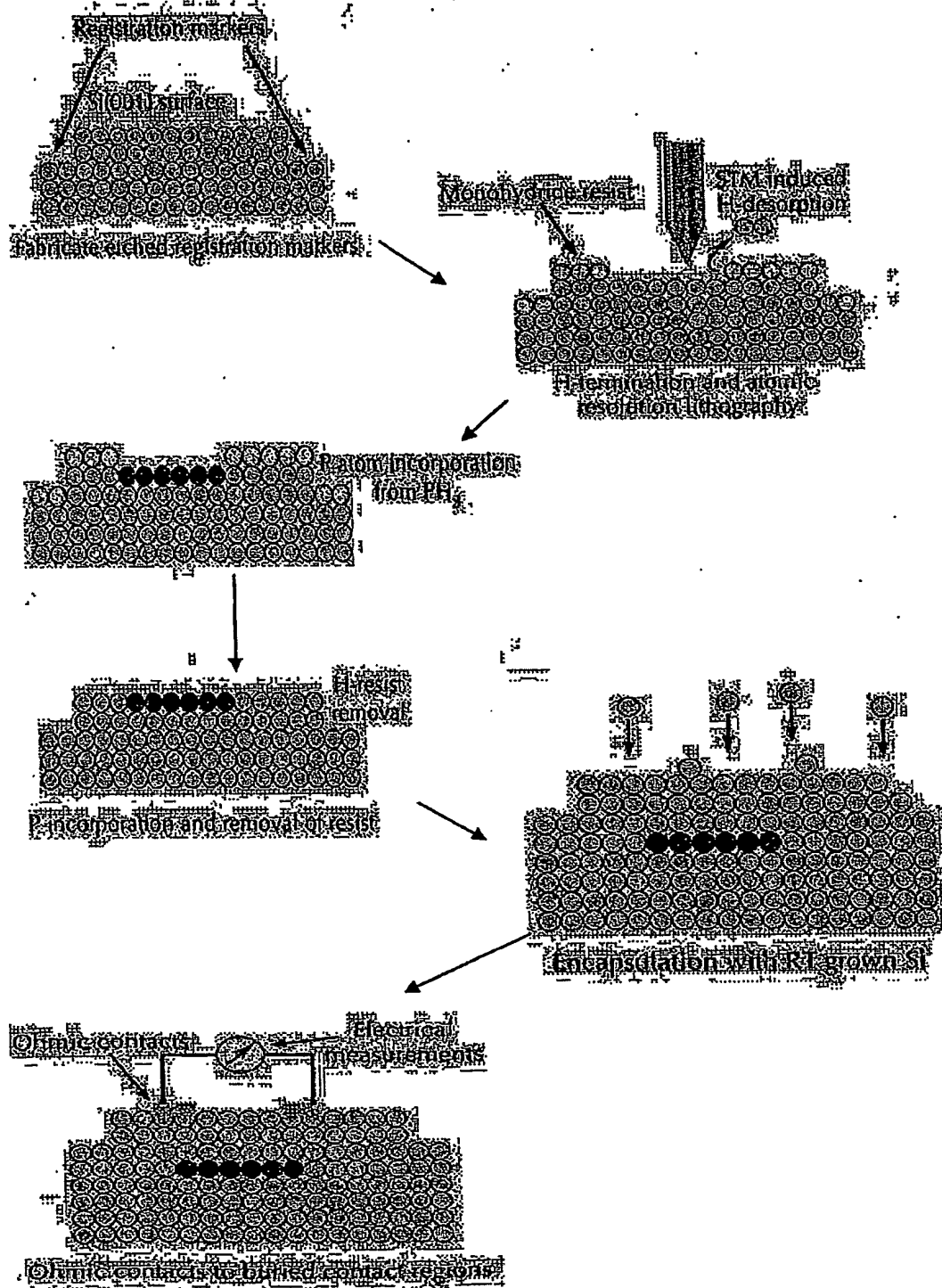


FIG. 25

49/53

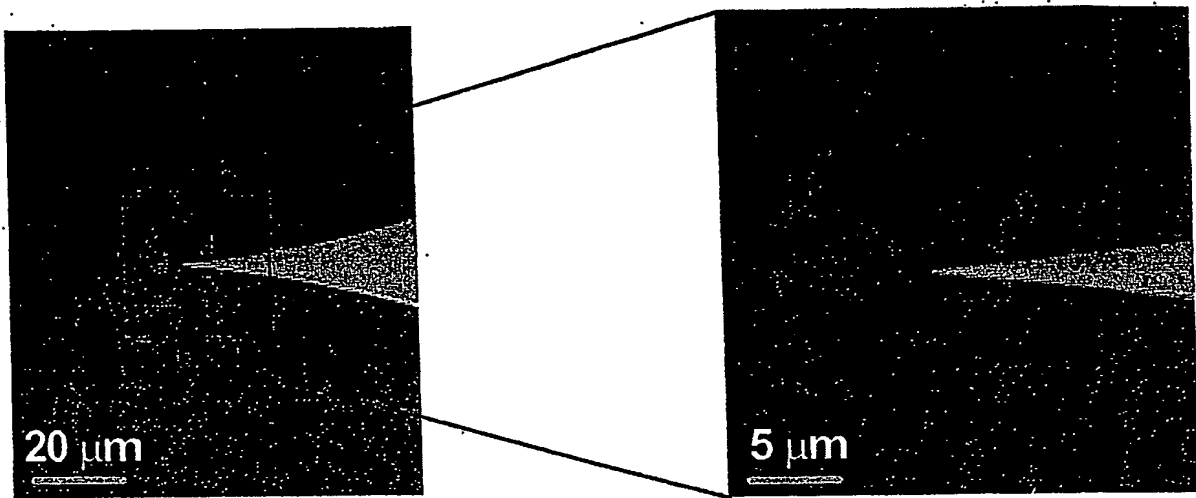


FIG. 26

50/53

FIG. 27a

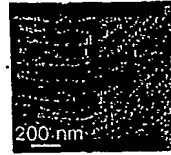


FIG. 27b

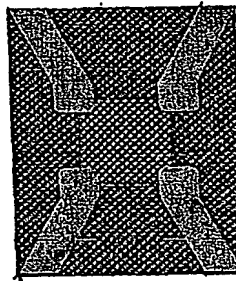
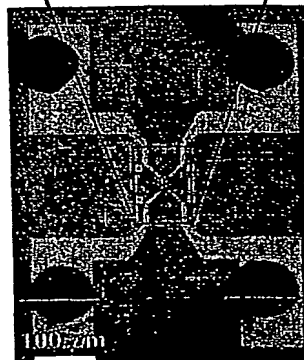


FIG. 27c



FIG. 27d



51153

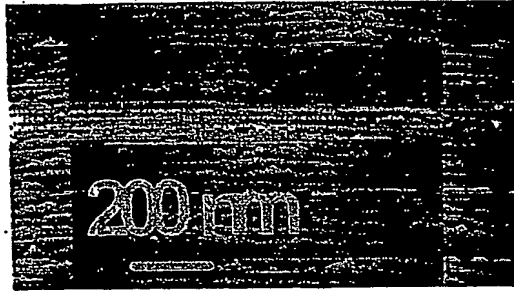


FIG. 28a

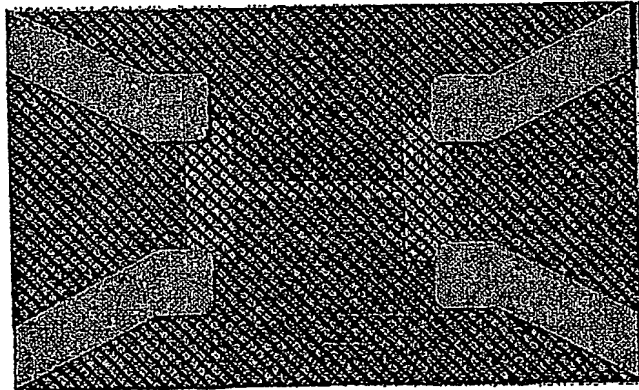


FIG. 28b

S2/S3

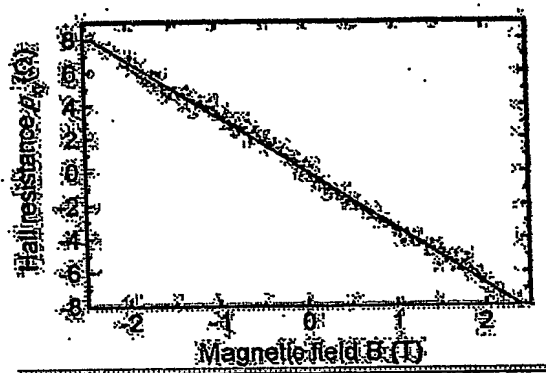


FIG. 29a

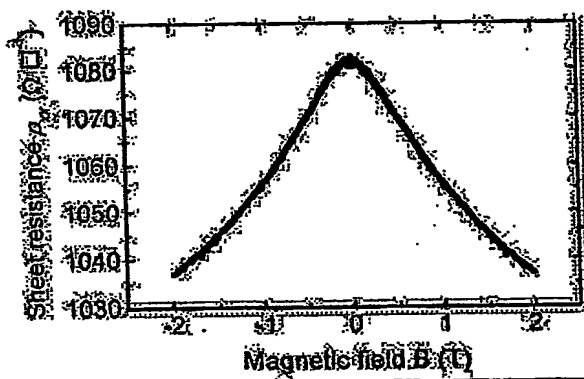


FIG. 29b

53/53

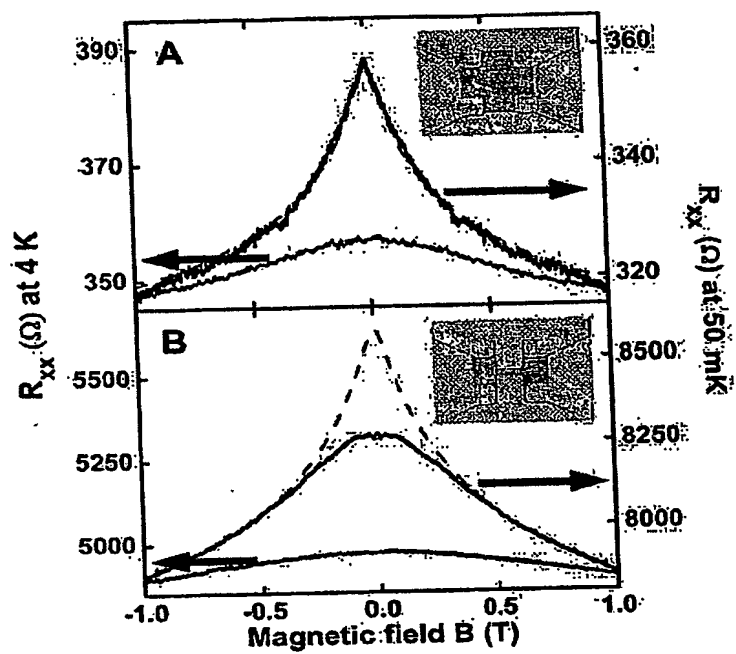


Fig. 30

**This Page is Inserted by IFW Indexing and Scanning
Operations and is not part of the Official Record**

BEST AVAILABLE IMAGES

Defective images within this document are accurate representations of the original documents submitted by the applicant.

Defects in the images include but are not limited to the items checked:

☒ BLACK BORDERS

☐ IMAGE CUT OFF AT TOP, BOTTOM OR SIDES

☒ FADED TEXT OR DRAWING

☐ BLURRED OR ILLEGIBLE TEXT OR DRAWING

☐ SKEWED/SLANTED IMAGES

☒ COLOR OR BLACK AND WHITE PHOTOGRAPHS

☐ GRAY SCALE DOCUMENTS

☒ LINES OR MARKS ON ORIGINAL DOCUMENT

☐ REFERENCE(S) OR EXHIBIT(S) SUBMITTED ARE POOR QUALITY

☐ OTHER: _____

IMAGES ARE BEST AVAILABLE COPY.

As rescanning these documents will not correct the image problems checked, please do not report these problems to the IFW Image Problem Mailbox.